Helsinki University of Technology
Department of Signal Processing and Acoustics
Espoo 2008   Report 2

PROPAGATION PARAMETER ESTIMATION IN MIMO SYSTEMS

Cássio Barboza Ribeiro

Dissertation for the degree of Doctor of Science in Technology to be presented with due permission of the Department of Electrical and Communications Engineering for public examination and debate in Auditorium S4 at Helsinki University of Technology (Espoo, Finland) on the 25th of April, 2008, at 12 o'clock noon.

Helsinki University of Technology
Faculty of Electronics, Communications and Automation
Department of Signal Processing and Acoustics

Teknillinen korkeakoulu
Elektroniikan, tietoliikenteen ja automaation tiedekunta
Signaalinkäsittelyn ja akustiikan laitos

ABSTRACT OF DOCTORAL DISSERTATION	HELSINKI UNIVERSITY OF TECHNOLOGY P. O. BOX 1000, FI-02015 TKK http://www.tkk.fi

Author	Cássio Barboza Ribeiro

Name of the dissertation
Propagation Parameter Estimation in MIMO Systems

Manuscript submitted	07 December, 2007	Manuscript revised	25 February, 2008

Date of the defence	25 April, 2008

☐ Monograph ☒ Article dissertation (summary + original articles)

Faculty	Faculty of Electronics, Communications and Automation
Department	Department of Signal Processing Laboratory and Acoustics
Field of research	Sensor Array Signal Processing
Opponent(s)	Prof. Reiner Thomä and Prof. Christoph Mecklenbräuker
Supervisor	Prof. Visa Koivunen
Instructor	Prof. Visa Koivunen

Abstract

Multiple antenna techniques are in the heart of modern and next-generation wireless communications systems, such as 3GPP Long-Term Evolution (LTE), IEEE 802.16e (WiMAX), and IMT-Advanced (IMT-A). Such techniques are considered for the high link capacity gains that are achievable from spatial multiplexing, and also for the system capacity, link reliability, and coverage benefits that are possible from spatial diversity, beamforming, and spatial division multiple access techniques. Accurate spatial channel models play a key role on the characterization of the propagation environment and determination of which techniques provide higher gains in a given scenario. Such models are also fundamental tools in network planning, link and system performance studies, and transceiver development.

Realistic channel models are based on measurements. Hence, there is a need for techniques that extract the relevant information from huge amount of data. This may be achieved by estimating model parameters from the data. Most estimation algorithms are based on the assumption that the channel can be modeled as a combination of a finite number of specular, highly-concentrated paths, requiring estimation of a very large number of parameters. In this thesis, estimators are derived for the parameters of the concentrated propagation paths and the diffuse scattering component that are frequently observed in Multiple-Input Multiple Output (MIMO) channel sounding measurements. Low complexity methods are derived for efficient computation of the estimates. The derived methods are based on a stochastic channel model, leading to a lower-dimensional parameter set that allow a reduction in computational complexity and improved statistical performance compared to methods found in the literature.

Simulation results demonstrate that high quality estimates are obtained. The large sample performance of the estimators are studied by establishing the Cramér-Rao lower bound (CRLB) and comparing it to the variances of the estimates. The simulations show that the variances of the proposed estimation techniques attain the CRLB for relatively small sample size for most parameters, and no bias is observed.

VÄITÖSKIRJAN TIIVISTELMÄ	TEKNILLINEN KORKEAKOULU
	PL 1000, 02015 TKK
	http://www.tkk.fi

Tekijä	Cássio Barboza Ribeiro

Väitöskirjan nimi

Etenemisparametrien estimointi moniantennijärjestelmissä

Käsikirjoituksen päivämäärä	07.12.2007	Korjatun käsikirjoituksen päivämäärä	25.02.2008

Väitöstilaisuuden ajankohta	25.04.2008

☐ Monografia   ☒ Yhdistelmäväitöskirja (yhteenveto + erillisartikkelit)

Tiedekunta	Elektroniikan, tietoliikenteen ja automaation tiedekunta
Laitos	Signaalinkäsittelyn ja akustiikan laitos
Tutkimusala	Tietoliikenteen signaalinkäsittely
Vastaväittäjä(t)	Prof. Reiner Thomä and Prof. Christoph Mecklenbräuker
Työn valvoja	Prof. Visa Koivunen
Työn ohjaaja	Prof. Visa Koivunen

Tiivistelmä

Moniantennitekniikat ovat keskeisessä osassa kehittyneissä uuden sukupolven langattomissa tietoliikennejärjestelmissä kuten 3GPP Long-Term Evolution (LTE), IEEE 802.16e (WiMAX) ja IMT-Advanced (IMT-A). Näillä tekniikoilla saavutetaan tietoliikennejärjestelmissä merkittäviä etuja: radiospektriä voidaan hyödyntää tehokkaammin ja radiolinkin kapasiteetti moninkertaistaa useaa datavirtaa tukevilla moniantenni (MIMO) lähetin-vastaanotin rakenteilla. Toisaalta systeemin kapasiteettia, tiedonsiirron luotettavuutta ja tiedonsiirron kattavuutta voidaan parantaa lähetysdiversiteettimenetelmien, keilanmuodostuksen ja tilajakoisen kanavoinnin avulla. Tarkat ja realistiset moniulotteiset kanavamallit ovat avainasemassa etenemisympäristön karakterisoinnissa, ja edellytys edellämainittujen moninantennitekniikoiden suorituskyvyn vertailulle erilaisissa käyttöympäristöissä. Nämä kanavamallit ovat myös keskeisiä työkaluja radiolähettimien ja vastaaonottimien kehitystyössä, radioverkkojen suunnittelussa, ja suorituskyvyn tarkastelussa sekä linkki- että systeemitasolla.

Realistiset kanavamallit kehitetään mittauksiin perustuen eristämällä relevantti informaatio valtavasta mittausaineistosta. Tämä voidaan saavuttaa tilastollisilla menetelmillä estimoimalla mallin parametreja tehdyistä havainnoista. Useimmat kirjallisuudessa esitetyt menetelmät perustuvat oletukseen, jossa kanava koostuu suuresta määrästä peiliheijastuksia. Tällöin estimoitavien parametrien määrä muodostuu hyvin suureksi. Tässä tutkimuksessa on johdettu estimaattoreita keskittyneiden etenemispolkujen ja diffuusin sirontakomponentin parametreille, jotka esiintyvät yleisesti MIMO-kanavan luotausmittauksissa. Tutkimuksessa on lisäksi johdettu laskennallisesti tehokkaita menetelmiä estimaattien muodostukseen. Kehitetyissä menetelmissä käytetyn stokastisen kanavamallin ansiosta tuntemattomia parametrejä on vähemmän kuin kirjallisuudesta löytyvissä menetelmissä. Tämän vuoksi kehitetyt menetelmät ovat laskennallisesti tehokkaampia ja tilastolliselta suorituskyvyltään parempia.

Simulaatiotulokset osoittavat, että lasketut estimaatit ovat korkealaatuisia. Estimaattoreiden asymptoottista suorituskykyä on tutkittu johtamalla Cramér-Rao alarajat (CRLB) eri parametreille ja vertaamalla sitä estimaattoreiden variansseihin. Simulaatiot osoittavat, että useimpien parametrien tapauksessa johdettujen estimaattoreiden varianssit saavuttavat Cramér-Rao alarajan suhteellisen pienelläkin otoskoolla ja että estimaatit ovat harhattomia.

Asiasanat	Moniantennijärjestelmät, parametrien estimointi, radiokanavan mallinnus, kanavaluotaus

ISBN (painettu)	978-951-22-9302-5	ISSN (painettu)	1797-4267
ISBN (pdf)	978-951-22-9303-2	ISSN (pdf)	
Kieli	Englanti	Sivumäärä	102s. + liit. 94s.

Julkaisija	Teknillinen korkeakoulu, Signaalinkäsittelyn ja akustiikan laitos

Painetun väitöskirjan jakelu	Teknillinen korkeakoulu, Signaalinkäsittelyn ja akustiikan laitos

☒ Luettavissa verkossa osoitteessa http://lib.tkk.fi/Diss

Preface

The research work for this doctoral thesis was carried out at the Signal Processing Laboratory, Helsinki University of Technology, during the years 2003-2005. The Statistical Signal Processing research group, led by Prof. Visa Koivunen, is a part of SMARAD (Smart and Novel Radios Research Unit) Center of Excellence in research nominated by the Academy of Finland.

First, I wish to express my gratitude to my supervisor, Prof. Visa Koivunen, for his continuous encouragement, guidance and support during the course of this work. It has been an honor to work with such a deeply dedicated scientist and outstanding group leader.

Then, I would like to thank the thesis pre-examiners, Prof. Christoph Mecklenbräucker and Dr. Juha Ylitalo for their constructive and helpful comments. Furthermore, Prof. Iiro Hartimo, the director of the Graduate School in Electronics, Telecommunications and Automation (GETA) and the GETA coordinator Marja Leppäharju are highly acknowledged. Lab secretaries Mirja Lemetyinen and Anne Jääskeläinen deserve also many thanks for assisting with all practical issues and arrangements.

I am grateful to my colleagues in the lab and especially co-workers Dr. Andreas Richter and Dr. Esa Ollila, with whom I co-authored several publications, as well as Dr. Stephan Werner, Dr. Timo Roman, and Dr. Fabio Belloni. Prof. Risto Wichman, Prof. Timo Laakso, Jussi Salmi, Eduardo Zacarias, Traian Abrudan, Dr. Maarit Melvasalo, Mei Yen Cheong, Dr. Jan Eriksson, Dr. Mihai Enescu, Karol Schober, Pekka Jänis, and Helka-Liina Määttänen are also acknowledged for our valuable discussions. Special thanks to Dr. Fernando Gregorio and Dr. Paulo Esquef, for the many discussions and personal support.

I am also grateful to my colleagues at Nokia Research Center, who gave me support during the final steps of the thesis. Special thanks to Dr. Juha Laurila and Dr. Klaus Hugl for their encouragement and effective support when finalizing the manuscript. My colleagues Elena Virtej, Petteri Lunden, Markku Kuusela, Tero Henttonen, Klaus Doppler,

I wish to express my warmest gratitude to my family, my parents José Marcos and Vera Lúcia as well as my brother Leonardo for their permanent encouragement and support, despite the distance to Brazil. My friends in Brazil and Finland also deserve many thanks for providing those precious moments when the mind is diverted from tough scientific work.

Foremost, I would like to thank my wife Patricia, whose love and care have been absolutely essential during the whole duration of this work, and that is currently taking very special care of our first child, who will become an integral part of our life in the next few months.

Espoo,
April 2008,

Cássio Ribeiro

Contents

x

List of original publications

(I) C. B. Ribeiro, E. Ollila, and V. Koivunen. "Stochastic maximum likelihood method for propagation parameter estimation," in *IEEE International Symposium on Personal, Indoor and Mobile Radio Communications*, Barcelona, Spain, Sep. 2004, vol. 3, pp. 1839–1843.

(II) C. B. Ribeiro, E. Ollila, and V. Koivunen, "Cramér-Rao bound for angular propagation parameter estimation in MIMO systems," in *Asilomar Conference on Signals, Systems, and Computers*, Pacific Grove, CA, USA, Nov. 2004, vol. 2, pp. 1785–1789.

(III) C. B. Ribeiro, E. Ollila, and V. Koivunen, "Propagation parameter estimation in MIMO systems using mixture of angular distributions model," in *Proc. IEEE Int. Conf. on Acoustics, Speech and Signal Processing, ICASSP 2005*, Philadelphia, PA, USA, Mar. 2005, vol. 4, pp. 885–888.

(IV) C. B. Ribeiro, E. Ollila, and V. Koivunen, "Stochastic maximum-likelihood method for MIMO propagation parameter estimation," *IEEE Transactions on Signal Processing*, vol. 55, no. 1, pp. 46–55, 2007.

(V) C. B. Ribeiro, A. Richter, and V. Koivunen, "Stochastic maximum likelihood estimation of angle- and delay-domain propagation parameters," in *IEEE International Symposium on Personal, Indoor and Mobile Radio Communications*, Berlin, Germany, Sep. 2005, vol. 1, pp. 624–628, *Best Paper Award*.

(VI) C. B. Ribeiro, A. Richter, and V. Koivunen, "Detecting specular propagation paths in the presence of distributed scattering in angle and delay domains," in *Asilomar Conference on Signals, Systems, and Computers*, Nov. 2006.

(VII) C. B. Ribeiro, A. Richter, and V. Koivunen, "Joint angular and delay domain

MIMO propagation parameter estimation using approximate ML method," *IEEE Transactions on Signal Processing*, vol. 55, no. 10, pp. 4775–4790, 2007.

List of abbreviations and symbols

Abbreviations

3GPP	Third-generation partnership project
BLAST	Bell Labs layered space time
BS	base station
CRLB	Cramér-Rao lower bound
CSI	channel state information
D-BLAST	Diagonal BLAST
DFT	discrete Fourier transform
DDIR	double directional impulse responses
DDDPS	double-directional delay power spectrum
DML	deterministic maximum likelihood
DoA	direction of arrival
DoD	direction of departure
DSC	diffuse scattering component
EM	expectation-maximization
ESPRIT	estimation of signal parameters via rotational invariance techniques
FDTD	finite difference time domain
FIM	Fisher Information Matrix
FFT	fast Fourier transform
GAM	generalized array manifold
H-BLAST	Horizontal BLAST
LoS	line-of-sight
LS	least squares
LTE	long-term evolution

MCSS	multi-carrier spread spectrum signal
MIMO	multiple-input multiple-output
MISO	multiple-input single-output
ML	maximum likelihood
MMSE	minimum mean squared error
MoM	method of moments
MRC	maximum-ratio combining
MS	mobile station
MSE	mean squared error
MT	mobile terminal
MUSIC	multiple signal classification
NLoS	non line-of-sight
PAP	power angular profile
PDF	probability density function
PDP	power delay profile
RMS	root mean square
RX	receiver
SAGE	space-alternating generalized expectation-maximization
SDMA	spatial division multiple access
SINR	signal-to-interference plus noise ratio
SIMO	single-input multiple-output
SISO	single-input single-output
SML	stochastic maximum likelihood
SNR	signal-to-noise ratio
STBC	space-time block code
STC	space-time coding
STTC	space-time trellis code
SVD	singular value decomposition
TDD	time-division duplex
TLS	total least squares
TX	transmitter
UCA	uniform circular array
ULA	uniform linear array

URA	uniform rectangular array
VNA	vector network analyzer
ZF	zero-forcing

Symbols

j	imaginary unit
$*$	convolution product
$\odot$	Schur-Hadamard (i.e., element-wise) product
$\otimes$	Kronecker (tensor) product
$\|\cdot\|$	Euclidean norm
arg	argument of a complex number
arg min	minimizing argument
arg max	maximizing argument
$E[\cdot]$	expectation operator
exp	exponential function
min	minimum
max	maximum
$\Re\{\cdot\}$	real part of complex scalar
$\Im\{\cdot\}$	imaginary part of complex scalar
$(\cdot)^*$	complex conjugate
$(\cdot)^T$	transpose of a matrix
$(\cdot)^H$	Hermitian transpose of a matrix
$(\cdot)^{-1}$	inverse of a matrix
$(\cdot)^{-H}$	inverse Hermitian transpose of a matrix
$(\cdot)^\dagger$	Moore-Penrose pseudo-inverse of a matrix
$\mathrm{vec}(\cdot)$	stacks columns of a matrix on top of each other
$\mathrm{mat}(\cdot, M, N)$	arranges a vector into a $M \times N$ matrix
$\mathrm{tr}(\cdot)$	trace of a matrix
$\det(\cdot)$	determinant of a matrix
$\mathrm{diag}(\cdot)$	diagonal matrix of the argument vector
$\mathbf{I}$	identity matrix
$\mathbf{1}$	vector whose elements are 1's
$\mathbf{F}$	DFT matrix
$T(\cdot)$	a linear mapping of the argument
$\widehat{a}$	estimate of a
$I_0(\cdot)$	modified Bessel function of the first kind of order zero

$\delta(\cdot)$	Dirac delta
C	Shannon capacity
M_t	number of Tx antennas
M_r	number of Rx antennas
M_f	number of frequency samples
M_o	$M_o = M_t M_r M_f$
M_s	number of observations
K	number of specular components
L	number of clusters
$B_T(f),\ B_R(f)$	frequency response of the measurement system at the transmitter and receiver, respectively
$s(t)$	transmitted symbol
$\mathbf{s}(t)$	transmitted symbol vector
$y(t),\ y(f)$	received signal in time and frequency domain, respectively
$\mathbf{y}(t),\ \mathbf{y}(f)$	received signal vector in time domain and frequency domain, respectively
$\mathcal{Y}$	stacked version of $\mathbf{y}(f)$, i.e., $\mathrm{vec}([\,\mathbf{y}(0)\ \cdots\ \mathbf{y}(M_f-1)\,])$
$\mathcal{Y}'$	pre-whitened version of $\mathcal{Y}$
σ_s^2	transmitted signal power
$\mathbf{D}$	diagonal matrix with the power weights for each symbol stream
$\mathbf{u}(t),\ \mathbf{u}(f)$	array output vector corresponding to one observation of a specular path in time and frequency domain, respectively
$\overline{\mathbf{u}}$	stacked version of $\mathbf{u}(f)$
$\mathbf{H}$	MIMO channel matrix
$\mathbf{H}_w$	MIMO channel matrix with i.i.d. elements
$\mathbf{h}$	SIMO channel vector
$h(t),\ H(f)$	SISO (scalar) channel in time and frequency domain, respectively
$\mathbf{U}$	left singular vectors of $\mathbf{H}$
$\boldsymbol{\Sigma}$	matrix with the singular values of $\mathbf{H}$ in the main diagonal
$\mathbf{V}$	right singular vectors of $\mathbf{H}$
$\mathbf{n}(t),\ \mathbf{n}(f)$	noise vector in time and frequency domain, respectively

$\overline{\mathbf{n}}$	stacked version of $\mathbf{n}(f)$
σ_n^2	noise variance
ρ	signal-to-noise ratio
$\boldsymbol{\Theta}$	parameter vector
$\boldsymbol{\Theta}_{\mathrm{sp}}$	parameter vector for specular components
$\boldsymbol{\Theta}_w$	parameter vector for frequency-domain DSC parameters
$\boldsymbol{\Theta}_h$	parameter vector for angular-domain DSC parameters
$\boldsymbol{\Theta}_{wn}$	parameter vector for frequency-domain DSC parameters and noise power
$\boldsymbol{\Theta}_{dn}$	parameter vector for DSC parameters and noise power
N_p	number of elements in $\boldsymbol{\Theta}_{dn}$
$\mathbf{v}(\boldsymbol{\Theta}_w)$	correlation function in frequency domain
β_d	normalized coherence bandwidth of DSC
γ	maximum power of DSC
τ_d	base delay of DSC
ϵ	mixture proportion of DSC
γ	complex gain of specular component
ν	maximum Doppler spread of specular component
τ	delay of specular component
θ	angle of arrival/departure in azimuth direction
θ_R	(azimuth) direction of arrival
θ_T	(azimuth) direction of departure
$\overline{\theta}$	angle of arrival/departure in azimuth direction relative to a reference angle (cluster mean angle)
φ	angle of arrival/departure in elevation direction
φ_R	(elevation) direction of arrival
φ_T	(elevation) direction of departure
$\overline{\varphi}$	angle of arrival/departure in elevation direction relative to a reference angle (cluster mean angle)
$\mathbf{c}(\tau)$	delay vector for a specular component with delay τ
$\mathbf{a}_R(\theta_R, \varphi_R)$	steering vector of the receive antenna array
$\mathbf{a}_T(\theta_T, \varphi_T)$	steering vector of the transmit antenna array
$\mathbf{A}$	steering matrix with steering vectors in its columns

$\mathbf{A}_R$, $\mathbf{A}_T$	steering matrix at the receive and transmit antenna array, respectively
$\widetilde{\mathbf{A}}$	steering matrix from virtual channel representation
$\widetilde{\mathbf{A}}_R$, $\widetilde{\mathbf{A}}_T$	steering matrix from virtual channel representation at the receive and transmit antenna array, respectively
$\mathbf{\Omega}$	matrix representing the coupling between DoAs and DoDs
ω	spatial frequency
σ_ω	standard deviation of spatial frequency
υ	wavelength
$\mathbf{n}_d(f)$	diffuse scattering component (DSC) in frequency domain
$\overline{\mathbf{n}}_d$	stacked version of $\mathbf{n}_d(f)$
$\mathbf{w}$	one observation of the frequency-dependent content of the DSC
$\mathbf{h}$	one observation of the angular content of the DSC
$\mathbf{R}_w$	$E[\mathbf{w}\mathbf{w}^H]$
$\mathbf{R}_h$	$E[\mathbf{h}\mathbf{h}^H]$
$\mathbf{R}_{\text{full}}$	covariance matrix of MIMO channel
$\mathbf{R}_{\text{T}}$, $\mathbf{R}_{\text{R}}$	channel covariance matrices at the transmitter and receiver side, respectively
$\mathbf{R}_n$	noise covariance matrix
$\mathbf{R}_s$	covariance matrix of the transmitted signal vector
$\mathbf{R}_y$	covariance matrix of the received signal vector
$\mathbf{p}_{ys}$	cross-correlation between received signal vector and transmitted signal
$f(\cdot)$	probability density function
$g_m(\theta)$	response of m-th element of the antenna array to a signal at angle θ
α	angle of transmit array
β	angle of receive array
Δ	angular spread at the transmitter side
R	radius of the ring of scatterers around the receiver
μ	symmetry center ("mean angle") of von Mises PDF
κ	scatter parameter in von Mises PDF

Ω	path-loss
D	distance between transmitter and receiver
$d_{p \to q}$	distance between elements p and q
d	element displacement in uniform linear arrays
$\mathbf{r}$	element position vector
R_a	radius of uniform circular array
$\mathbf{w}$	weight vector
$\mathbf{W}$	weight matrix
$\mathbf{P}$	precoding matrix
$\mathbf{V}_y, \mathbf{V}_w, \mathbf{V}_h$	eigenvectors of $\mathbf{R}_y, \mathbf{R}_w, \mathbf{R}_h$, respectively
$\mathbf{\Lambda}_y, \mathbf{\Lambda}_w, \mathbf{\Lambda}_h$	diagonal matrices with the eigenvalues of $\mathbf{R}_y, \mathbf{R}_w, \mathbf{R}_h$, respectively
$\boldsymbol{\lambda}$	vector with the diagonal elements of $\mathbf{\Lambda}$
λ	eigenvalue
$P(\mathbf{w})$	output power after linear processing at the receiver with weight vector $\mathbf{w}$
$P_{\mathrm{BF}}(\theta)$	spatial spectrum of conventional beamformer as a function of θ
$P_{\mathrm{CAP}}(\theta)$	spatial spectrum of Capon's beamformer as a function of θ
$P_{\mathrm{MUSIC}}(\theta)$	MUSIC spatial pseudo-spectrum
$\mathcal{L}(\cdot)$	log-likelihood function
$\mathbf{E}$	pre-whitening matrix
$\mathcal{I}$	Fisher information matrix
$\mathbf{D}_1, \mathbf{D}_2$	matrices containing the partial derivatives with respect to all N_p elements of the parameter vector $\mathbf{\Theta}_{dn}$
σ_θ	standard deviation of the distribution of angles of rays around a mean direction
$\mathbf{v}$	spatial signature

Chapter 1

Introduction

1.1 Motivation of the thesis

Multiple antenna techniques are a key enabling technology in modern and next-generation wireless communications systems, such as 3GPP Long-Term Evolution (LTE) [1] and IEEE 802.16e (WiMAX) [2], as well as fixed wireless communications and last-mile networks [3]. Figure 1.1 illustrates a system with multiple antennas at transmitter and receiver, usually known as multiple-input multiple-output (MIMO) system. Such techniques are considered for the high link capacity gains that are achievable from spatial multiplexing, but also for the system capacity benefits, improved link reliability, and extended range that are possible from spatial diversity, beamforming, spatial division multiple access, and interference cancellation techniques [4, 5, 6, 7]. In general, all these gains cannot be achieved simultaneously, as they are dependent on antenna configuration and scattering environment. Hence, good knowledge of the characteristics of the propagation environment is crucial for maximizing the achievable MIMO gains. In fact, the very demanding performance targets set for next-generation systems are virtually impossible to reach without an efficient utilization of multiple antennas both at transmitter and receiver side.

The decision on which techniques should be employed in each situation in order to obtain higher performance gains depends on many factors, such as the type of data/voice traffic, the number of users in the system, the quality of service parameters, and, very importantly, the characteristics of the propagation environment. It is well known that while beamforming techniques benefit from strong spatial correlation among the antennas, spatial multiplexing techniques obtain higher gains for rich scattering environments [4]. Hence, deep understanding of propagation phenomena and accurate knowledge of the
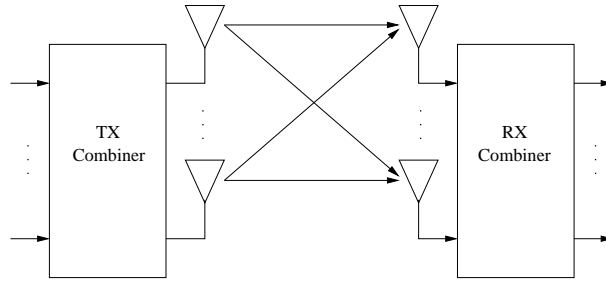
Figure 1.1: Illustration of a typical MIMO system, where the transmitter has M_t antennas and the receiver has M_r antennas.

propagation environment is required in order to meet the ambitious targets of such systems.

Accurate multidimensional spatial channel models play a key role in the characterization of the propagation environment [8]. Although wireless propagation mechanisms have been studied for a long time, modern wireless communications systems are assumed to operate on higher frequencies and with larger bandwidth than previous systems. Moreover, previous single antenna measurements do not allow for characterization of spatial information. Hence, there is a need of new measurement campaigns that utilize transmitters and receivers equipped with multiple antennas. Realistic channel models are based on measurements, and, consequently, there is a need for techniques for estimation of model parameters from data. Typically, MIMO channel measurements are very high dimensional, implying that a huge amount of data is collected. Hence, it is important to condense the relevant information to a few parameters. This is also useful for development of low-complexity channel models for specific scenarios, to be used, e.g., by system designers.

Advanced estimation algorithms have been derived as well, with the goal of extracting high-precision estimates of the parameters that describe the spatial channel, like the SAGE-based method in [9] and RIMAX [10]. Most estimation algorithms are based on the assumption that the channel can be modeled as a combination of rays that travel from the transmitter to the receiver reflecting on objects scattered around the environment, as illustrated in Figure 1.2. Such models are useful for describing a variety of propagation scenarios, but since a large number of rays might be needed to characterize the environment, the estimation algorithms based on such deterministic models become highly complex [9, 10].

One approach to solve this problem and obtain powerful models with few parameters is to utilize a stochastic model instead of a deterministic model [11, 12]. Such a model
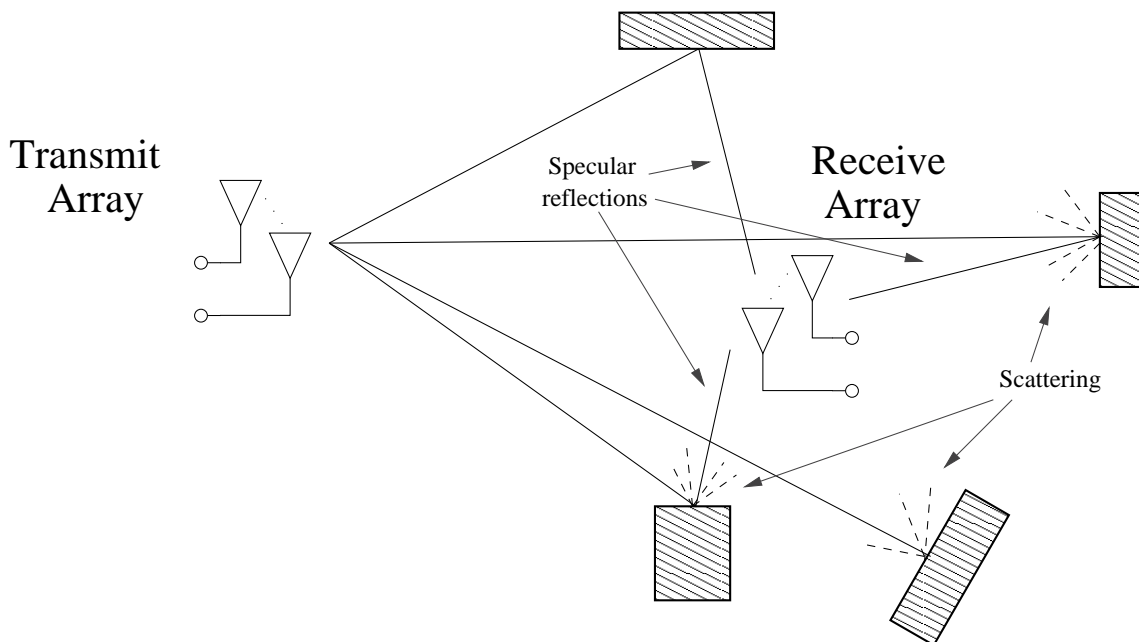
2

Figure 1.2: Illustration of MIMO propagation channel.

is suitable to describe diffuse scattering, which is the part of the received signal that cannot be resolved into distinct specular paths. Even tough diffuse scattering is usually neglected and considered as noise, recent investigations have shown that both specular and diffuse propagation mechanisms contribute significantly to the wave propagation [8, 13]. Moreover, it should be noted that diffuse scattering is a significant part of the rich scattering that gives diversity and multiplexing gains in MIMO systems [14]. In [10] a data model for channel parameter estimation is proposed, which combines these two models. It is shown that an estimator that accounts for both, concentrated propagation paths and distributed scattering, outperforms estimators that ignore either of the channel components. However, in [10] the estimator is derived assuming that the contribution of the distributed scattering is an i.i.d. process in the angular domain at TX and RX. It only accounts for the correlation of the distributed scattering in the time-delay and the frequency domain and ignores the correlation in angular domain. So far no channel parameter estimation results have been published which provide more information about the angular properties of diffuse scattering in radio channels.

Parameter estimation algorithms based on the assumption of slightly-scattered sources can be found in the literature , such as GAM [15] and Spread-F [16] methods, among others [16, 17, 18]. Such algorithms are based on the assumption that scattering around the mean

angle is small, and hence cannot be applied for the estimation of angular characteristics of the diffuse scattering component of the channel.

It should be noted that the problem of MIMO channel sounding is closely related to that of MIMO radars [19, 20], where the goal is to detect and track moving targets. Hence, the algorithms and analysis derived in this thesis are applicable to the context of MIMO radars as well.

1.2 Scope of the thesis

The scope of this thesis is to develop novel estimation techniques for channel sounding applications in MIMO systems. This thesis contributes to physical layer research in wireless multiantenna communications systems, e.g., 3GPP Long-Term Evolution (LTE) [1], IEEE 802.16e (WiMAX) [2], and IMT-Advanced [21] systems. The developed techniques can be applied for development of accurate MIMO channel models, which are fundamental tools in network planning, link- and system-level studies, and transceiver development. In particular, the developed techniques take into account the diffuse scattering, which is commonly neglected in measurement campaigns.

The goal of this thesis is to develop efficient estimation algorithms that gives high-precision estimates with a reduced parameter space. By explicitly modeling the diffuse scattering component, the number of parameters is reduced significantly compared to commonly used techniques. Such simplified models are important tools for transceiver design, for example. In order to keep the overall complexity low, the proposed algorithms must also be computationally efficient. This allows their application in practical measurement campaigns, which can be used, e.g., for standardization of next generation wireless systems and network planning.

1.3 Contributions and structure of the thesis

This dissertation contributes to the field of propagation parameter estimation. Realistic channel models are derived from measurements, and hence optimal or close to optimal estimation of model parameters is necessary. The estimation methods derived in this thesis are particularly useful for propagation environments where a significant portion of energy is received as a result of diffuse scattering. In particular, the derived estimation methods jointly estimate the parameters of the concentrated propagation paths and the distributed

4

scattering component that are frequently observed in Multiple-Input Multiple Output (MIMO) channel sounding measurements. The diffuse scattering component is modeled using a stochastic model, which allows a compact description of the scattering phenomena, resulting in efficient estimation methods. Diffuse scattering component provides significant part of MIMO gains. If the concentrated component is estimated only and diffuse part ignored, the designer may get a biased view of the MIMO system performance.

The joint angular-delay domain model leads to a correlation matrix with high dimensionality, which makes direct implementation of a maximum-likelihood (ML) estimator unfeasible. Novel low complexity methods are derived for computing approximate ML estimates that exploit the structure of the covariance matrices. An iterative two stage procedure is proposed that alternates between the estimation of the parameters of the concentrated propagation paths and the parameters of the distributed scattering. For the distributed scattering, the estimator first optimizes the parameters describing their time-delay structure. Then, using the estimated time-delay parameters, the parameters of the angular distributions are optimized.

A model for the diffuse scattering component in spatial domain is proposed that is based on a mixture of von Mises PDFs, which is a suitable PDF for angular data [22]. The estimation methods are derived taking the mixture model into account, which allows for flexible characterization of a variety of propagation environments, covering from uniform distribution to highly concentrated angular distributions.. The mixture model allows modeling of multimodal and skewed angular data, which correspond to clusters of scatterers often observed in measurement campaigns.

Optimality of the proposed methods is analyzed by establishing the Cramér-Rao lower bound (CRLB), which gives a lower bound for the variance of unbiased estimators. The simulation results show that the variances of the proposed estimation techniques reach the CRLB for relatively small sample size for most parameters, and no bias is observed for any parameter. Estimated time-delay and angular distributions are compared to the actual distributions, demonstrating that high quality estimates are obtained.

This thesis is organized as follows. Chapter 2 presents an overview of multiple antenna systems, describing the many benefits such system can present over single antenna systems. Moreover, it is highlighted how different techniques are more suitable for certain propagation environments. Chapter 3 gives an overview on channel sounding. Several recently developed MIMO channel models are presented. Chapter 4 presents several pa-

rameter estimation techniques, including recent developments for estimation of scattered sources. Spectral-based estimation techniques are presented for comparison. Chapter 5 describes the main contributions of this thesis. The joint angle- and delay-domain estimation method is described, together with performance bounds, and simulation results. Finally, Chapter 6 summarizes the results and the contributions of the thesis.

1.4   Summary of the publications

This thesis consists of an introductory part and seven original publications. The publications are listed at page xi, and appended at the end of the manuscript starting from page 103. The first four publications address the estimation of diffuse scattering parameters, with emphasis on angular-domain parameters. In Publications I and IV, it is also developed a method for estimation of delay-domain parameters assuming a pseudo-noise sequence is used for channel sounding. The CRLB for the angular parameters is derived in Publication II. In Publication IV, the estimation procedure and CRLB are developed for an extended angular model, including parameters from the transmit antenna array as well. In Publication III a model of the diffuse scattering based on a mixture of angular distribution is introduced, and the estimation method is extended to suit the model.

The last three publications address the joint estimation of angular- and delay-domain parameters. In Publications V and VII a computationally efficient estimation procedure for joint estimation of angular- and delay-domain parameters is developed. A procedure for searching new specular paths is derived in Publication VI, and it is applied for the detection of a weak specular path in the presence of diffuse scattering, using the estimation procedure derived in publications V and VII. An initialization procedure for the estimation method, and CRLB for the angular and delay parameters are also derived in Publication VII.

All the simulation software for all the original publications included in this dissertation was written solely by the author, except for the initialization phase of the estimation method in Publications V, VI, and VII, which uses in part the software for the RIMAX estimation method.

In Publications I-VII, the original estimation procedure was the idea of the first author. All derivations and simulations were performed by the first author as well. The co-authors provided guidance in the theoretical modeling, in the design of the experiments, and helped in writing the papers.

Chapter 2

Overview of MIMO Systems

Multiple-input multiple-output (MIMO) systems using multiple transmit and receive antennas are considered as one of the main enabling technologies for future wireless communications systems. Signal streams can be combined by adaptive algorithms at the transmitter and the receiver in order to use the wireless channel efficiently. In this chapter we summarize the main aspects and advantages of MIMO systems, which motivate the MIMO channel modeling and parameter estimation techniques described in the remaining chapters. A review of MIMO systems and their applications can be found, e.g., in [5, 7, 4].

2.1 Introduction

Figure 2.1 illustrates a typical MIMO system, with M_t transmit (TX) antennas, and M_r receive (RX) antennas. The multiple channels connecting the individual channel elements at both sides give extra degrees of freedom for the design of the communications system. If the multiple channels are fading independently, it is possible to design the combiners at both TX and RX such that *diversity gain* is obtained. In this case, the gain comes from the fact that the probability that all channels will fade at the same time is small [5]. By coherently combining the signals, it is possible to obtain also *array gain* (also called *power gain*), since the effective total received power scales with the number of receive antennas [7]. Moreover, multiple channels can be used in order to create parallel data pipes, thus providing *multiplexing gain*.

The benefits and applications that can be obtained from the above mentioned gains include [4]

- *Coverage*: the receiver can form an antenna pattern matched to the MIMO chan-
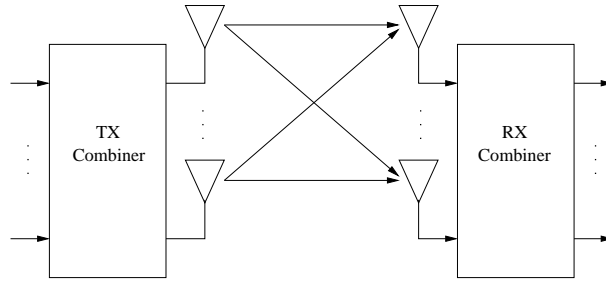
Figure 2.1: Illustration of a typical MIMO system, where the transmitter has M_t antennas and the receiver has M_r antennas.

nel between the transmitter and the receiver, increasing signal-to-noise ratio (SNR) compared to a single-antenna reception. Hence, in a noise-limited cellular system, this increase in SNR extends the coverage area of a base station (BS). If angular information is available, this procedure is equivalent to forming a beam in the direction of the received signal.

- *System capacity*: MIMO systems can increase the signal-to-interference plus noise ratio (SINR), allowing for more users to be active in the system. If channel state information (CSI) of the receivers is known, it is possible for the transmitter to create beams in the direction of each receiver, allowing simultaneous transmission to different terminals on the same time-frequency resources.

- *Increased user throughput*: transmission quality on each link is improved, implying that transmission with higher data rates are possible. Moreover, it is possible to exploit the different subchannels between each transmit and receive antennas in order to create parallel data streams that increase user throughput.

- *Improved spectral-efficiency*: higher spectral efficiency (measured in bits/s/Hz) is obtained as a combination of the increased user throughput and higher system capacity.

- *Location*: information about the direction of arrival (DoA) of the terminals can be used for location-based services, and also to locate users in emergency situations.

There is a trade-off in achieving these gains, and not all gains can be obtained simultaneously. Correlation between signals in each antenna element of the arrays is a key factor for the realization of MIMO gains. For example, DoA estimation algorithms described in

Chapter 4 require high correlation among the antenna elements. However, higher multiplexing gains are obtained when correlation between antenna elements is close to zero, as seen in Section 2.2. Similarly, high correlation between antenna elements is required in order to use beamforming techniques, while highest diversity gains are obtained if the individual channels are fading independently. In the following sections, the main results from MIMO systems are presented from an information theoretic point of view, and the most relevant design strategies are reviewed as well.

2.2 Information-theoretic aspects

Let us assume a narrowband (or frequency flat) system model, where the relative time delays experienced by the impinging signals are small compared to the symbol period. In this case, the model for the system in Figure 2.1 can be written as

$$\mathbf{y} = \mathbf{Hs} + \mathbf{n}, \tag{2.1}$$

where $\mathbf{y}$ is the length-M_r vector with the signals at the output of each antenna element of the receive array, $\mathbf{s}$ is the length-M_t vector with the originally transmitted symbols, $\mathbf{n}$ is the length-M_r vector with measurement noise, and $\mathbf{H}$ is the $M_r \times M_t$ matrix with the channel response. $\mathbf{H}$ is defined as

$$\mathbf{H} = \begin{bmatrix} h_{0,0} & \dots & h_{0,M_t-1} \\ \vdots & & \vdots \\ h_{M_r-1,0} & \dots & h_{M_r-1,M_t-1} \end{bmatrix}, \tag{2.2}$$

where entries $h_{i,j}$ are the transfer functions from the j-th transmit antenna element to the i-th receive antenna element. Different strategies for modeling the elements of $\mathbf{H}$ are discussed in Chapter 3.

For a memory-less single-input single-output (SISO) system with non-fading channel, capacity is given by [4]

$$C = \log_2(1 + \rho|h|^2) \quad \text{b/s/Hz}, \tag{2.3}$$

where ρ is the SNR at any RX antenna. Considering now the case where there multiple antennas at both transmitter and receiver ends, the capacity can be shown to be given by

[4, 5]

$$C = \log_2 \left[\det \left(\mathbf{I}_{M_r} + \frac{\rho}{M_t} \mathbf{H} \mathbf{R}_s \mathbf{H}^H \right) \right] \quad \text{b/s/Hz,} \tag{2.4}$$

where $\mathbf{I}_{M_t}$ is the $M_t \times M_t$ identity matrix and $\mathbf{R}_s$ is the covariance matrix of the transmit data. It is intuitive that capacity in equation (2.4) increases linearly with $\min(M_t, M_r)$, since the number of non-zero eigenvalues of $\mathbf{H} \mathbf{R}_s \mathbf{H}^H$ is upper-bounded by $\min(M_t, M_r)$. If only the receiver or only the transmitter has more antennas this result does not hold, since in this case the capacity can be shown to grow logarithmically with respect to the number of antennas [5].

The MIMO channel can be used to create parallel data pipes, which can be used to improve rate or diversity [4, 5]. Spatial multiplexing techniques usually transmit different signals from each antenna, thus increasing the data rate. Diversity and beamforming techniques, on the other hand, transmit the same signal from all antennas, with the goal of improving the SINR at the receiver. If link adaptation is used, these techniques also increase data rate indirectly, since higher-order modulations and higher-rate codewords can be used.

For the capacity formulas shown above, it is assumed that the channel is deterministic. For flat-fading channels this capacity definition is not applicable, since the channel coefficients are random variables. In this case, two different capacity definitions are commonly used: *ergodic capacity* and *outage capacity*. Ergodic capacity denotes the expected value of capacity, while outage capacity denotes the capacity achieved over a certain amount of channel uses, e.g., 90% or 95% [23, 4].

It is an important issue to determine the impact of correlation between the signals at any (or both) ends of the MIMO system to capacity. For a given SNR, maximum capacity is achieved when the channel matrix is full-rank with equal singular values [4]. Channel correlation increase the singular value spread, thus reducing system capacity, even if the channel matrix is still full-rank. Even though this result is taken as a rule of thumb for MIMO systems, it should be noted that the high capacity gains of i.i.d. channels are observed for relatively high SNR values, and it is possible that correlated channels have higher capacity at low SNR [24].
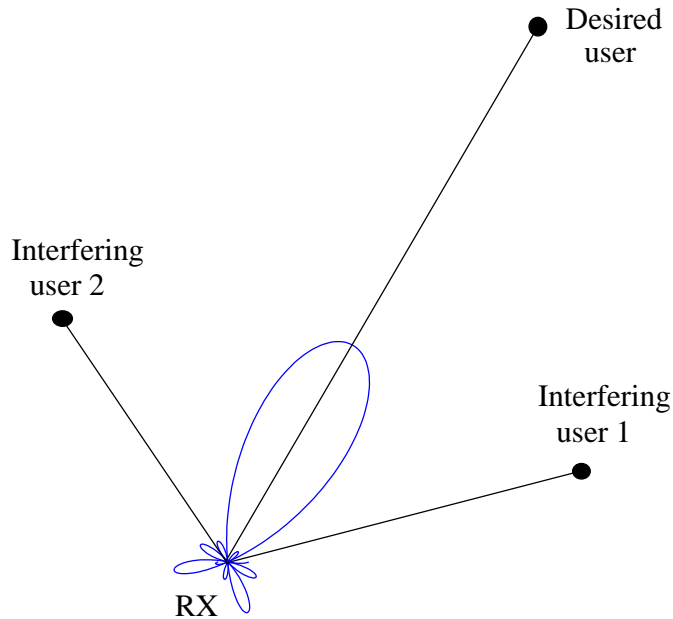
Figure 2.2: Illustration of the beamforming principle.

2.3 MIMO Processing and Beamforming

This section describes techniques that exploit the diversity gain of the MIMO channel, as well as interference rejection obtained by steering the array response in favor of the desired signals. We denote by *beamforming* those techniques that use directional beams aligned to the angles of the multipath components. The term *array processing* will be used to denote techniques that exploit the MIMO channel without explicit knowledge of angular information.

2.3.1 Beamforming

The concept of beamforming is to concentrate transmission or reception on relevant directions that maximize the signal at the receiver, or rather to receive energy from preferred directions only. The basic principle behind this idea is that most of the energy that reaches the receiver propagates in limited directions, e.g., in a line-of-sight (LoS) situation, as illustrated in Figure 2.2 [25, 26, 27, 28, 29, 4]. The main goal of beamforming techniques is to provide SINR gain, usually denoted as *beamforming gain* or *array gain*.

Beamforming requires partial channel state information in order to be applied. In case of transmit beamforming, usually this information can be obtained by means of feedback from the receiver. In time-division duplex (TDD) systems utilizing beamforming at the

base station, CSI can also be estimated from previous transmission from the terminal, assuming the channel is reciprocal.

Beamforming benefits from highly-correlated signals at the antennas, thus favoring system setups with closely-spaced antenna elements and locations with low angular spread. In principle, beamforming can also be applied for uncorrelated signals, but in this case the main directions are dependent on current channel realization and fast adaptation is required in order to achieve the beamforming gain. A review of beamforming techniques can be found in [29, 30].

2.3.2   Receive Diversity

If the receiver is equipped with multiple antennas, the signals arriving at each antenna element can be combined in order to obtain array or diversity gain. The combiner can be designed for minimization of some metric based on the instantaneous channel realization, without explicitly taking angular information into account, e.g., using maximum-ratio combining (MRC) or zero-forcing (ZF) criteria [31, 8]. Another important design method is the minimum mean squared error (MMSE) receiver [32], which is based on the (estimated) covariance matrix of the received signal, thus taking the statistics of noise component into account.

Receive diversity techniques are often derived for the uplink direction, given that it is more common that the base station will employ multiple antennas. However, in advanced wireless systems like 3GPP LTE and WiMAX, most mobile terminals are assumed to be equipped with at least two antennas, making it possible to apply the receive diversity techniques in the downlink direction as well.

2.3.3   Transmit Diversity

Transmit diversity schemes frequently involve the design of multiple correlated signals without CSI information at the transmitter side. This can be achieved by jointly encoding the individual streams at each transmit antenna, which in turn reduce the data rate and increase the correlation between the signals, introducing robustness against channel fading and noise. Such schemes are commonly denoted by *space-time coding* (STC) [33, 5].

Initial developments of STC are in the form of space-time trellis codes (STTC), which require a multidimensional algorithm at the receiver for decoding. However, the true popularity of STC came with the development of space-time block codes (STBC), which
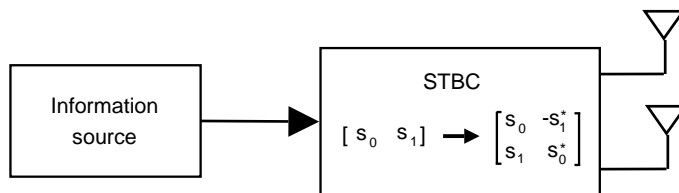
Figure 2.3: Transmit diversity with STBC (Alamouti). The symbol transmitted by antennas 0 and 1 are denoted by s_0 and s_1, respectively.

require only linear processing at the receiver. It has been shown that STBC can achieve the same spatial diversity order as STTC, but the former cannot obtain the coding gain that is possible with STTC [5]. Nevertheless, most of the research on STC is currently done on STBC, since its simple design rules and receiver processing allows for implementation in practical wireless communications systems. In fact, STBC can be found in standards of modern wireless communications systems, as in 3GPP HSDPA and LTE [1].

A very popular STBC for a two transmit antennas setup was developed by Alamouti [31], which is illustrated in Figure 2.3. In this scheme orthogonal signals are transmitted from each antenna, which greatly simplifies receiver design. Even tough originally developed for systems with two transmit antennas and one receive antenna, the Alamouti scheme can be extended for M_r receive antennas, obtaining a diversity order of $2M_r$ [31, 5]. The resulting scheme can be seen as a combination of the 2×1 Alamouti scheme with maximum ratio combining, and hence the diversity order is the same as that of a $2 \times M_r$ MRC scheme [31, 5].

While Alamouti scheme is widely used due to its simple construction and design, a better detection performance can be obtained if the STBC is concatenated with outer channel coding (e.g. convolutional), in which case, however, transmission rate is lower than one. The interested reader can find general STBC design techniques and analysis in [5, 33, 6].

2.4 Spatial Multiplexing

The previous section was concerned about the utilization of the multiple antennas at transmitter or receiver side (or both) with the goal of increasing diversity and consequently obtaining higher SINR at the receiver. If such schemes are combined with link adaptation mechanisms, higher throughput can be obtained indirectly, since data can be transmitted

with higher coding rates and higher-order modulations. In this section we will present techniques whose primary goal is to increase throughput directly, by utilizing the MIMO channel to create data pipes through which different data streams can be transmitted. The transmitter and receiver can be designed such that interference from one data stream to the other is small or non-existent.

Joint encoding of the streams combined with maximum likelihood detection at the receiver can provide a near-capacity performance [4]. However, the complexity of such scheme is prohibitive for a large number of antennas. The so-called layered structures have been proposed to overcome this problem by decomposing the receiving procedure in several steps with small complexity. These techniques are usually called *BLAST* (Bell Labs layered space time) [34, 35].

If full CSI is available at the transmitter and receiver, then it is possible to create orthogonal data pipes, thus simplifying the decoding process at the receiver. The orthogonal data pipes can be created, e.g., by designing the transmitter to be orthogonal to the matrix with the right singular vectors of $\mathbf{H}$. In this case the receiver can be designed as a matrix orthogonal to the left singular vectors of $\mathbf{H}$ (see Section 2.4.3). Even though this information is not necessarily available, modern wireless communications standards such as 3GPP LTE define feed back channels that contain partial CSI and CQI information. The partial CSI is defined such that the transmitter can create approximately orthogonal data pipes. This technique is called here *eigenbeamforming* [8].

Incremental gain from additional receive antennas may diminish if the number of receive antennas is much larger than the number of transmit antennas, since the extra antennas cannot be used to create parallel data streams, but only provide diversity gain. If the receiver is combined with an antenna selection mechanism that selects a subset of the "best" antennas, it is possible to achieve full multiplexing gain with a reduced complexity, since only a limited number of RF receiving chains are needed [36, 37, 8].

In this section we briefly describe the Horizontal BLAST, Diagonal BLAST, and Eigenbeamforming schemes. The interested reader can find more details in [4, 8].

2.4.1 Horizontal BLAST

In Horizontal BLAST (H-BLAST)[1], the data streams that are to be input to different antennas are encoded independently, as shown in Figure 2.4. The receiver separates the

---

[1]Initially, Horizontal BLAST was called Vertical BLAST, but this definition was changed in [35].
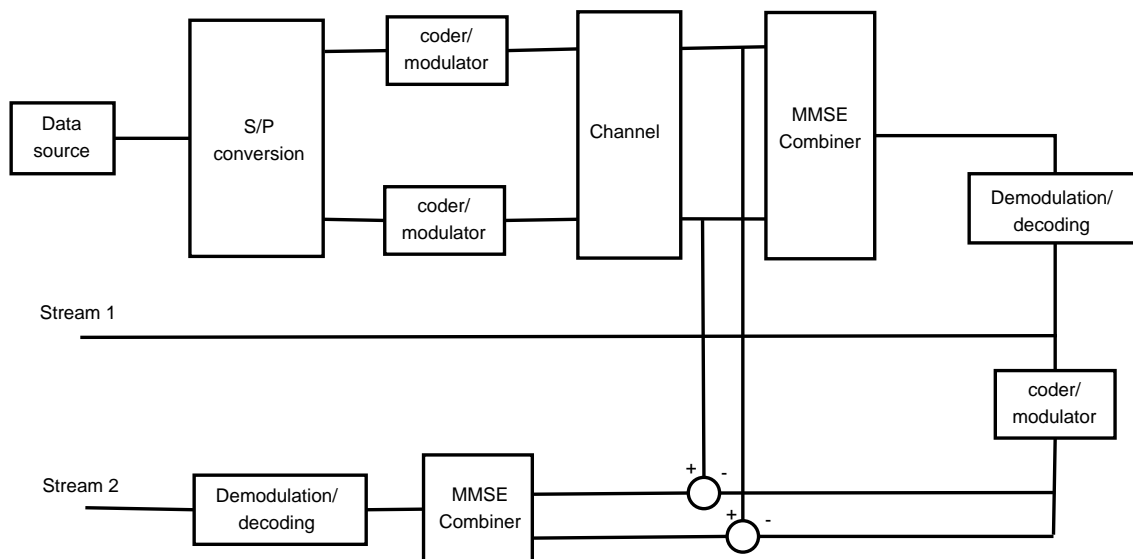
Figure 2.4: Block diagram of the H-BLAST transceiver.

streams by successively applying an MMSE receiver and interference cancellation [4]. H-BLAST scheme is simple, in particular from the transmitter point of view. It suffers, however, from error propagation, since if one stream is not decoded correctly, then the interference is not properly subtracted from the received signal, reducing the probability that the next stream will be decoded correctly. Moreover, H-BLAST does not achieve full diversity [4].

2.4.2 Diagonal BLAST

The Diagonal BLAST (D-BLAST) scheme cycles the data streams through all possible transmit antennas. Each data stream is divided in sub-blocks, which are transmitted from one antenna at a time. This is illustrated in Figure 2.5. The receiver is similar to the one in H-BLAST, where each decoded block is subtracted from the received signal. The difference here is that the decoding order for each data stream is alternating for every sub-block, so that all data streams experience all diversity orders. This scheme can be shown to provide higher capacity than H-BLAST scheme, due to the increased diversity of all streams [4].

2.4.3 Eigenbeamforming

If both transmitter and receiver are equipped with multiple antennas, and assuming the channel is known in both sides, beamforming can also be applied to generate an orthogonal

$$S_{\text{H-BLAST}} = \begin{bmatrix} \boxed{s_0 \quad s_4 \quad s_8 \quad s_{12}} \\ \boxed{s_1 \quad s_5 \quad s_9 \quad s_{13}} \\ \boxed{s_2 \quad s_6 \quad s_{10} \quad s_{14}} \\ \boxed{s_3 \quad s_7 \quad s_{11} \quad s_{15}} \end{bmatrix} \qquad S_{\text{D-BLAST}} = \begin{bmatrix} s_0 \quad s_4 \quad s_8 \quad s_{12} \\ s_1 \quad s_5 \quad s_9 \quad s_{13} \\ s_2 \quad s_6 \quad s_{10} \quad s_{14} \\ s_3 \quad s_7 \quad s_{11} \quad s_{15} \end{bmatrix}$$
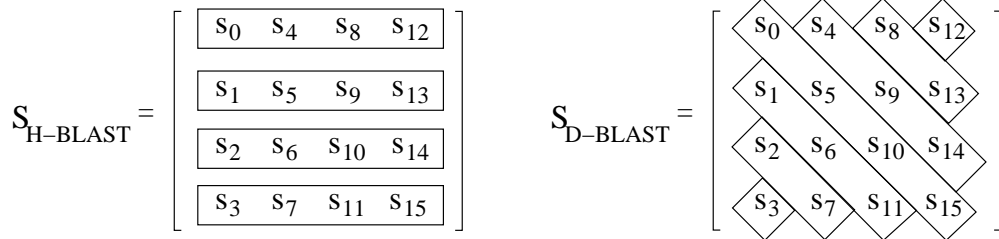
Figure 2.5: Schematic representation of the mapping of data streams to transmit antennas in D-BLAST.

set of spatial filters. By properly designing the transmitter, it is possible to direct the signals into orthogonal eigenmodes of the channel, which can be extract by the receiver without interference. The gain at each orthogonal eigenmode is given by the singular values of the channel matrix $\mathbf{H}$ [8].

The singular value decomposition of $\mathbf{H}$ is given by

$$\mathbf{H} = \mathbf{U}\boldsymbol{\Sigma}\mathbf{V}^H, \tag{2.5}$$

where the columns of the $M_r \times M_r$ matrix $\mathbf{U}$ and the $M_t \times M_t$ matrix $\mathbf{V}$ contain the left and right singular vectors of $\mathbf{H}$, respectively, and the diagonal elements of $\boldsymbol{\Sigma}$ are the singular values. With the channel known at the transmitter and receiver, it is possible to design the linear combiners at transmitter and receiver in order to create a virtual MIMO channel where the different streams are orthogonal to each other. The estimated symbols at the receiver are given by

$$\widehat{\mathbf{s}} = \mathbf{W}^H \mathbf{H} \mathbf{P} \mathbf{s} + \mathbf{W}^H \mathbf{n}, \tag{2.6}$$

where $\mathbf{P}$ is the linear combiner at the transmitter.

From equations (2.5) and (2.6), the parallel data streams are created if the linear combiners are selected as $\mathbf{P} = \mathbf{V}$ and $\mathbf{W} = \mathbf{U}$. With this choice of $\mathbf{P}$ and $\mathbf{W}$, the estimated symbol vector at the receiver is given by

$$\mathbf{y} = \boldsymbol{\Sigma}\mathbf{s} + \mathbf{U}^H \mathbf{n}. \tag{2.7}$$

From equation (2.7) it is clear that the linear combiner at the transmitter directs the signals into orthogonal eigenmodes of the channel, which can be extract by the receiver without interference. The gain at each orthogonal eigenmode is given by the singular
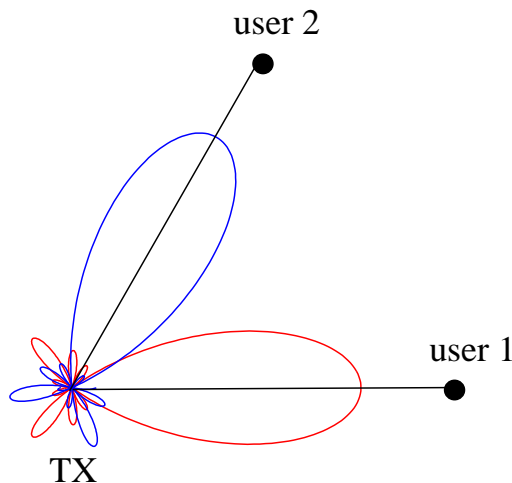
Figure 2.6: Illustration of a spatial division multiple access system.

values of $\mathbf{H}$.

If the data streams belong to different users, this scheme can be used for spatial division multiple access (SDMA), where several users share the same physical resources, and separated only by the different spatial channels. While such scheme can be implemented both in spatially uncorrelated and spatially correlated scenarios, performance is supposed to be better in correlated scenarios. This is due to the fact that in correlated scenarios the eigenbeams correspond to propagation directions, which change relatively slowly over time (and frequency), depending on movement of the mobile terminal and of the scattering environment. This principle is illustrated in Figure 2.6, where the transmitter directs one beam toward each user, simultaneously minimizing the interference from one user to the other. On the other hand, in uncorrelated scenarios the eigenbeams vary much more often for every channel realization, and hence it is more difficult to keep both transmitter and receiver directed at the same eigenbeams.

Even though full-CSI at the transmitter is not practical, wireless standards like 3GPP LTE define feed back channels that can transmit partial CSI and CQI. The partial CSI usually contains an indication of the (quantized) right singular vectors that should be used for transmission. The CQI information can be used to perform link adaptation for each stream. Such a scheme approximates the eigenbeamforming method described in this section, and the quality of the approximation depends basically on the vector quantization of the singular vectors and the delays associated with the feed back channel.

Chapter 3

MIMO Channel models

Accurate multidimensional spatial channel models play a key role in the characterization of the propagation environment. Different models have been developed for MIMO channels in the literature with the goal of characterizing the wireless propagation mechanisms when multiple antennas are used in the transmitter and the receiver. As a rule of thumb, the more aspects and detail the model tries to capture, the more complex it gets. Complexity might become so high that the model is not suitable for practical use. Hence, the trade-off between model accuracy and complexity has to be taken into account when developing a model.

Models can be designed to capture specific characteristics of the MIMO channel, for example beamforming, multiplexing, or diversity gains. The level of application of the model is also important, since system-level models have different requirements than link-level models. Regardless of the application, good models must be supported by actual channel measurements and validated by objective metrics. Different metrics emphasize the various aspects of the MIMO channel [8]. The number of parameters required by the model is also relevant, since a large parameter set often leads to complex estimators and relatively high variance of the estimates.

In this chapter several channel models presented in literature are described. Section 3.1 describes the basic principles of propagation modeling based on electromagnetic theory and introduces the concept of propagation scenarios. Ray tracing methods and the introduction of a stochastic component to represent the diffuse scattering are discussed as well.

Section 3.2 describes a basic MIMO channel model as the superposition of specular (concentrated) and diffuse scattering components. This model serves as a basis for most

of the models described in Section 3.4. An extensive review of MIMO channel models can be found in [38, 8, 39]. Antenna array configurations are discussed in Section 3.3.

Finally, Section 3.7 gives an overview on the MIMO channel model derived during COST273 action [8], which encompasses both link- and system-level aspects of MIMO systems, and have been throughly investigated based on actual channel measurements.

3.1 Propagation modeling

Electromagnetic theory describes how electromagnetic waves propagate in different media and interact with objects. Hence, it is essential in propagation modeling. In case of wireless communications systems, three types of objects are especially relevant: terrain, buildings, and moving objects. Scenarios can be defined taking into account the presence or absence of these objects, and depending on the relative position and motion of the objects with respect to the transmitter and receiver. For example, outdoor scenarios usually consider that the transmitter is situated well above a roof top and not surrounded by local scatterers. On the other hand, indoor scenarios assume the transmitter and receiver are on same height, and both can be surrounded by nearby objects. Figure 3.1 shows an example of propagation environment where the receiver is surrounded by local scatterers, and a few remote scatterers are present. The characterization of these scenarios depend also on other factors, such as interference, spatial correlation, correlation of multiuser MIMO channels, etc. A detailed description of MIMO scenarios can be found in [8]. In this section we introduce a few methods and models utilized in propagation studies, in special for next generation MIMO systems.

Deterministic propagation modeling aims at studying and reproducing the propagation of electromagnetic waves and their interactions with the environment [40, 41]. This type of technique is specially suited for environments dominated by man-made objects, such as buildings, hallways, rooms, due to their simpler geometrical description. The information about the objects can be stored in databases and used for the reconstruction of the propagating fields by analytical formulas and/or computer programs.

Statistical models, on the other hand, employ probability distributions with a few parameters, such as moments, and characterize the output of the propagation mechanisms. Due to the inherent many-to-one mapping, statistical models do not allow for investigation of the exact propagation mechanisms and object interactions that generate a certain
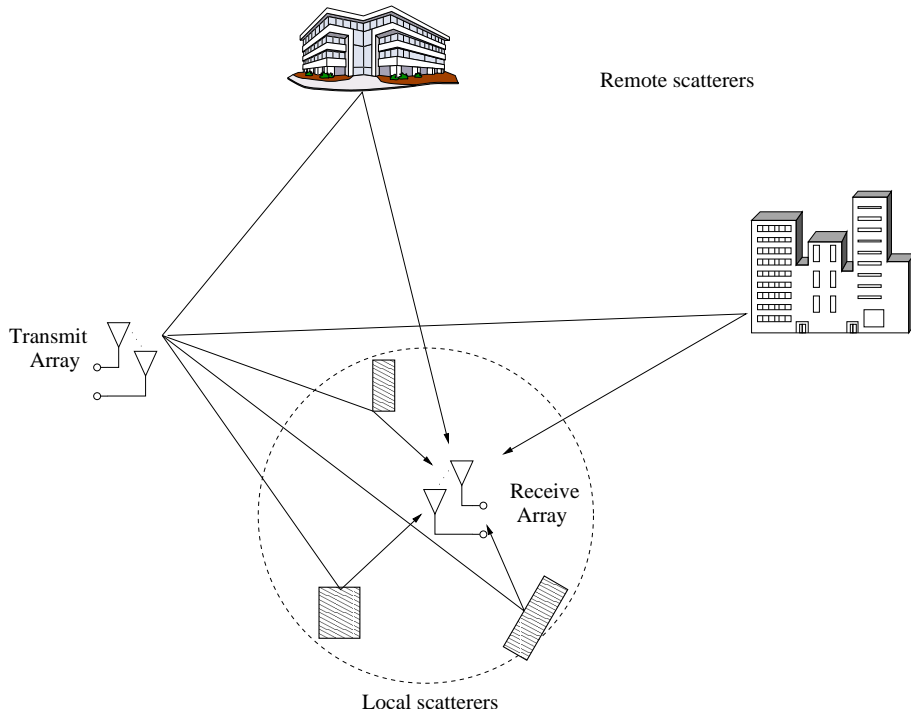
Figure 3.1: Example of propagation environment where the receiver is surrounded by local scatterers, and a few remote scatterers are present.

output. However, such models are in general simpler and faster than deterministic models. Combinations of deterministic and statistical models are also employed in order to reduce complexity and decrease computation time [42].

Electromagnetic models that (approximately) solve Maxwell's equations are used for deterministic field prediction. Several models have been proposed to simplify computation while retaining good modeling accuracy, such as finite element method, finite difference time domain (FDTD), and method of moments (MoM) [8]. If the wavelength is small compared to the interacting objects, then the ray approximation from geometrical optics can be employed. With the ray approximation, the electromagnetic field is described as a collection of rays or beams. Beams have a finite (non-zero) transverse dimension while rays have zero transverse dimension. Due to their inherent lower resolution, beam-based methods are more suitable for coverage prediction over large areas, while ray-based methods are used to describe the propagation environment with higher level of detail. Ray-based models have high complexity which is directly related to the database size and accuracy of the underlying electromagnetic models. Such models are very specific and applicable to the defined propagation environment.

Conventional ray models only accounts for waves that are reflected by flat surfaces (specular or concentrated reflections) or diffracted in rectangular edges. Diffuse scattering, meaning signals that are scattered in directions other than the specular direction due to imperfections on object surfaces, are neglected in the models. Scattering also appears in urban environments due to objects near to wall surfaces, such as street signs, trees, etc. It has been observed in measurement campaigns such as [43, 44, 45, 8] that diffuse scattering can be significant, and even dominant, especially in non line-of-sight (NLoS) situations. Hence, inclusion of diffuse scattering in traditional ray-based models is needed to improve multidimensional and wideband prediction performance. Recent developments in this field include the approach in [40], which is similar to Kirchoff formulations and models a stochastic component resulting in instantaneous realizations of the scattering processes. In [41], the diffuse scattering is added in a mean, statistical way, according to the effect roughness model, which assumes the scattering to be originated from surface roughness. A detailed survey of recent propagation models can be found in [8].

3.2 MIMO Channel Modeling

Based on the discussion in Section 3.1, we describe the basic MIMO channel model as the superposition of specular and diffuse scattering components. The specular components account for the concentrated portion of the signal that can be modeled as the result of specular reflections, while the diffuse scattering component (DSC) accounts for part of the signal that is the result of scattering. Typically, a deterministic model is used for the specular component, while the DSC is better described by a stochastic model.

3.2.1 Specular Component

The following assumptions will be considered:

1. Waves impinging at the receiver array are planar (far-field assumption).

2. Narrowband assumption: relative bandwidth with respect to center frequency is small such that the time delay between the antenna elements are represented as phase shifts.

3. Array aperture is small enough such that there is no significant magnitude variation between the signal received by each antenna element.

4. Parameters for each wavefront are time invariant.

5. Signal bandwidth is smaller than antenna bandwidth at the carrier frequency.

Given the assumptions above, the response of a SISO link between the transmitter and receiver in frequency domain is given by [10]

$$H(f,t) = \gamma_k \, B_T(f) B_R(f) e^{-j2\pi f \tau_k} e^{-j2\pi \nu_k t}, \tag{3.1}$$

where γ_k is the complex gain for the k-th specular reflection, $B_T(f)$ and $B_R(f)$ are the system responses of the transmitter and receiver, respectively, ν_k is the Doppler spread, and τ_k is the delay. Since the channel is linear the superposition principle applies. Hence, we can write for K specular reflections

$$H(f,t) = B_T(f) B_R(f) \sum_{k=0}^{K-1} \gamma_k \, e^{-j2\pi f \tau_k} e^{-j2\pi \nu_k t}. \tag{3.2}$$

In order to describe the response of the whole MIMO system, we define the steering vector of the receive antenna array as the $M_r \times 1$ complex vector $\mathbf{a}_R(\theta_R, \varphi_R)$, where θ_R and φ_R are the azimuth and elevation angles, respectively. Similarly, we define the steering vector of the transmit antenna array as the $M_t \times 1$ complex vector $\mathbf{a}_T(\theta_T, \varphi_T)$. The definition of the elements of the steering vectors $\mathbf{a}_R(\theta_R, \varphi_R)$ and $\mathbf{a}_T(\theta_T, \varphi_T)$ depend on the array geometry (c.f. Section 3.3 and [10]). With these definitions, the MIMO radio channel response for the specular components can be written as

$$\mathbf{H}(f,t) = B_T(f) B_R(f) \sum_{k=0}^{K-1} \gamma_k \, \mathbf{a}_R(\theta_{R,k}, \varphi_{R,k}) \, \mathbf{a}_T^T(\theta_{T,k}, \varphi_{T,k}) \, e^{-j2\pi f \tau_k} \, e^{-j2\pi \nu_k t}. \tag{3.3}$$

3.2.2   Diffuse Scattering

Most of the MIMO gains achieved by techniques described in Chapter 2 require propagation environments with rich scattering. In such environments, diffuse scattering mechanisms are likely to be relevant. In [10] the author presents a MIMO model that combines multipath components resulting from specular reflections and diffuse scattering. Based on physical arguments, it is assumed that the diffuse scattering can be modeled as a stochastic process with zero-mean complex circular Gaussian distribution. Since very limited information is available in the literature about the spatial properties of the diffuse scattering, the phases are assumed to be distributed uniformly in the interval $(-\pi, \pi)$ [8].

22

Due to the assumption of Gaussian distribution, the diffuse scattering may be completely characterized by its mean and covariance matrix.

In channel measurements, the correlation of components of the diffuse scattering at different delays is frequently observed as an exponential decay over time and a base delay which is related to the distance between the transmitter and receiver. Hence, we can model correlation for different delays as

$$
\psi(\tau) = \begin{cases} 0, & \tau < \tau'_d \\ \gamma/2, & \tau = \tau'_d \\ \gamma e^{-B_d(\tau - \tau'_d)}, & \tau > \tau'_d \end{cases}, \tag{3.4}
$$

where B_d is the coherence bandwidth, γ denotes the maximum power, and τ'_d is the base delay. Note that equation (3.4) assumes infinite bandwidth.

The Fourier transform of (3.4), the correlation function of the channel in the frequency domain, is given by

$$
\psi(\Delta f) = \frac{\gamma}{\beta_d + j2\pi\Delta f} e^{-j2\pi\Delta f \tau'_d}, \tag{3.5}
$$

where $\beta_d = B_d/B_m$ is the normalized coherence bandwidth, and B_m is the measurement bandwidth. Let us define the sampled version of the correlation function $\mathbf{v}(\mathbf{\Theta}_w)$, $\mathbf{\Theta}_w = \{\gamma, \beta_d, \tau_d\}$, in frequency-domain as

$$
\mathbf{v}(\mathbf{\Theta}_w) = \frac{\gamma}{M_f} \left[\frac{1}{\beta_d} \quad \frac{e^{-j2\pi\tau_d}}{\beta_d + j\frac{2\pi}{M_f}} \quad \cdots \quad \frac{e^{-j2\pi(M_f-1)\tau_d}}{\beta_d + j2\pi\frac{M_f-1}{M_f}} \right], \tag{3.6}
$$

where τ_d is the normalized base delay.

The covariance matrix of the diffuse scattering (assuming the received signal is spatially-white) may be modeled as a Toeplitz matrix

$$
\mathbf{R}_w = \mathrm{toep}\big(\mathbf{v}(\mathbf{\Theta}_w), \mathbf{v}(\mathbf{\Theta}_w)^H\big), \tag{3.7}
$$

where $\mathrm{toep}(\mathbf{a}, \mathbf{b}^H)$ denotes a Toeplitz matrix with $\mathbf{a}$ as its first column and $\mathbf{b}^H$ as its first row, with $a_1 = b_1^*$.

The specular components are considered as deterministic waves with unknown parameters, and thus incorporated to the model as local mean values of the distribution of the scattered energy. High-resolution parameter estimation like ESPRIT [46], SAGE [9], and

RIMAX [10] (c.f. Chapter 4) can be used for joint estimation of the diffuse scattering and specular components.

3.3 Antenna Arrays

The configuration of the antenna arrays at the transmitter and/or receiver side influence the performance of different MIMO techniques. Moreover, several methods for MIMO channel estimation have been developed that rely on properties of the array structure, e.g., Root-MUSIC and ESPRIT.

Figure 3.2 shows the representation of one element of an antenna array in a 2-D coordinate system, where the position of the m-th element is represented by the vector $\mathbf{r}_m = [x_m \ y_m]^T$. Assuming far-field conditions, and that the array aperture is much less than the inverse relative bandwidth (narrowband assumption), the output in baseband as a function of the angle in azimuth direction can be modeled as [47]

$$u_m(t) = g_m(\theta)e^{-j\frac{2\pi}{\upsilon}(x_m\cos\theta + y_m\sin\theta)}s(t),\tag{3.8}$$

where $g_m(\theta)$ is the response of m-th element, assumed to be constant over the signal bandwidth, and υ is the signal wavelength. Let us define the array output vector as $\mathbf{u}(t) = [u_0(t) \ \cdots \ u_{M-1}(t)]^T$, where M is the number of antenna elements in the array. Hence, for an M element array with arbitrary geometry, we can write the array response as

$$\mathbf{u}(t) = \mathbf{a}(\theta)s(t),\tag{3.9}$$

where the $M \times 1$ steering vector $\mathbf{a}(\theta)$ is given by

$$\mathbf{a}(\theta) = \begin{bmatrix} g_0(\theta)e^{-j\frac{2\pi}{\upsilon}(x_0\cos\theta + y_0\sin\theta)} \\ \vdots \\ g_{M-1}(\theta)e^{-j\frac{2\pi}{\upsilon}(x_{M-1}\cos\theta + y_{M-1}\sin\theta)} \end{bmatrix}.\tag{3.10}$$

Figure 3.3 shows some commonly used antenna arrays.

Antenna arrays consisting of cross-polarized antenna elements have been considered lately in the literature. The benefits of such array constructions include robustness of the rank of the channel matrix due to polarization diversity, which in turn improves performance of spatial multiplexing techniques [48, 49].
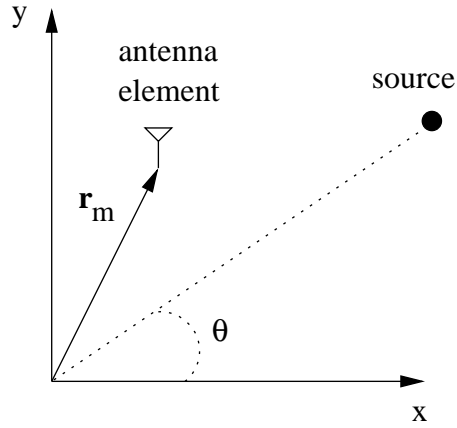
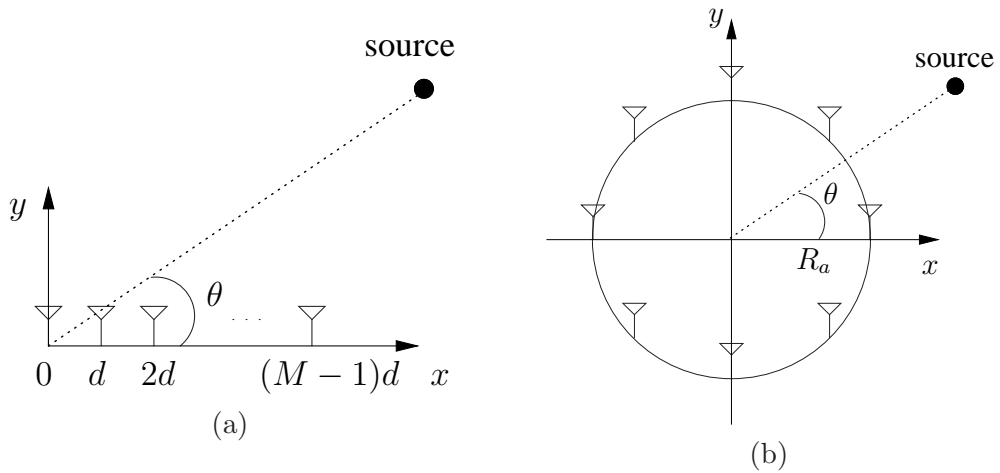Figure 3.2: Representation of 2-D array geometry.

Figure 3.3: Common array structures: (a) uniform linear array, (b) uniform circular array.

Assuming the system to be linear, the superposition principle can be applied in case there are K impinging waves, i.e., the system output in case of K impinging waves can be written as

$$\mathbf{y}(t) = \sum_{k=0}^{K-1} \mathbf{a}(\theta_k) s_k(t). \tag{3.11}$$

A review of other antenna array configurations and antenna calibration techniques can be found in [10, 8].

3.4 Spatial models

The double-directional channel models presented in this section describe the MIMO channel matrix directly, which combines the spatial channel and array geometry. Following the
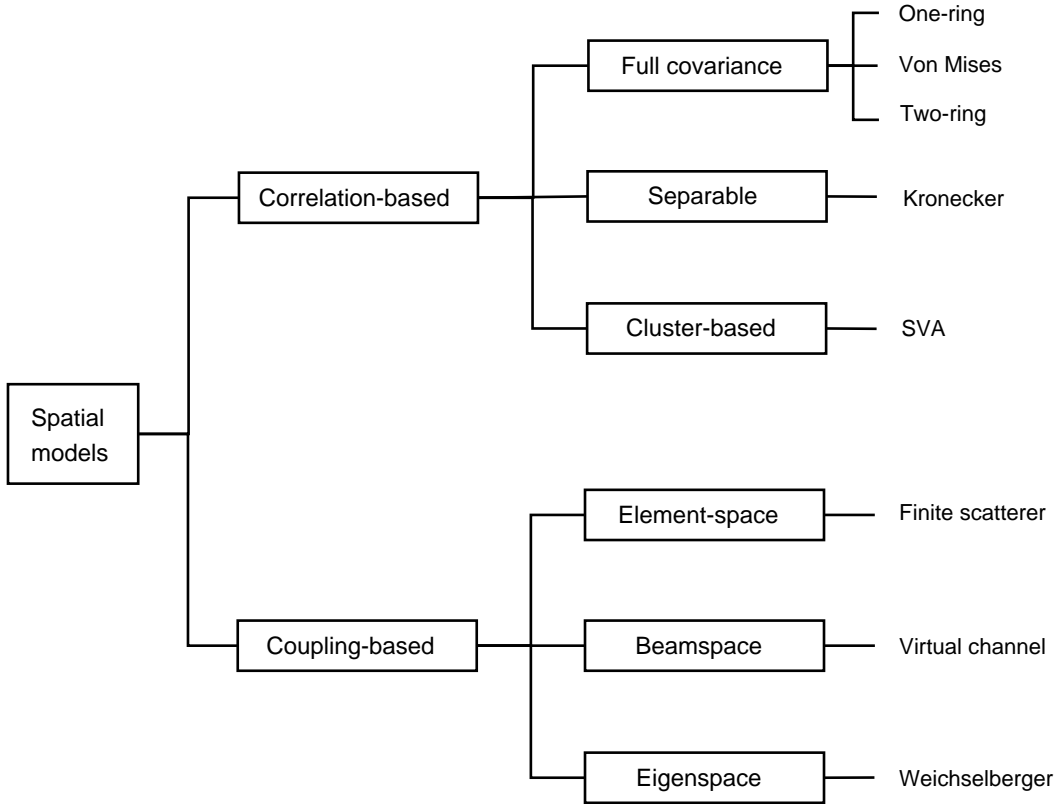
Figure 3.4: Categorization of models described in Section 3.

approach in [8], the MIMO channel models will be categorized in correlation-based models and coupling-based models.

The basic assumption behind correlation-based models is that the channel obeys a circularly symmetric Gaussian distribution, and hence it is fully described by its first- and second-order statistics. Coupling-based models represent the coupling of DoA and DoD directly, most of them assuming a limited number of specular paths connect the transmitter and the receiver.

Further categorization is possible, and one possible example is shown in Figure 3.4. The different categories in Figure 3.4 will be described in this Section together with the description of each model. The categorization is not unique, and different variations of the channel models would allow different classification of the models. For example, the SVA model is separable if only one cluster is present. Detailed review of spatial channel models can be found in [38, 8].

3.4.1 Correlation-based models

The covariance matrix of the MIMO channel may be written as

$$\mathbf{R}_{\text{full}} = E[\text{vec}(\mathbf{H})\text{vec}(\mathbf{H})^H], \qquad (3.12)$$

where the $\text{vec}(\cdot)$ operator stacks the columns of the argument into a larger vector. Equivalently, channel realizations following a zero-mean, circularly symmetric complex Gaussian process with the correlation matrix given in equation (3.12) can be obtained as

$$\text{vec}(\mathbf{H}) = \mathbf{R}_{\text{full}}^{1/2}\,\mathbf{H}_w, \qquad (3.13)$$

where $\mathbf{H}_w$ is a $M_r \times M_t$ matrix whose elements are i.i.d. following a zero-mean, circularly symmetric complex Gaussian distribution with unit variance.

Direct characterization of $\mathbf{R}_{\text{full}}$ is a very complex task. In this section we describe different approaches in the literature that decompose this problem into smaller ones, thus simplifying this task.

3.4.1.1 Kronecker model

Assuming that fading at each antenna element is independent, it has been proposed in [50, 51, 52] to decompose the channel covariance matrix as

$$\mathbf{R}_{\text{full}} = \frac{1}{\text{tr}(\mathbf{R}_R)}\mathbf{R}_T \otimes \mathbf{R}_R, \qquad (3.14)$$

where $\otimes$ denotes the Kronecker product, $\text{tr}(\cdot)$ denotes the trace, $\mathbf{R}_T$ and $\mathbf{R}_R$ are the covariance matrices at the transmitter and receiver side, respectively, defined as [8]

$$\mathbf{R}_T = E[(\mathbf{H}^H\mathbf{H})^T] \qquad (3.15)$$

$$\mathbf{R}_R = E[\mathbf{H}\mathbf{H}^H]. \qquad (3.16)$$

From equations (3.14) and (3.13), the channel matrix for the Kronecker model can be written as

$$\mathbf{H} = \frac{1}{\sqrt{\text{tr}(\mathbf{R}_R)}}\mathbf{R}_R^{1/2}\,\mathbf{H}_w(\mathbf{R}_T^{1/2})^T. \qquad (3.17)$$

This model has been widely used, e.g., in EU IST SATURN (Smart Antenna Technology
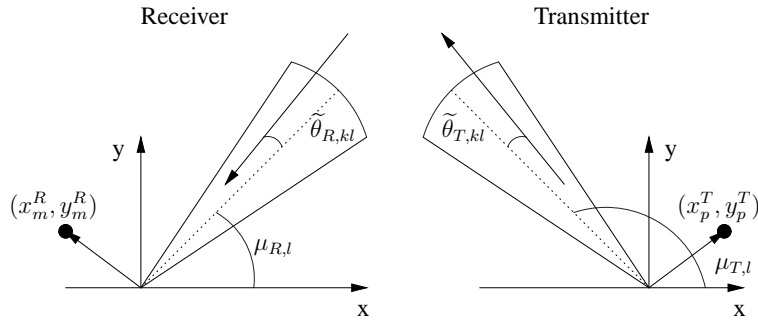
Figure 3.5: Parameters for a single cluster in the SVA model.

in Universal bRoadband wireless Networks) project [53], since it allows for simplified analytical treatment and simulations. However, it should be noted that such a model assumes statistical independence of DoD and DoA, and hence cannot be applied if the joint angular power spectrum is not separable.

3.4.1.2 SVA model

In [54, 11], the authors propose an extension of the Saleh-Valenzuela SISO channel model [55] to incorporate DoD and DoA statistics. The extended Saleh-Valenzuela model will be denoted as the *SVA model* in the remainder of this document.

Based on channel measurements, it has been observed that the multipath components arrive in clusters in both space and time. The SVA model characterizes the channel by a weighted sum of clusters, each cluster characterized by the amplitude, arrival time, and DoA/DoD of its multipath components. Figure 3.5 shows the parameters for a single cluster in the SVA model.

Assuming there are L clusters and K multipath components, the directional channel impulse response between one transmit antenna element and one receive antenna element is given by

$$h(\theta_R, \theta_T) = \frac{1}{\sqrt{LK}} \sum_{l=0}^{L-1} \sum_{k=0}^{K-1} \gamma_{kl}\, \delta(\theta_T - \mu_{T,l} - \widetilde{\theta}_{T,kl})\, \delta(\theta_R - \mu_{R,l} - \widetilde{\theta}_{R,kl}), \qquad (3.18)$$

where θ_T and θ_R are the transmit and receive angles, γ_{kl} is the complex gain of the k-th multipath component in the l-th cluster, $\mu_{T,l}$ and $\mu_{R,l}$ are the transmit and receive mean angles for the l-th cluster, and $\widetilde{\theta}_{T,kl}$ and $\widetilde{\theta}_{R,kl}$ are the transmit and receive angles of the k-th multipath component in the l-th cluster relative to the cluster's mean angle.

Average ray power in each cluster is assumed constant so that γ_{kl} follows a zero-mean circular complex Gaussian distribution with variance $|\gamma_l|^2$. The cluster amplitude is assumed to be Rayleigh distributed and the cluster arrival time distribution is conditionally exponential with a normalized unit arrival rate [55, 11].

From equation (3.18), the channel response from transmit antenna element p to receive antenna element m is given by

$$h_{m,p} = \int_0^{2\pi} \int_0^{2\pi} W_m^R(\theta_R) h(\theta_R, \theta_T) W_p^T(\theta_T) d\theta_T d\theta_R, \tag{3.19}$$

where $W_a^B(\theta) = g_a^B(\theta) \exp[j\psi_a^B(\theta)]$, $g_a^B(\theta)$ is the antenna gain pattern, $\psi_a^B(\theta) = 2\pi[x_a^B \cos(\theta) + y_a^B \sin(\theta)]$, $a \in \{m, p\}$, $B \in \{T, R\}$. In [11] it is suggested that the DoD/DoA follows a Laplacian distribution.

Given the assumptions above, the channel response in equation (3.19) is a weighted sum of zero-mean complex Gaussian random variables, and hence $h_{m,p}$ is zero-mean complex Gaussian distributed. Assuming independent ray gains and that ray DoA/DoD are i.i.d., the average covariance matrix can be written as [11]

$$E[h_{m,p} h_{n,q}^*] = \frac{1}{L} \sum_{l=0}^{L-1} |\gamma_l|^2 L_{m,n}^R(\mu_{R,l}) L_{p,q}^T(\mu_{T,l}), \tag{3.20}$$

where

$$L_{a_1,a_2}^B(\mu_{B,l}) = \int f^B(\widetilde{\theta}) g_{a_1}^B(\mu_{B,l} + \widetilde{\theta}) g_{a_2}^B(\mu_{B,l} + \widetilde{\theta}) \exp[j\psi_{a_1,a_2}^B(\mu_{B,l} + \widetilde{\theta})] \, d\widetilde{\theta}, \tag{3.21}$$

with $\{a_1, a_2\} \in \{m, p\}$, $B \in \{T, R\}$, $f^B(\widetilde{\theta})$ is the PDF for the ray DoD/DoA,

$$\psi_{a_1,a_2}^B(\theta) = 2\pi d_{a_1 \to a_2}^B \cos(\theta - \phi_{a_1,a_2}^B) \tag{3.22}$$

$d_{a_1 \to a_2}^B$ is the distance between elements a_1 and a_2, and

$$\phi_{a_1,a_2}^B = \tan^{-1}[(y_{a_1}^B - y_{a_2}^B)/(x_{a_1}^B - x_{a_2}^B)]. \tag{3.23}$$

3.4.1.3 One-ring model

The one-ring model was first proposed by [56] and further extended by [50] in order to study the capacity distribution under spatial correlation. The one-ring model is derived
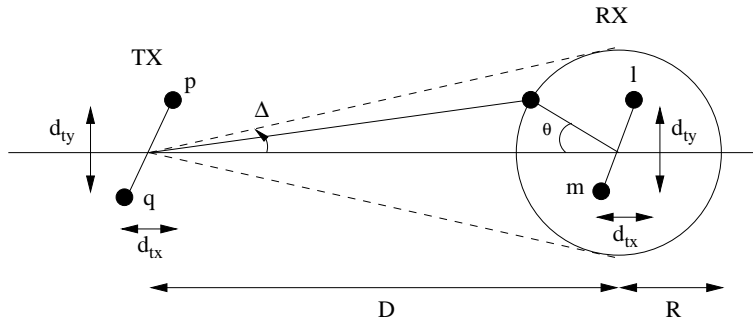
Figure 3.6: Illustration of the geometrical configuration of a 2x2 channel with local scatterers at the receiver, where D is the distance between the transmitter and receiver arrays, R is the radius of the ring of scatterers around the receiver.

for an application of fixed wireless communications, where the transmitter is elevated and unobstructed by local scatterers, and the receiver is surrounded by scatterers.

Figure 3.6 illustrates the one-ring model, where D is the distance between the transmitter and receiver arrays, R is the radius of the ring of scatterers around the receiver, and Δ is the angle spread at the transmitter as seen by a particular antenna element. Assuming $D >> R$, the angle spread at the transmitter can be approximated as $\Delta \approx \arcsin(R/D)$.

Denote by $S(\theta)$ a scatterer located in the ring around the receiver at angle θ. The one-ring model is basically a ray-tracing model that computes the propagation from the transmitter to each receiver on the ring of scatterers. It is assumed that the scatterers are distributed uniformly in θ, and the radius R is determined by the root mean square (RMS) delay spread of the channel. Each scatterer is associated with a phase shift ϕ assumed to be uniformly distributed in $(-\pi, \pi)$ and i.i.d. on θ. Only rays that are reflected by the effective scatterers once are considered for computation of the channel response, and it is assumed that all rays reach the receiver with equal power (one-bounce model).

Assuming there are K effective scatterers $S(\theta_k)$, $k = 0, \ldots, K-1$, the complex channel coefficient between the p-th transmit antenna element to the l-th receive antenna element is given by

$$h_{l,p} = \frac{1}{2\pi} \int_0^{2\pi} \frac{1}{\sqrt{K}} \sum_{k=0}^{K-1} \delta(\theta - \theta_k) \exp\left\{ \frac{-2\pi j}{\upsilon} \left(d_{p \to S(\theta_k)} + d_{S(\theta_k) \to l} \right) + j\phi(\theta_k) \right\} d\theta, \quad (3.24)$$

where $d_{X \to Y}$ denotes the distance from object X to object Y, and υ is the wavelength. In the limit when the number of scatterers is infinite, we can conclude from the Central Limit Theorem that $h_{l,p}$ is Gaussian distributed. The covariance between channels $h_{l,p}$

30

and $h_{m,q}$ is given by [50]

$$E[h_{l,p}, h_{m,q}] = \frac{1}{2\pi} \int_0^{2\pi} \exp\left\{\frac{-2\pi j}{\upsilon}\left[d_{p\rightarrow S(\theta)} - d_{q\rightarrow S(\theta)} + d_{S(\theta_k)\rightarrow l} - d_{S(\theta_k)\rightarrow m}\right]\right\} d\theta$$

$$(3.25)$$

In general, equation (3.25) has to be evaluated numerically, but for small angle spread at the transmitter some approximations are possible. The interested reader may refer to [50] for more detailed formulas and results.

3.4.1.4 Two-ring model

The two-ring model proposed in [57] assumes both transmitter and receiver are surrounded by scatterers. Since in this model each ray is reflected twice, once in each ring of scatterers (two-bounce model), the rays impinging the receiver are not independent in general. Moreover, even if the number of scatterers in both rings go to infinity, the channel coefficients do not follow a Gaussian distribution. Hence, mean and covariance matrix are not enough to characterize the process. It was suggested in [57] to generate the channel coefficients by ray-tracing.

3.4.1.5 Von Mises Distribution

Similarly to the one-ring model, a narrowband model was proposed in [12] that uses the von Mises distribution as the angular PDF at the receiver side. The von Mises PDF is a widely used distribution for directional data, and plays a similar role as Gaussian distribution for angular data, and is characterized by its mean and dispersion [22]. This model also takes the Doppler spread into account. This channel model assumes a ring of scatterers around the receiver, as depicted in Figure 3.7 for any 2 antennas at the transmitter and receiver[1].

Assuming that $D \gg R \gg \max(d_{p\rightarrow q}, d_{l\rightarrow m})$, the angle spread at the transmitter can be approximated as $\Delta \approx \arcsin(R/D)$.

It can be shown that the cross-correlation between any two sub-channels lp and mq is given by [12]

$$E[h_{l,p}h_{m,q}^*] = \Omega \exp(c_{pq}\cos\alpha) \int_{-\pi}^{\pi} \exp(c_{pq}\Delta\sin(\alpha)\sin(\theta) + b_{lm}\cos(\theta - \beta))f(\theta)d\theta, \quad (3.26)$$

where Ω is the path loss, $f(\theta)$ is any angular PDF of θ, $c_{pq} = j2\pi d_{p\rightarrow q}/\upsilon$, $b_{lm} = j2\pi d_{l\rightarrow m}/\upsilon$,

---

[1]Note that some variable definitions are modified in Figure 3.7 with respect to the one-ring model in Figure 3.6.
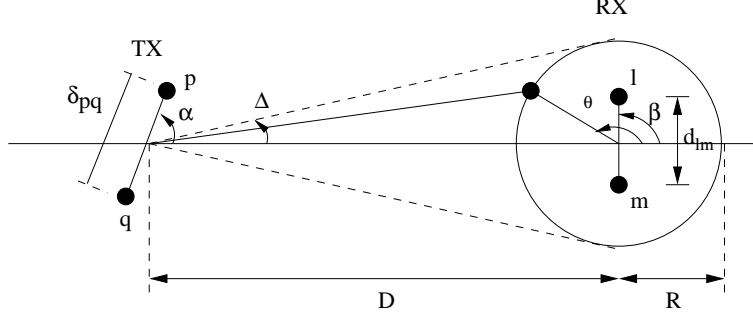
Figure 3.7: Illustration of the geometrical configuration of a 2x2 channel with local scatterers at the receiver, where D is the distance between the transmitter and receiver arrays, R is the radius of the ring of scatterers around the receiver, and $d_{l \to m}$ is the distance between elements l and m in the receive array.

v is the transmitted signal wavelength. Parameter α denote the angle of the transmit array relative to the line connecting the transmit and receive arrays, respectively. In [12] the correlation is derived including the Doppler spread considering the terminal is moving. The interested reader can find more details in [12].

An angular PDF must satisfy $f(\theta) = f(\theta + 2\pi k)$ for any integer k. Hence, a Gaussian PDF can not be used. A suitable angular PDF is the von Mises [22], defined as

$$f(\theta) = \frac{1}{2\pi I_0(\kappa)} \exp(\kappa \cos(\theta - \mu)), \tag{3.27}$$

where μ is the symmetry center ("mean direction"), κ can be chosen between 0 (isotropic scattering) and ∞ (extremely concentrated), and $I_0(\cdot)$ is the modified Bessel function of the first kind of order zero. Figure 3.8 illustrates the von Mises PDF for different values of κ. Using the von Mises PDF the cross correlation in (3.26) may be written as [12]

$$E[h_{l,p}h_{m,q}^*] = \Omega \frac{\exp(c_{pq}\cos(\alpha))}{I_0(\kappa)} I_0(\{c_{pq}^2 \Delta^2 \sin^2(\alpha) + 2c_{pq}\Delta \sin(\alpha)(b_{lm}\sin(\beta) + \kappa \sin(\mu)) +$$

$$+ 2\kappa b_{lm} \cos(\mu - \beta) + \kappa^2 + b_{lm}^2\}^{\frac{1}{2}}). \tag{3.28}$$

An extension of this model to multiple scatterer clusters is found in Publication III, where the angular distribution is a mixture of von Mises PDFs. A mixture model is used with Laplace and Gaussian PDFs in [58].
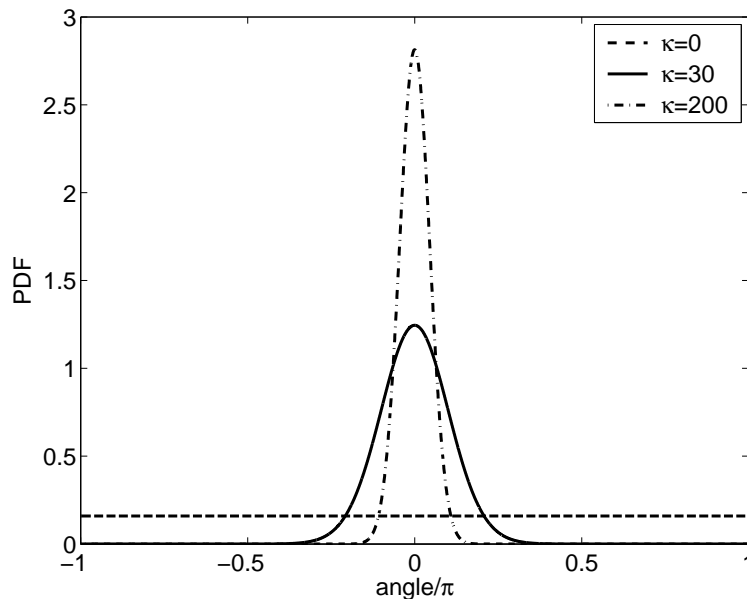
Figure 3.8: Von Mises PDF for different values of κ, with $\mu = 0$.

3.4.2 Coupling-based models

Spatial channel models relying on separability assumption, such as the Kronecker model in Section 3.4.1.1, do not provide an accurate representation of the MIMO channel when there is strong coupling between DoAs and DoDs. This is especially true for large arrays with high angular resolution, as reported in [59]. The coupling-based models presented in this Section attempt to solve this problem by explicitly modeling the coupling between DoDs and DoAs.

3.4.2.1 Finite scatterer model

Assuming there are K scatterers between the transmitter and receiver, the MIMO channel matrix can be written as [60]

$$\mathbf{H} = \sum_{k=0}^{K-1} \gamma_k \, \mathbf{a}_R(\theta_{R,k}) \, \mathbf{a}_T^T(\theta_{T,k}), \tag{3.29}$$

where γ_k is the complex gain for the k-th scatterer, $\theta_{T,k}$ and $\theta_{R,k}$ are the DoD and DoA, respectively, and $\mathbf{a}_T(\theta_{T,k})$ and $\mathbf{a}_R(\theta_{R,k})$ are the array responses at the transmitter and receiver, respectively. For an uniform linear array the array response vectors at both sides

are given by (see Section 3.3)

$$\mathbf{a}_T(\theta_{T,k}) = \begin{bmatrix} 1 \\ e^{-j\frac{2\pi}{v}d_T\cos(\theta_{T,k})} \\ \vdots \\ e^{-j\frac{2\pi}{v}(M_t-1)d_T\cos(\theta_{T,k})} \end{bmatrix} \tag{3.30}$$

$$\mathbf{a}_R(\theta_{R,k}) = \begin{bmatrix} 1 \\ e^{-j\frac{2\pi}{v}d_R\cos(\theta_{R,k})} \\ \vdots \\ e^{-j\frac{2\pi}{v}(M_r-1)d_R\cos(\theta_{R,k})} \end{bmatrix}, \tag{3.31}$$

where d_T and d_R are the element spacing at the transmitter and receiver arrays, respectively.

This model can be written in a more general form as [8]

$$\mathbf{H} = \mathbf{A}_R\left(\mathbf{\Omega}\odot\mathbf{H}_w\right)\mathbf{A}_T^H, \tag{3.32}$$

where $\odot$ denotes the element-wise Schur-Hadamard product. The columns of the $M_r \times K$ matrix $\mathbf{A}_R$ and of the $M_t \times K$ matrix $\mathbf{A}_T$ are the steering vectors related to each individual scatterer at the receiver and transmitter side, respectively, and the $K \times K$ matrix $\mathbf{\Omega}$ is a coupling matrix that contains the complex path gains.

Equation (3.29) is obtained from equation (3.32) by proper ordering of the steering vectors and defining $\mathbf{\Omega}$ as a diagonal matrix. However, equation (3.32) is more general, since $\mathbf{\Omega}$ can be designed as to represent multiple coupling between DoD and DoA.

3.4.2.2   Virtual channel representation

The channel representation in Section 3.4.2.1 is linear in $\mathbf{\Omega}$, but it is non-linear in the steering vectors. One alternative representation that is linear is obtained by modeling the MIMO channel in the beamspace with predefined steering vectors [61, 8],

$$\mathbf{H} = \widetilde{\mathbf{A}}_R\left(\mathbf{\Omega}\odot\mathbf{H}_w\right)\widetilde{\mathbf{A}}_T^H, \tag{3.33}$$

where the $M_r \times M_r$ matrix $\widetilde{\mathbf{A}}_R$ and the $M_t \times M_t$ matrix $\widetilde{\mathbf{A}}_T$ are the steering matrices corresponding to the receiver and transmitter, respectively. Both $\widetilde{\mathbf{A}}_R$ and $\widetilde{\mathbf{A}}_T$ are unitary

and correspond to fixed angles. In fact, $\widetilde{\mathbf{A}}_R$ and $\widetilde{\mathbf{A}}_T$ can be defined as discrete Fourier transform (DFT) matrices [61]. However, in contrast to Section 3.4.2.1, the coupling matrix $\mathbf{\Omega}$ is not diagonal in general. The accuracy of the virtual channel representation depends on the number of virtual angles, which cannot be chosen arbitrarily, but is related to the array construction [8].

3.4.2.3   Weichselberger model

The Weichselberger model represents the MIMO channel in the eigenspace instead of the beamspace [8], allowing for an arbitrary coupling between the transmit and receive eigenbeams. The main idea is to relax the separability constraint of the Kronecker model described in Section 3.4.1.1, which is responsible for mismatches of predicted performance when comparing to measured channels [59].

The eigenvalue decomposition of the receive and transmit covariance matrices is given by

$$\mathbf{R}_{\mathrm{R}} = \mathbf{V}_R \mathbf{\Lambda}_R \mathbf{V}_R^H, \tag{3.34}$$

$$\mathbf{R}_{\mathrm{T}} = \mathbf{V}_T \mathbf{\Lambda}_T \mathbf{V}_T^H. \tag{3.35}$$

Assuming all transmit and receive eigenmodes are mutually uncorrelated, the channel matrix can be written as

$$\mathbf{H} = \mathbf{V}_R \left(\mathbf{\Omega} \odot \mathbf{H}_w \right) \mathbf{V}_T^T. \tag{3.36}$$

This model includes the Kronecker model as a special case [8], but in general there is coupling between the transmit and receive eigenmodes, given by $\mathbf{\Omega}$.

3.4.2.4   Keyhole channels

MIMO models with complex Gaussian statistics are not able to reproduce a situation where there is rich scattering at both sides of the link, but the channel matrix is still rank deficient. This could happen if the signals from the scatterers around the transmitter reach the scatterers around the receiver through a very narrow pipe. In [62] a generalization of the Kronecker model is presented

$$\mathbf{H} = \frac{1}{\sqrt{S}} \mathbf{R}_{\mathrm{R}}^{1/2} \mathbf{H}_{R,w} \left(\mathbf{\Omega} \odot \mathbf{H}_w \right) \mathbf{H}_{T,w} \left(\mathbf{R}_{\mathrm{T}}^{1/2} \right)^T, \tag{3.37}$$

where the elements of $\mathbf{H}_{R,w}$ and $\mathbf{H}_{T,w}$ are i.i.d. complex Gaussian distributed, and S is a normalization factor. The keyhole effect is observed if the coupling matrix $\boldsymbol{\Omega}$ is not full rank. In an extreme case of a rank one $\boldsymbol{\Omega}$, the channel transfer matrix $\mathbf{H}$ is rank one as well, even though the channel correlation matrices at both rank may have full rank. Note that the channel matrix in equation (3.37) is not Gaussian distributed, and hence cannot be described only by first- and second-order statistics.

This channel model has been verified by experimental results where one antenna array was located inside a shielded chamber, which was connected to the an adjacent room where the other antenna array was located by a wave guide [63]. It is shown that the keyhole channel shows a double-Rayleigh distribution, as expected from equation (3.37). However, keyhole channels have not been observed in natural environments.

3.5   3GPP Spatial Channel Model

In 3GPP, the Spatial Channel Model (SCM) has been proposed for link- and system-level MIMO simulations [64], which is among the first full MIMO channel models. The 3GPP SCM channel model is widely used outside 3GPP context as well, due to its simpler implementation compared to the more sophisticated channel models that will be described in the next sections.

In 3GPP SCM, a simple procedure is defined to generate the channel matrices:

1. Select a propagation environment, which can be either suburban macro, urban macro, and urban micro cell.

2. Determine user parameters, associated with the propagation environment: angular spread, shadowing, delay spread, pathloss, antenna orientation, speed, and antenna gains. Based on these parameters, generate angles of arrival and departure, path delays, and path power.

3. Generate channel coefficients

In addition to the propagation environments mentioned above, four cases are specified for link-level simulations, usually designated as Case A, B, C, and D. The differences among the cases are in existence of line-of-sight component or not, PDP, and angular spreads. Case A corresponds to a single-path channel. Polarized arrays, far scatter clusters, and urban canyons can also be added as optional system simulation features.

In 3GPP SCM there are always 6 paths (except for Case A), each composed of a combination of 20 subpaths. The angular distance between the subpaths is constant and defined as a parameter dependent on the environment, such that the corresponding angular spread is generated. The DoAs and DoDs of the paths are generated randomly from a Gaussian distribution. The phases of the subpaths are i.i.d. and uniformly distributed. After all user parameters are generated, the channel matrix coefficients are generated by a mapping function [64].

3.6 COST259 model

A detailed channel model for macro- micro- and pico-cell environments was developed in COST259 action [65]. A layered approach is used in order to characterize different propagation environments, due to the complexity of the propagation mechanisms under consideration. The COST259 channel model was one of the first to consider directional information, and it served as a basis for more advanced channel models, as the one developed in COST273 action (cf. Section 3.7). In this section we summarize the main aspects of COST259 channel model, especially those regarding directional information. Further details and parameters can be found in [66, 67].

The double directional impulse response (DDIR) of the radio channel is given by the sum of multipath components (MPC) [68, 66]. Each MPC is described by its elevation and azimuth angles of incidence at the BS, the elevation and azimuth angles of departure at the MS, the delay, and a complex polarimetric 2×2 matrix. The MPCs result from the specular reflections in interacting objects (IO) which are scattered in the environment. The position of the IOs is such that they correspond to a pre-defined PDP/PAS [66], assuming only single interactions.

it is observed from channel measurements that MPCs usually arrive in clusters [66]. The expected number of clusters in COST259 channel model is close to one for most scenarios, except for "Bad Urban" scenario, where the expected number of cluster is approximately equal to two [66].

The COST259 channel model defines the concept of the *visibility region*, which model the appearance and disappearance of clusters [67]. Each cluster is associated with one visibility region. Each visibility region is a physical region in a coverage area which is defined such that if the MT is in that region, the cluster is considered as active and
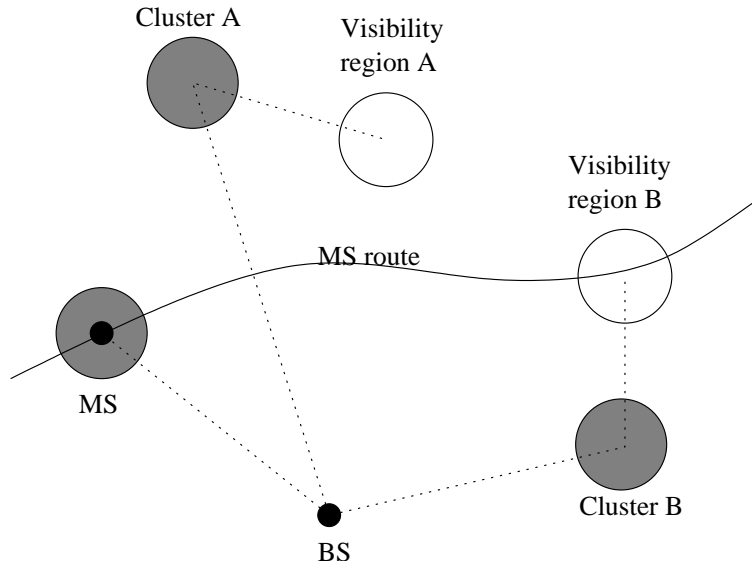
Figure 3.9: Example of visibility regions for a given MS trajectory. The white circles represent the visibility areas and the shaded circles denote the associated clusters.

contribute to the final DDIR. Figure 3.9 illustrates the concept of visibility region. For the exemplified MS trajectory, visibility region A will not be activated at any time. The visibility regions are circular and defined by their radii. A transition region around the visibility region provides a smooth transition between cluster activity/inactivity states.

The concepts laid out in COST259 channel model have been extended and enhanced during COST273 action, that will be described in next section.

3.7   COST273 model

During the course of COST273 action, a generic channel model for next generation wireless systems was developed [8]. The goal was to develop one channel model that would fit all evaluated scenarios. In this section we summarize the main aspects of the COST273 MIMO model, in particular those topics related to the generation of the double directional impulse responses (DDIR) [68]. Detailed information on the evaluated scenarios and related parameters can be found in [8].

Following the concept of the COST259 channel model [66, 67], the signal is assumed to arrive in clusters. The total DDIR can then be written as a sum of each cluster DDIR. This model assumes that, within one cluster, azimuth spread, elevation spread, and delay spread are independent at the transmitter and receiver. The resulting model, however, does not correspond to the Kronecker model if more than one cluster is present, since different

clusters have different statistics, implying that the overall covariance matrix cannot be decomposed into a Kronecker structure.

In the COST273 channel model, the mean angles and delays of the clusters are modeled by a geometric approach [66, 69], while the intracluster spreads and small scaled fading are generated either by a geometric approach or by a tapped delay line representation. One of the main differences between COST259 and COST273 channel models is the inclusion of multiple interaction mechanisms. Three kinds of clusters are defined to model different types of interaction mechanisms: *local clusters* around the transmitter and/or receiver, *clusters with single interaction*, and *twin clusters*. Not all kinds of clusters are supposed to be present in all environments. For example, in macrocells the single-interaction cluster is the dominant propagation mechanism, while in microcell multiple interaction processes concentrate most of the energy [8].

Local clusters are assumed to be always present at the mobile terminal (MT) side, resulting in large angular spread. The local cluster is generated from a single-scattering assumption. The size of the local cluster is given by their delay spreads and the distribution of multipath components inside the cluster.

Similarly to COST259 channel model, COST273 channel model employs the concept of visibility regions. Each cluster is associated with one visibility region. Each visibility region is a physical region in a coverage area which is defined such that if the MT is in that region, the cluster is considered as active and contribute to the final DDIR.

The positions for single-interaction clusters are determined in a geometric way. Initially the visibility regions are distributed throughout the cell, and each visibility region is associated with one specific cluster. The radial position from the base station (BS) is defined from an exponential distribution, and the angle of the cluster center is drawn at random from a Gaussian distribution. The minimum delay, azimuth spread as seen from transmitter and receiver are then obtained by simple geometrical relationships.

For the multiple-interaction clusters, the mean DoA, DoD, and minimum delay are derived from random realizations of the marginal distributions, which implies that delay and angles are independent. Another approach for generation of multiple-interaction case is to have each cluster divided into a cluster corresponding to the transmitter side and one corresponding to the receiver side. The angular dispersions at both sides are modeled independently, but in order to limit complexity the clusters behave like twins, having the same distributions of scatterers and long-term behaviors. This concept is illustrated in
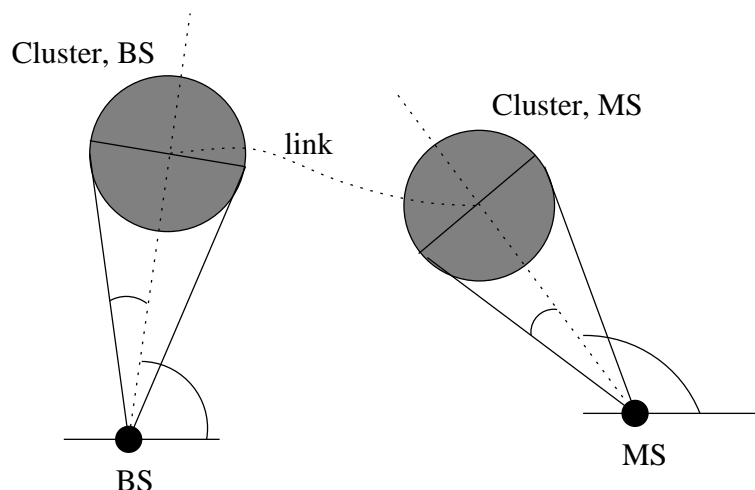
Figure 3.10: Illustration of the twin cluster concept.

Figure 3.10.

The line of sight (LoS) component is modeled stochastically for some environments using an approach very similar to that of visibility regions for clusters.

The double-directional delay power spectrum (DDDPS) is defined as the squared magnitude of the DDIR and can be characterized for each cluster by its dispersion in the following domains: delay, azimuth at BS, elevation at BS, azimuth at MT, and elevation at MT. In the delay domain an exponentially-decaying power profile is used. The angular spectra at both BS and MT are defined by Laplacian power spectra, which can be shown to provide a good fit to experimental data [70, 71].

Diffuse scattering is defined as the part of the measured signal which cannot be resolved in the temporal domain. The PDP of the diffuse component is modeled uniformly in azimuth and exponentially in decay.

3.8 WINNER Model

The Wireless World Initiative New Radio (WINNER) project aims to develop an ubiquitous radio system to provide wireless access in a wide range of environments and support different applications [72]. The WINNER channel model is a system-level and link-level model, and hence the model parameters include both large-scale (e.g. shadow fading, delay and angular spreads) and small-scale parameters (e.g. delays, power, direction of arrival/departure). In this section only those parameters related to generation of DDIR are described. Detailed information on the evaluated scenarios and related parameters can

be found in [73] [2]

During the first phase of the WINNER project, the 3GPP SCM channel model [64] was extended from 5 MHz to 100 MHz bandwidth for initial evaluation of the system concept [74]. For the second phase of the WINNER project, however, more advanced channel model has been derived, in order to fully support the considered scenarios and applications. The current version of the WINNER channel model utilizes a generic channel model which is antenna independent, and hence it can be applied to different antenna configurations. Channel realizations are obtained by summing contributions of rays (specular reflections). Similarly to COST259 [66] and COST273 [8] model described in Section 3.7, it is assumed that the signals arrive in clusters. In the context of WINNER channel model, a cluster is defined as a "propagation path diffused in space, either or both in delay and angle domains." [73] Angles of arrival and departure are generated randomly from a truncated Gaussian distribution, and the relative angles of rays within one cluster are fixed.

The concept of *channel segment* is defined similarly to the concept of *drops* in static channel models [75]. During a channel segment it is assumed that the probability distributions of the parameters are unchanged, and some large-scale parameters are kept constant during this time. Small-scale parameters are generated independently between channel segments. This creates discontinuity of parameters such as delays, DoA/DoD, which do not correspond to behavior observed from measurements. Several approaches exist for modeling the time evolution of small-scale parameters. Current approach in WINNER is to provide a smooth transition between two segments by replacing clusters from one segment to the other sequentially. The power of each cluster is ramped up and down linearly, and the clusters are substituted one at a time, until only clusters from the new channel segment remain. This process is illustrated in Figure 3.11. Alternative approaches for smooth transition of channel segments are currently under investigation in WINNER project.

Reduced complexity models are proposed as well, which can be used for faster studies. These models employ cluster delay lines (CDL), similarly to widely used tapped-delay-line models. In the context of these simplified models, a cluster is defined as a tap spread over angle domain, but all rays are equally powered with the same delay. Relative angles of rays within one cluster are fixed.

---

[2]It should be noted that the WINNER project will continue until the end of year 2007, and hence the proposed channel model and system concept may still evolve.
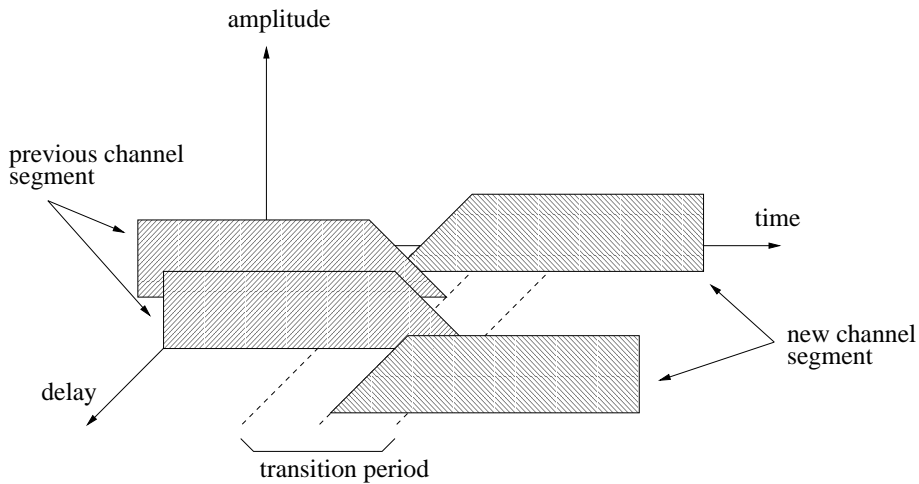
Figure 3.11: Illustration of the transition between channel segments.

3.9 Summary and discussion

In this chapter several MIMO channel models were presented. Section 3.4 describes link-level models, which are suitable to describe the spatial characteristics of the channel between a transmitter and receiver. Sections 3.5, 3.6, 3.7, and 3.8 describe the main aspects of 3GPP SCM, COST259, COST273, and WINNER channel models, respectively, which are complex system-level models, and hence combine propagation and link-level models for a large variety of scenarios.

The models are derived from different sets of assumptions and targeting characterization of different aspects of the MIMO channel. Covariance-based channel models are in general useful for generation of channel responses for simulation purposes, which can be easily obtained from, e.g., the Cholesky decomposition of the correlation matrix. On the other hand, coupling-based models are better suited for the characterization of angular properties of the double-directional channel, since coupling between DoAs and DoDs is modeled explicitly. In particular, the finite scatterer model in Section 3.4.2.1 is widely used in the literature, for example for the derivation of estimators for the parameters of the underlying waves and for assessment of beamforming applications. While this model is very powerful to characterize propagation environments that are dominated by specular-like reflections, it is not suitable to describe diffuse scattering. It is also common to model the cluster behavior observed from measurement campaigns using the finite scatterer model where there is a superposition of scatterers which are concentrated around the mean angle/delay of the respective clusters, as in the COST273 and WINNER models described

in Sections 3.7 and 3.8, respectively. However, if the clusters are not clearly separated in angle and/or delay domains, it is a non-trivial task to identify which waves belong to the clusters when estimating the parameters of the model from channel measurements. The same is not true for an estimator derived from cluster-based models, like the SVA model described in Section 3.4.1.2, where the spread and mean angles of the clusters are identified explicitly.

The categorization of spatial models utilized in Section 3.4 and further detailed in Figure 3.4 is not unique, since models share some properties that would allow them to be classified in more than one category. For example, the SIMO version of the von Mises model in Section 3.4.1.5 corresponds to the receive correlation in the SVA model in Section 3.4.1.2, and hence the SIMO correlation matrix from the von Mises model can be used as a building block for the SVA model, allowing for a closed form solution to the corresponding MIMO correlation matrix. Moreover, the separability principle used in the Kronecker model is employed cluster-wise in the SVA model, and also on COST273 and WINNER models. Finally, the Weichselberger model in Section 3.4.2.3 is based on eigenvectors obtained from channel covariance matrix, and hence could also be considered as a correlation-based model.

The system-level models described in Sections 3.7 and 3.8 are intended for simulation of large systems with several terminals and base stations, and also for the evaluation of the transmission techniques in realistic deployment scenarios. Hence, such models are commonly simplified in order to keep complexity as low as possible. Traditionally, look-up tables are used to make the mapping between link-level and system-level simulations, in order to avoid computation of receiver and transmitter procedures in system-level simulations [75]. However, both COST273 and WINNER projects came to the conclusion that for the characterization of the MIMO channel it is not possible to draw a clear division between link-level and system-level issues, and hence part of receiver and transmitter procedures have to be implemented in system-level as well, increasing the need for simplification of the MIMO channel model. The WINNER project approaches this problem by proposing two channel models, with different levels of complexity, and, naturally, different levels of accuracy.

The COST273 channel model describes features of the MIMO channel, like time evolution of spatial parameters and birth and death of clusters in a more natural and intuitive form than WINNER model by explicitly placing clusters in the propagation environment

and by the concept of visibility regions. The WINNER model may have lower complexity, however, due to the concept of channel segments, and simplified schemes for smooth transition between channel segments. Since both models are very recent and work on WINNER project is still ongoing, no direct objective comparison between the models can be found in literature so far.

The dynamic behavior of the MIMO channel is perhaps one of the major challenges for future development of channel models, especially taking into account that the channel model must remain simple to be of practical use in link-level and system-level simulators. Since tracking the evolution of a large number of parameters is likely to be highly complex, channel models that capture the main features of the MIMO channel with few parameters are desirable. Channel models that describe the diffuse scattering component explicitly might be one step toward this objective, since they are able to describe the MIMO channel with smaller number of specular-like components. Hence, a better characterization of the diffuse scattering mechanisms is required. While COST273 addresses the diffuse scattering already, no measurement campaigns have measured the diffuse scattering component in spatial domain.

Chapter 4

Propagation parameter estimation

Advanced estimation algorithms are needed in order to obtain the parameters for the models described in Chapter 3. Estimators vary in their design criteria, statistical properties, resolution, computational complexity, dimensionality of parameter space, etc. Estimators based on maximum likelihood (ML) criterion are optimal in the sense that the variance of the estimates asymptotically converge to the theoretical bound given by the CRLB [76]. However, the complexity of such estimators can become prohibitively high. Numerical methods for finding ML estimates with reduced complexity have received a lot of attention recently. Some of the most relevant methods are discussed in Section 4.4. These estimators are designed for obtaining several parameters regarding each individual specular reflection reaching the receiver array, including DoA/DoD, delay, Doppler spread, and complex gain.

Simpler estimators dedicated to a few parameters are still required, for example for initialization of complex iterative ML algorithms, or for shorter studies where only spatial characteristics of the channel are needed. Such estimators include well-known techniques like beamforming, MUSIC, and ESPRIT, which are briefly described in Section 4.3.

Finally, the estimators shown in Section 4.6 are designed taking into account that the signals that reach that receiver array arrives in clusters, as observed in recent measurement campaigns and in COST273 and WINNER channel models described in Chapter 3. Such estimators estimate mean angle and angular spread of each clusters assuming the angular spread is small.

4.1 Principles of channel sounding

The operation of a channel sounder consists of transmitting a known signal from one antenna at a given location and receiving this signal from another antenna which is in a different location. The signals is received after being distorted by the channel, and since it is known to the receiver, it is possible to model the channel from the received signal with high precision. A channel sounder can be built as dedicated hardware or by utilizing a vector network analyzer (VNA), the latter being adequate for short-range measurements only. There is a large similarity between the MIMO channel sounding and MIMO radars [19, 20], where the goal is to use antenna arrays at the transmitter and receiver to detect moving targets.

For directional measurements, the transmitter and/or receiver must be equipped with multiple antennas. For single-directional measurements, an antenna array must exist at the receiver side at least. It is possible to employ parallel receivers for each antenna element, but a commonly used approach is time-domain multiplexing the signal received from each antenna element to a single RF front-end. An alternative approach is the use of a synthetic array, where a single antenna element is moved to the position of each antenna element in a virtual array [77, 78]. The advantage of the latter method is that existing SISO hardware can be used for the measurement, and there is no need for calibration of the antenna elements. However, measurement is limited to static environments due to the time consuming operation of positioning the antenna, and very accurate positioning devices are needed. For double-directional measurements, antenna arrays must exist at both transmitter and receiver. Time domain multiplexing of signals at both transmitter and receiver ends is the most commonly used technique [79, 80]. This technique is illustrated in Figure 4.1.

Array geometries play an important role in the performance and resolution of angular estimation methods. In order to avoid aliasing in the angular spectrum, the antenna spacing must be smaller than or equal to half a wavelength. Azimuth-only measurements can use, e.g., a uniform linear array (ULA) or a uniform circular array (UCA) (c.f. Section 3.3). The ULA has the advantage of higher resolution in the broadside for the same number of elements, while the UCA has the advantage of uniform resolution for all angles [8].

For joint azimuth and elevation angle estimation, a two-dimensional array structure is
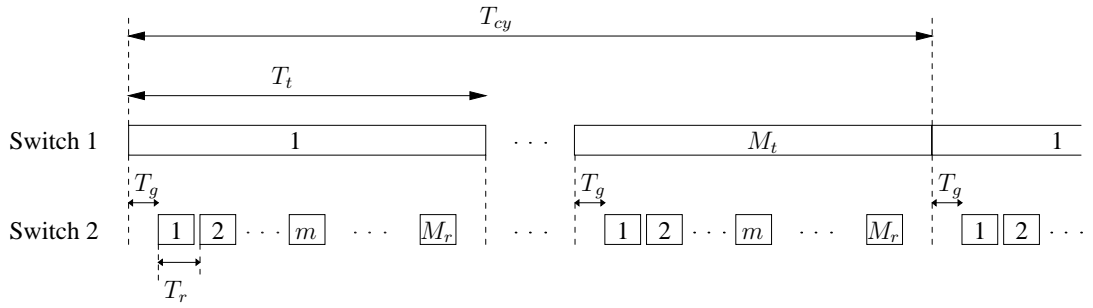
Figure 4.1: Time-domain multiplexing of a channel sounding system, where T_t denotes the period that the sounding signal is applied at the input of each element of the transmit array, T_r is the period that each antenna element of the receive array is active, T_{cy} is the total time it takes to cycle through all transmit and receive antennas, and T_g is a guard time to account for the switching time at the transmitter.
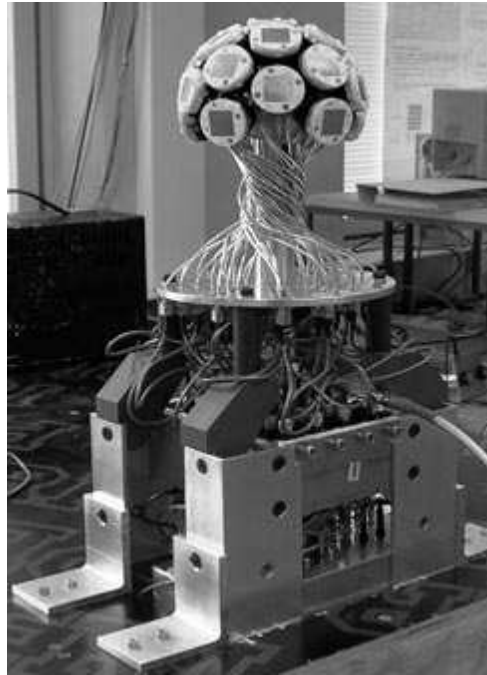
Figure 4.2: Spherical array from Radio Laboratory, TKK.

needed. A UCA may also be used for this purpose, or, alternatively, a uniform rectangular array (URA). In order to avoid ambiguity between angles below or above the horizontal plane, three-dimensional array structures must be employed, such as a spherical array, a circular cylindrical array, or a rectangular solid array [8, 10]. Figure 4.2 shows an example of spherical array from Radio Laboratory, TKK.

4.2 Assumptions

The channel is assumed to be narrowband except when explicitly mentioned otherwise. For most of the estimation methods described in this chapter it will be assumed that the channel is described by the finite scatterer model in Section 3.4.2.1. For the techniques described in Section 4.6, the channel model is a simplified version of the COST273 model in Section 3.7.

The number of specular components (scatterers) will be assumed as known. An overview on techniques for the estimation of number of sources is given in Section 4.5. The estimation procedures described here assume that noise is zero-mean circular complex white Gaussian distributed. For colored noise, pre-whitening of the observation is required [76, 81].

From (2.1) and Section 3.4.2.1, the covariance matrix of the received signal $\mathbf{y}$ is given by

$$\mathbf{R}_y = \mathbf{A}\mathbf{R}_s\mathbf{A}^H + \sigma_n^2\mathbf{I}. \tag{4.1}$$

In practice, the covariance matrix of the received signal, $\mathbf{R}_y$, has to be estimated from the received data. An estimate of $\mathbf{R}_y$ is given by the sample covariance matrix

$$\widehat{\mathbf{R}}_y = \frac{1}{M_s} \sum_{t=0}^{M_s-1} \mathbf{y}(t)\mathbf{y}^H(t), \tag{4.2}$$

where M_s is the number of observations.

4.3 Estimation of Directional Parameters

4.3.1 Spectral-Based Estimation

The techniques presented in this section construct a spectrum from which the channel directional parameters are estimated. The algorithms are designed such that the DoAs correspond to peaks on the spectrum.

Conventional Beamformer

The conventional (Bartlett) beamformer is defined as the weight vector that maximizes the output power assuming that the received signal has only one component, which arrives

from direction θ [47]. The spatial spectrum is obtained as

$$P_{\mathrm{BF}}(\theta) = \frac{\mathbf{a}^H(\theta)\widehat{\mathbf{R}}_y\mathbf{a}(\theta)}{\mathbf{a}^H(\theta)\mathbf{a}(\theta)}. \tag{4.3}$$

The DoAs can then be identified as the values of θ corresponding to peaks in the spectrum defined in (4.3).

Capon's Beamformer

Several modifications have been proposed to the conventional beamformer in order to overcome its limitations, especially with respect to the angular resolution of the spatial spectrum and the ability of the beamformer to separate closely spaced sources. One approach to increase resolution of the spatial spectrum is given by the Capon's beamformer, which minimizes the output power in all directions except for the direction of interest. The spatial spectrum is obtained as

$$P_{\mathrm{CAP}}(\theta) = \frac{1}{\mathbf{a}^H(\theta)\widehat{\mathbf{R}}_y^{-1}\mathbf{a}(\theta)}. \tag{4.4}$$

The Capon's beamformer utilizes all degrees of freedom for nulling directions other than the direction of interest [82]. This results in a better capability to separate closely spaced sources than the conventional beamformer [47]. Figure 4.3 shows an example output of the Capon and Bartlett beamformers, for two sources at 80° and 110°, where the higher resolution of Capon's beamformer is clearly observed.

MUSIC

Subspace-based methods, which rely on the separation of signal and noise subspaces, provide even higher resolution for closely-spaced sources. The multiple signal classification (MUSIC) technique [83, 84] was derived specifically for the problem of estimating directional information in MIMO systems, and is based on the structure of the signal covariance matrix. Similarly to beamforming methods, the directional estimates correspond to the peaks of the MUSIC pseudo-spectrum, given by

$$P_{\mathrm{MUSIC}}(\theta) = \frac{\mathbf{a}^H(\theta)\mathbf{a}(\theta)}{\mathbf{a}^H(\theta)\widehat{\mathbf{V}}_n\widehat{\mathbf{V}}_n^H\mathbf{a}(\theta)}, \tag{4.5}$$

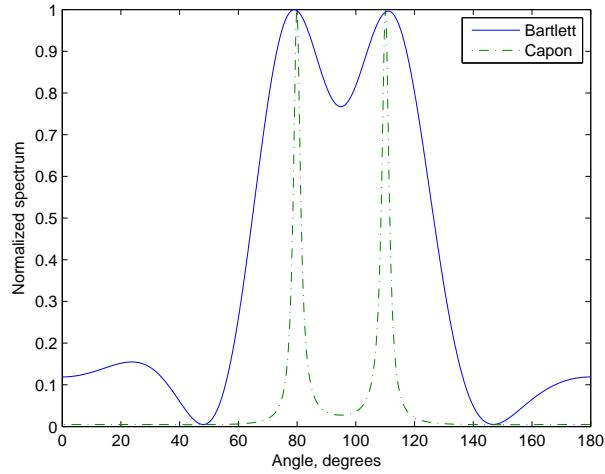where the columns of matrix $\widehat{\mathbf{V}}_n$ are the eigenvectors of the noise subspace [83, 84].

Figure 4.3: Example of spatial spectrum obtained with Bartlett and Capon's beamformers for two sources at 80° and 110°.

Equation (4.5) does not actually define a spectrum, but only a measure of the distance between signal and noise subspaces. It exhibits peaks corresponding to those directions of the actual directions, due to the orthogonality between signal and noise subspaces. The resolution of the MUSIC spectrum is much higher than that obtained with Capon's beamformer, as shown in Figure 4.4 for two sources at 80° and 90°. In fact, the resolution of MUSIC estimates is not dependent on array construction, but on SNR, sample size, and accuracy of the signal model. However, there is performance degradation if signals are highly-correlated, as a result of multipath propagation, for example. In the extreme case of coherent signals the method fails to yield consistent estimates. Several extensions of MUSIC have been derived in the literature to overcome these limitations and improve estimation performance in general.

4.3.2 Estimators for Specific Antenna Configurations

The estimators in this section are not based on an angular spectrum, but they utilize the array structure in order to directly compute the estimates.

Root-MUSIC

The Root-MUSIC method is a polynomial version of MUSIC applied to the ULA case, that exploits the Vandermonde structure of the steering matrix [47]. The roots of the Root-MUSIC polynomial that are close to the unit circle correspond to the DoAs/DoDs. While the root music method does not require maximization of non-linear functions its
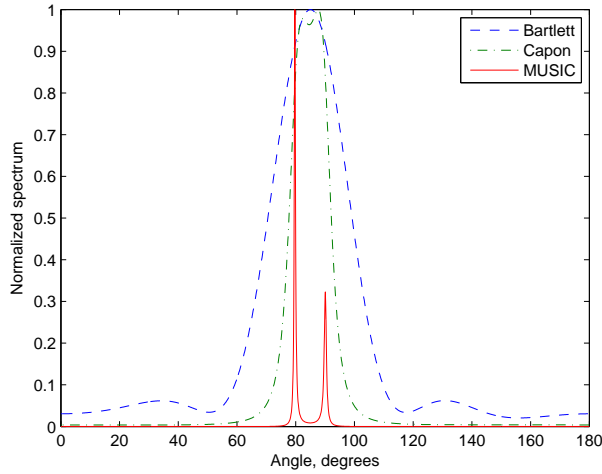
50

Figure 4.4: Example of spatial spectrum obtained with Bartlett and Capon's beamformers and the MUSIC spectrum for two sources at 80° and 90°.

application is limited to ULA only. Extensions of the Root-MUSIC method to non-ULA configurations exist, e.g., using manifold separation approach [85].

ESPRIT

The ESPRIT method [46, 86, 47] exploits the array structure in a different way than the Root-MUSIC method. The basic assumption in ESPRIT is that the array can be divided in two subarrays that are identical except for a fixed displacement vector. It is straightforward to verify that this principle can be applied to the ULA configuration, but in fact it is useful for other configurations as well, as exemplified in Figure 4.5. The ESPRIT solution is given in closed form, and hence application of ESPRIT does not require numerical optimization of a cost function.

4.4   Estimation of Complete Set of Model Parameters

In contrast with the methods described in Section 4.3, the methods presented in this section are not constrained to directional estimates, and application to estimation of complete set of model parameters is straightforward. Complexity is usually higher than that of spectral-based methods but high-precision estimates are obtained. Most methods assume either a correlation-based model (c.f. Section 3.4.1) or the finite scattering model (c.f. Section 3.4.2.1). An exception is the RIMAX method described in Section 4.4.3, which is based on a combination of both correlation-based and finite-scatter models.
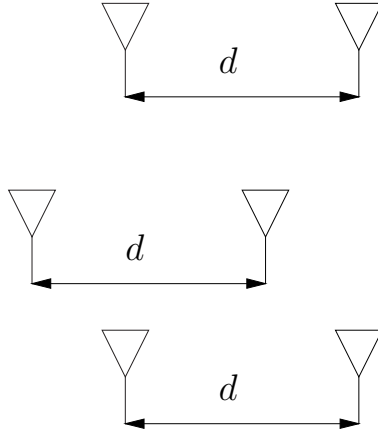
Figure 4.5: Example of array division for application of ESPRIT method.

Most commonly used parameter estimation methods for channel sounding application rely on the maximum likelihood (ML) principle, and the estimates correspond to those parameter values that maximize the likelihood function, or an approximation of it. The methods described in Sections 4.4.1, 4.4.2, 4.4.1.1, and 4.4.3 all fall into this category.

4.4.1 Deterministic Maximum-Likelihood

The basic assumption for the deterministic maximum likelihood (DML) techniques is that the impinging signals are deterministic signals with unknown parameters [84, 87, 47]. Hence, these techniques are well suited to estimate parameters of the finite scatterer model. From the assumption that the noise is zero-mean circularly complex Gaussian, the received signals are also circularly complex Gaussian distributed. Hence, we can write the log-likelihood function for M_s observations of the measurement vector $\mathbf{y}(t)$ as

$$\mathcal{L}(\mathbf{y}(0),\ldots,\mathbf{y}(M_s{-}1))=-M_r M_s \log \pi - M_r M_s \log \sigma_n^2 - \frac{1}{\sigma_n^2}\sum_{t=0}^{M_s-1}\left\|\mathbf{y}(t)-\sum_{k=0}^{K-1}\mathbf{u}(t,\mathbf{\Theta}_k)\right\|^2, \quad (4.6)$$

where $\mathbf{u}(t,\mathbf{\Theta}_k)$ is the array output vector corresponding to one observation of k-th, $k = 0,\ldots,K-1$, specular path, and $\mathbf{\Theta}_k$ is the corresponding parameter vector, which includes DoD/DoA, delay, Doppler frequency, and amplitude. Noise variance can also included in the parameter set. In case of dual-polarized arrays, polarization parameters can be included as well [88, 89]. The maximum-likelihood estimates are those parameter values that maximize the log-likelihood function in equation (4.6) [76].

In general, a multidimensional search has to be performed in order to find the maximum

of (4.6). Given a good initial guess, a Gauss-Newton search usually converges quickly [47]. Spectral-based methods like those described in Section 4.3.1 are natural candidates for initial parameter estimates.

4.4.1.1 SAGE-Based Method

The expectation-maximization (EM) method has been formulated as an iterative method for solving ML problems where part of the observations are missing or censored [90, 91]. The EM algorithm can be applied also to the problem of estimating superimposed signals in noise, which is the problem being considered in this section. An extension of the EM algorithm has been proposed in [92], the space-alternating generalized expectation-maximization (SAGE) algorithm. The SAGE algorithm is particularly suitable to problems where it is possible to sequentially update small groups of elements of the parameter vector. A parameter estimation technique for channel sounding applications has been proposed based on the SAGE algorithm [9]. This method is typically called SAGE in the literature, but here we call it SAGE-based method to differentiate from the original technique developed in [92]. The SAGE-based method is essentially a DML technique derived for estimation of parameters of the finite scatterer model.

The EM algorithm rely on the notions of *complete* and *incomplete* data. The complete data cannot be observed directly, but only by a many-to-one mapping to the incomplete data. The choice of the sets of complete and incomplete is not unique, and it influences the convergence rate of the algorithm. In the problem of estimating superimposed signals in noise, the individual signals corrupted by a part of the additive noise constitute a natural choice for the complete data. The received signal, $\mathbf{y}(t)$, is identified as the incomplete data.

Once the complete and incomplete data have been identified, the EM algorithm consists of two steps: *expectation* and *maximization*. During the expectation step, the incomplete data and the current knowledge of the parameters are used to compute an estimate of the log-likelihood function of the complete data, denoted by $Q(\boldsymbol{\Theta})$, where $\boldsymbol{\Theta}$ is the parameter vector. The maximization step consists of refining the current estimate of the parameter vector by maximizing $Q(\boldsymbol{\Theta})$ with respect to $\boldsymbol{\Theta}$.

The advantage of this method stems from the fact that from the definition of complete data given above it is possible to estimate the parameters of each impinging wave independently. Hence, the number of parameters involved in the multidimensional search

for finding the maximum of $Q(\boldsymbol{\Theta})$ is reduced by a factor of K, where K is the number of waves. The algorithm proceeds by iterating the E- and M-steps until convergence is obtained or a maximum number of iterations is reached.

The SAGE algorithm is an extension of the EM algorithm where the concept of complete data is generalized to that of *hidden-data*, which allows the mapping to the incomplete data space to be random. Moreover, each iteration of the SAGE algorithm is an EM iteration to re-estimate only a subset of the parameters while keeping the estimates of the other parameters fixed [92]. For the estimation problem at hand, the incomplete data is defined as in the EM algorithm, and the hidden-data sets are defined as subsets of the parameter set. Hence, the maximization step can be substituted by several one-dimensional searches, one for each parameter in $\boldsymbol{\Theta}$. A detailed description of this procedure can be found in [9, 80].

Both EM and SAGE algorithms have the important feature that the sequence of likelihood values is monotonically nondecreasing. Moreover, given some mild regularity conditions, the likelihood values always converge to a local maximum. Good initial values are necessary for early convergence of the algorithm and also to ensure that the algorithm converges to a value close to the optimum, which can be obtained by a successive interference cancellation method or by using spectral-based algorithms, such as MUSIC [9, 93]. For global convergence, multiple initial estimates are needed.

4.4.2 Stochastic Maximum-Likelihood

An alternative to the DML approach is obtained by using a stochastic model for the received signal waveforms. Typically, a zero-mean circularly complex Gaussian random processes is used as a model. The observation vector $\mathbf{y}$ is also zero-mean circularly Gaussian, with covariance matrix given by equation (4.1). This approach is known as stochastic maximum likelihood (SML) [94, 95]. The log-likelihood function is now given by

$$
\begin{aligned}
\mathcal{L}(\mathbf{y}(0), \ldots, \mathbf{y}(M_s - 1)) &= -M_r M_s \log \pi - M_s \log |\mathbf{R}_y| - \sum_{t=0}^{M_s - 1} \mathbf{y}^H(t) \mathbf{R}_y^{-1} \mathbf{y}(t) \\
&= -M_r M_s \log \pi - M_s \left[\log |\mathbf{R}_y| + \mathrm{tr}\{\mathbf{R}_y^{-1} \widehat{\mathbf{R}}_y\} \right].
\end{aligned}
\tag{4.7}
$$

The ML estimate is the covariance matrix $\mathbf{R}_y$ that maximizes the log-likelihood function in (4.7). The elements of $\mathbf{R}_y$ can be estimated explicitly, but smaller parameter space, with corresponding lower complexity and higher precision of estimates is obtained if $\mathbf{R}_y$

is parameterized as in Section 3.4.1.

As in case of DML methods, the estimates are obtained by a multidimensional search to find the maximum of (4.7). Once more the methods described in 4.3 are a natural choice to provide initial estimates for cluster mean angles.

4.4.3 RIMAX

Parameter estimation methods typically rely on models based on the finite scatterer model described in Chapter 3, which assumes that only waves resulting from specular reflections contribute to the received signal. However, if the power of the diffuse scattering component (DSC) is significant, these methods will attempt to estimate the diffuse scattering as a sum of several discrete waves, substantially increasing the number of parameters.

The RIMAX algorithm proposed in [10] addresses this problem by jointly estimating both specular components and diffuse scattering. The method performs multidimensional ML estimation, using the SAGE method in [92]. The application of the SAGE method in RIMAX is different from the SAGE-based method described in Section 4.4.1.1, since the latter alternates between parameters of the specular components themselves, while RIMAX is based on the observation that the specular components and the DSC are described by independent parameter sets. The parameters of specular components and diffuse scattering are estimated in an alternative manner using conjugate gradient based algorithms. Due to this separation, the RIMAX method can be seen as a combination of DML and SML techniques for the specular components and diffuse scattering, respectively. Since the DSC is estimated explicitly, computational complexity of RIMAX is reduced in comparison to DML methods, like the SAGE-based method described in Section 4.4.1.1, due to the reduced parameter space.

Direct optimization of the likelihood function is not feasible in this case, due to the high non-linearity of the problem and the large number of parameters. Since parameters of the specular components and DSC are independent, the SAGE algorithm can be applied to alternately estimate the two parameter sets. Hence, for the estimation of the DSC the current estimates of the specular components are removed from the received signal, and the likelihood function is similar to that of SML method given in equation (4.7), and denoted by $\mathcal{L}_{\mathrm{DSC}}(\mathcal{Y})$, where $\mathcal{Y}$ is the received signal. In [10] a Gauss-Newton algorithm is applied for the maximization of $\mathcal{L}_{\mathrm{DSC}}(\mathcal{Y})$, which exploits the Toeplitz structure of the covariance matrix $\mathbf{R}_y$, obtaining its spectral decomposition in an efficient manner.

Once refined estimates of the DSC are available, the maximization of the complete likelihood function with respect to the parameters of the specular components is equivalent to a non-linear weighted least squares problem [10], which is solved by using conjugate gradient algorithms. These algorithms require the computation of the gradient, Jacobian, and approximate Hessian. The approximate Hessian is an estimate of the Fisher Information Matrix, and since its computation is already required by optimization procedure, it can be used for the estimation of the variance of the estimates, and assist the model order selection [10].

Figure 4.6 shows an outline of the RIMAX parameter estimation algorithm. The search for new paths is based on SAGE-type algorithm, the optimization of DSC parameters is based on Gauss-Newton algorithm, and the nonlinear least-squares estimation of parameters of specular components is based on Levenberg-Marquadt algorithm. The reliability test that decides whether or not to keep an estimated path is based on the approximate Hessian. Since the parameters usually change little from one observation to the other, the parameters from the previous observation are used to provide initial estimates for the new observation.

4.5   Estimation of Number of Sources

A natural method for estimation of the number of sources is obtained from the eigen-decomposition of the covariance matrix of the received signal. Subspace-based methods, e.g. MUSIC, use the fact that for K sources, the smallest $M_r - K$ eigenvalues of the covariance matrx $\mathbf{R}_y$ are equal to the noise variance, σ_n^2. Hence, the number of sources could be estimated from the multiplicity of the smallest eigenvalue of $\mathbf{R}_y$. However, only an estimate of $\mathbf{R}_y$ is usually available, which implies that more sophisticated techniques would be required for an accurate estimation of K.

Objective criteria can be obtained from an information theoretic point of view, as the AIC measure introduced in [96] and the MDL measure introduced by Schwartz and Rissanen [97, 98, 99]. Both criteria involve minimizing a cost function that evaluates the
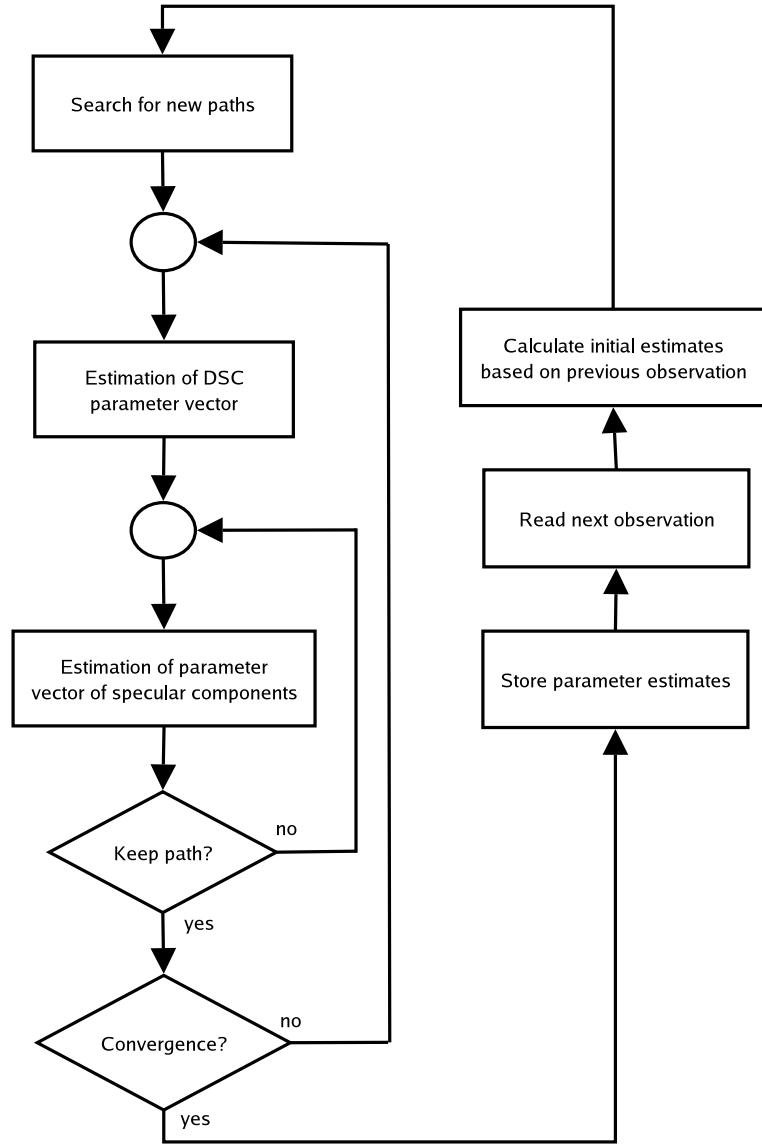
Figure 4.6: Outline of RIMAX parameter estimation algorithm.

model that best fits the data. The AIC criterion is given by

$$\text{AIC}(k) = -2\log\left(\frac{\displaystyle\prod_{m=k}^{M_r-1}\widehat{\lambda}_m^{1/(M_r-k)}}{\displaystyle\frac{1}{M_r-k}\sum_{m=k}^{M_r-1}\widehat{\lambda}_m}\right)^{(M_r-k)M_s} + 2k(2M_r-k), \qquad (4.8)$$

where M_s is the number of observations of the received signal vector, and $\widehat{\lambda}_m$ are the eigenvectors of the sample covariance matrix, with $\widehat{\lambda}_0 > \widehat{\lambda}_1 > \ldots > \widehat{\lambda}_{M_r-1}$. The term in the brackets is the ratio between the geometric mean to the arithmetic mean of the smallest eigenvalues, which can be seen as a symmetry test for the noise subspace, and

the term after the plus sign accounts for bias reduction due to the number of degrees of freedom. The MDL criterion is given by

$$\mathrm{MDL}(k) = -2 \log \left(\frac{\displaystyle\prod_{m=k}^{M_r-1} \widehat{\lambda}_m^{1/(M_r-k)}}{\displaystyle\frac{1}{M_r-k} \sum_{m=k}^{M_r-1} \widehat{\lambda}_m} \right)^{(M_r-k)M_s} + \frac{1}{2}k(2M_r - k) \log M_s. \tag{4.9}$$

The MDL criterion is very similar to AIC, expect for the bias compensation term. It can be shown that the MDL estimates are consistent, i.e., they converge to the true model order if the number of observations grows to infinity, while the AIC criterion tends to, asymptotically, overestimate the number of sources [99]. A review of model order estimation techniques based on information criterion is given in [100].

An alternative to techniques based on information criterion is given by the generalized likelihood ratio test (GLRT) [101]. Even tough these two approaches are usually considered as completely different in the literature, in [101] it is shown that the GRLT is equivalent to the generalized information criteria (GIC). Hence, information criteria methods can be seen as a direct implementation of the sequence of likelihood test performed in GRLT, or GIC methods can be seen as a way to provide the thresholds for the likelihood tests.

For the SAGE-based method in Section 4.4.1.1, one approach commonly used is to start the iterations algorithm assuming a very large number of waves, and reject those whose power is below a pre-determined threshold. While this method is simple and intuitive, it can overestimate the number of waves, since a single wave can be estimated as a superposition of two or more waves. The RIMAX method estimates the number of sources using an estimate of the Fisher information matrix, as described in Section 4.4.3.

4.6   Estimation of Scattered Sources

In channel sounding measurements, the signal is commonly observed as arriving in clusters in space and delay domains. This behavior is included in recent advanced channels models, as the COST273 and WINNER models, described in Sections 3.7 and 3.8, respectively. The estimators presented in this section assume scattered sources with small angular spreads, and estimate the mean angle and angular spread of the clusters directly.

An ML estimator for scattered sources is proposed in [102], where the angular distri-

bution is assumed to be Gaussian. The angular spread is assumed to be small, so that the correlation between the antenna elements can be approximated by a Taylor series expansion. In [15], for small angular spreads, the authors propose a first order Taylor expansion of the spatial signature of each source. This leads to the generalized array manifold (GAM) model, which can be used in conjunction with well-known subspace-based methods, such as MUSIC. This method provides a parametric model for an instantaneous realization of the fading channel, as shown in [103]. Again, by assuming small angular spreads, the authors in [16] show that it is possible to approximate a scattered source as a combination of two rays symmetrically located around the nominal direction. This approximation allows the use of computationally efficient algorithms such as ESPRIT and root-MUSIC. The resulting algorithms are called Spread ESPRIT, Spread root-MUSIC, and so on [16]. Other methods stemming from these can be found, e.g., in [17, 18].

For notational simplicity, the methods in this Section will be presented assuming only one source is present, but they can be easily extended for the case of multiple independent sources. See the references corresponding to each method for details.

ML Estimation of Scattered Sources

It is assumed that there is a large number of independent reflections impinging at an ULA. It is also assumed that the distribution of angles of the rays around the mean direction is Gaussian with standard deviation σ_θ. For small σ_θ, it can be shown that the covariance matrix of the received signal is approximated by [102]

$$\mathbf{R}_y = \sigma_s^2 \mathbf{a}(\mu)\mathbf{a}(\mu)^H \odot \mathbf{B}(\mu, \sigma_\theta) + \sigma_n^2 \mathbf{I}, \tag{4.10}$$

where μ is the mean angle, $\mathbf{a}(\mu)$ is the steering vector, d is the element displacement, $\odot$ denotes the Schur-Hadamard (element-wise) product, and the $\{i, j\}$-th element of matrix $\mathbf{B}(\mu, \sigma_\theta)$ is defined as

$$\mathbf{B}(\mu, \sigma_\theta)_{i,j} = e^{-2[\pi d(i-j)]^2 \sigma_\theta^2 \cos^2 \mu}. \tag{4.11}$$

It is assumed that the received signal is zero-mean circularly symmetric complex Gaussian distributed, and the estimation problem is similar to the SML estimator in Section 4.4.2. The estimates of the mean angle μ and angular deviation σ_θ are those values that maximize the likelihood function.

In [102] it is also proposed an alternative method that estimates the covariance matrix

by a least-squares fit, which results in an estimator with lower complexity since analytical expressions are found for the signal and noise power, and hence optimization has to be performed only for directional parameters.

Generalized Array Manifold

Assuming there is a large number of signals impinging at the receiver array concentrated around a mean direction, we can define the concept of *spatial signature* as

$$\mathbf{v} = \sum_{k=1}^{K} \gamma_k \mathbf{a}(\mu + \widetilde{\theta}_k), \tag{4.12}$$

where γ_k is the complex gain, $\mu + \widetilde{\theta}_k$ is the angle of arrival of the k-th scattered wave, and K is the number of scattered waves. The first order Taylor series expansion of (4.12) can be written as [15]

$$\mathbf{v} \approx \mathbf{a}(\mu) + \mathbf{d}(\mu)\phi, \tag{4.13}$$

where $\mathbf{d}(\mu)$ is the gradient $\mathbf{d}(\mu) = \partial \mathbf{a}(\mu)/\partial \mu$, and $\phi = \sum_{k=1}^{K} \gamma_k \widetilde{\theta}_k$. The structure in (4.13) is denoted by *generalized array manifold*.

In [104] a SAGE-based technique is derived for the estimation of slightly distributed sources using the GAM model, and a MUSIC-based approach is proposed in [15] for the estimation of μ and ϕ. For the model in (4.13), the MUSIC cost function becomes

$$P(\mu, \phi) = \frac{\overline{\phi}^H \overline{\mathbf{A}}^H(\mu) \overline{\mathbf{A}}(\mu) \overline{\phi}}{\overline{\phi}^H \overline{\mathbf{A}}^H(\mu) \widehat{\mathbf{V}}_n \widehat{\mathbf{V}}_n^H \overline{\mathbf{A}}(\mu) \overline{\phi}}, \tag{4.14}$$

where $\widehat{\mathbf{V}}_n$ contains the noise eigenvectors, $\overline{\mathbf{A}}(\mu) = [\mathbf{a}(\mu) \quad \mathbf{d}(\mu)]$, and $\overline{\phi} = [1 \quad \phi]^T$. It can be shown [15] that the maximum of (4.14) can be computed for μ without explicitly estimating $\overline{\phi}$.

Spread-F Techniques

It is assumed that the number of impinging rays at the antenna array is large, so that based on the Central Limit Theorem the received signal can be considered to be zero-mean circularly symmetric complex Gaussian distributed. The covariance matrix of the received

signal can be written as

$$\mathbf{R}_y = \sigma_s^2 \int_0^{2\pi} f(\widetilde{\theta}, \sigma_\theta)\, \mathbf{a}(\mu + \widetilde{\theta})\, \mathbf{a}^H(\mu + \widetilde{\theta})\, d\widetilde{\theta} + \sigma_n^2 \mathbf{I}, \qquad (4.15)$$

where $\widetilde{\theta}$ is the angle deviation around the mean angle μ, σ_θ is the standard deviation of the angle distribution, and $f(\widetilde{\theta}, \sigma_\theta)$ is an angular PDF. Also assume that σ_θ is small and that the angular PDF is symmetric around μ. Then, from a Taylor expansion of $\mathbf{a}_\omega(\omega + \widetilde{\omega})$ it can be shown that the covariance matrix of the received signal can be approximated as [16]

$$\mathbf{R}_y \approx \frac{1}{2}\sigma_s^2 \mathbf{A}_\omega(\omega + \sigma_\omega, \omega - \sigma_\omega)\mathbf{A}_\omega^H(\omega + \sigma_\omega, \omega - \sigma_\omega) + \sigma_n^2 \mathbf{I}, \qquad (4.16)$$

where $\mathbf{A}_\omega(\omega + \sigma_\omega, \omega - \sigma_\omega) = [\mathbf{a}_\omega(\omega + \sigma_\omega)\ \mathbf{a}_\omega(\omega - \sigma_\omega)]$, and $\sigma_\omega \approx \sigma_\theta 2\pi d \cos \mu$.

Equation (4.16) indicates that the rank of the signal subspace is approximately equal to 2. In [16] the authors present an algorithm for the estimation of μ and σ_θ that exploits the structure of $\mathbf{R}_y$ in (4.16). The algorithm is based on the existence of an estimation function $F(\widehat{\mathbf{R}}_y, K_F)$ that gives consistent estimates of the spatial frequencies, where K_F is the number of sources. Function $F(\widehat{\mathbf{R}}_y, K_F)$ must also satisfy some conditions specified in [16], which are in fact satisfied by most common DoA estimation algorithms. The estimation algorithm is called *Spread-F*, where F stands for the underling DoA estimation algorithm in use, e.g., Spread-ESPRIT or Spread root-MUSIC.

Given the observation that the signal subspace is approximately equal to 2 for a source with small angle spread, the Spread-F algorithm obtain estimates for the spatial frequency of the two virtual sources around the mean direction by means of the function $F(\widehat{\mathbf{R}}_y, 2)$. The mean angle and standard deviation are obtained by mapping the estimates using (4.16). See [16] for a detailed description of the algorithm.

The Spread-F algorithm allows for a straightforward utilization of well-known methods for the estimation of the mean angle and angular spread, without knowing the exact angular distribution. However, the algorithm can be difficult to apply if the number of sources is larger than one, due to its nature of exploiting the symmetry around the mean angle of each source. Unless the sources are well separated in angular domain with small angular spreads, it may be difficult to identify which pair of DoAs correspond to each individual source.

4.7 Summary and Discussion

In this chapter several estimators for MIMO channels were presented, with emphasis on their main features, the assumed channel model, and the criterion used in their derivation. A brief introduction to channel sounding principles and methodology was presented as well.

Since MIMO channel estimation is the main topic of this thesis, especial attention was paid to methods that estimate spatial parameters from measurements. A variety of estimators for the directional parameters were presented, starting with non-parametric estimators based on the beamforming principle (conventional beamformer and Capon's beamformer), and the MUSIC method, where the estimates are obtained from a pseudo-spectrum that represents the distance between signal and noise subspaces. The conventional beamformer is simple and useful for obtaining coarse estimates from data, but its limited resolution prevents the identification of closely-spaced sources. Capon's beamformer provides higher resolution by using all degrees of freedom for nulling directions other than the direction of interest. While these methods are based on standard estimation techniques, the MUSIC method is among the first methods derived with the purpose of estimating directional data. It uses the structure of the finite scatterer model for the identification of signal and noise subspaces, and uses the orthogonality between these subspaces to build a pseudo-spectrum that presents peaks corresponding to the actual directions. Resolution of MUSIC method is higher than that obtained with beamforming techniques. In fact, the resolution of MUSIC estimates is not dependent on array construction, but on SNR, sample size, and accuracy of the signal model.

Some estimators are derived for specific antenna configurations, exploiting the structure of the steering vectors to obtain estimates without a spatial spectrum. The root-MUSIC method is derived for ULA only, but there are extensions that allow application of the method to other array configurations. The ESPRIT method is more flexible, since it only requires that the array can be split in two parts that are related by a fixed displacement vector. The ESPRIT method is commonly derived considering either least squares (LS) or total least squares (TLS) criterion, and closed-form solution is obtained in both cases. Both root-MUSIC and ESPRIT methods obtain high-resolution directional estimates.

Commonly-used estimators for channel sounding applications are based on maximum likelihood (ML) principle, as SAGE and RIMAX estimators described in Section 4.4.

Estimators based on ML criterion are optimal in the sense that they attain the CRLB asymptotically, and hence high-precision estimates are obtained. However, such estimators usually require the maximization of the likelihood function using numerical methods. Since such functions are typically highly non-linear, good initial estimates are required in order to avoid convergence to local optima. The EM and SAGE principles to ML estimation result in a simplification of the numerical optimization procedures. In these methods the estimates are obtained by maximizing several simpler functions, which require optimization only for a subset of the parameters of interest. EM and SAGE can be shown to converge to the ML estimates, and hence they have the same optimality properties as the ML estimator.

A procedure for obtaining ML estimates based on the SAGE method in MIMO channel sounding applications is described in Section 4.4.1.1. This SAGE-based method is an interactive procedure that searches for each parameter of each specular reflection independently. While his procedure greatly reduces computational complexity, the number of iterations can be relatively high, especially for a larger number of waves and closely-spaced reflections. The reason for the slow convergence stems from the definition of parameter sets in the application of the SAGE method. In the method described in Section 4.4.1.1, the criterion used for the division of parameter sets is the simplification of the estimation procedure alone. It is not taken into account that the number of iterations can be high if there are correlated parameters belonging to different data sets. This can be particularly relevant for estimation of waves that belong to the same cluster, which are closely-spaced and correlated.

The RIMAX method presented in Section 4.4.3 proposes direct estimation of the parameters of specular reflections by using a non-linear least squares algorithm. This approach has the benefit that an estimate of the Fisher information matrix is computed, which allows for dynamic estimation of the number of sources based on the variances of the estimates. Moreover, the RIMAX algorithm models the diffuse scattering in delay domain, and the SAGE methodology is employed for interactive estimation of parameters of specular component and diffuse scattering component. Since these parameter sets are independent, convergence is achieved with few interactions. The explicit modeling of diffuse scattering in RIMAX has the benefit of reducing the parameter set, since parameters from a smaller number of waves are estimated. However, the diffuse scattering is assumed to be spatially white, and it is not straightforward to extend the RIMAX method for estimation

of parameters of spatially-correlated scattering.

The estimators presented in Section 4.6 assume that the MIMO channel can be modeled as a set of clusters with small angular spread, and the estimated parameters include the mean angle and angular spread of each cluster. Given the assumption of small angular spreads, these methods derive approximate solutions that are based on ML estimation or on the directional estimation methods described in Section 4.3. These methods estimate parameters of stochastic signals that are spatially correlated, which is a different approach compared to the methods discussed until this moment, which either assume only deterministic sources are present, or else it is assumed that the stochastic component of the channel is spatially white. However, the assumption of small angular spreads and well separated sources prevents the application of such methods for estimation of spatially-correlated diffuse scattering component, for example.

Chapter 5

Maximum Likelihood methods for propagation parameter estimation

Deterministic and Stochastic Maximum Likelihood techniques for parameter estimation were described in Chapter 4. In this chapter these methods are applied for parameter estimation in a channel sounding application, where the diffuse scattering component is not assumed to be spatially white.

5.1 Signal Model

Assuming a channel sounding arrangement with M_r antennas at the receiver and M_t antennas at the transmitter, the received signal in frequency-domain is given by

$$\mathbf{y}(f) = \mathbf{u}(f) + \mathbf{n}_d(f) + \mathbf{n}(f), \tag{5.1}$$

where $\mathbf{u}(f)$ represents the specular components of the propagation paths, $\mathbf{n}_d(f)$ represents the diffuse scattering component, and $\mathbf{n}(f)$ represents the zero-mean complex Gaussian measurement noise. The specular components are modeled as in Section 3.2.1, i.e.,

$$\mathbf{u}(f) = \sum_{k=0}^{K-1} \mathbf{u}_k(f) = \sum_{k=0}^{K-1} \gamma_k \mathbf{a}(\theta_{R,k}, \theta_{T,k}) \exp(-j2\pi f \tau_k) s(f), \tag{5.2}$$

where $s(f)$ is the transmitted signal, γ_k is the complex gain, $\mathbf{a}(\theta_{R,k}, \theta_{T,k})$ is the array response to receive azimuth angle $\theta_{R,k}$ and transmit azimuth angle $\theta_{T,k}$, and τ_k is the normalized delay for the k-th specular path $k = 0, \ldots, K-1$. The array response is given

as a function of the receive and transmit array responses, $\mathbf{a}(\theta_{R,k})$ and $\mathbf{a}(\theta_{T,k})$, respectively, as $\mathbf{a}(\theta_{R,k}, \theta_{T,k}) = \mathbf{a}(\theta_{R,k}) \otimes \mathbf{a}(\theta_{T,k})$, where $\otimes$ denotes the Kronecker product.

The excitation signal $s(f)$ is assumed to be a multi-carrier spread spectrum signal (MCSSS) [10], which is designed such that $|s(f)|$ is constant over the bandwidth of interest. Pseudo-noise sequences are also commonly used as excitation signal in channel sounding applications, and an estimation procedure for separate estimation in angular- and delay-domain is presented in Publications I and IV. For the MCSS excitation signal, a raw estimate of the channel observation can be determined without changing the statistics of the noise $\mathbf{n}(f)$, simply by dividing the received samples by the known excitation function $s(f)$. Hence, equation (5.2) can be rewritten as

$$\mathbf{u}(f) = \sum_{k=0}^{K-1} \mathbf{u}_k(f) = \sum_{k=0}^{K-1} \gamma_k \mathbf{a}(\theta_{R,k}, \theta_{T,k}) \exp(-j2\pi f \tau_k). \tag{5.3}$$

Let M_f be the number of observed frequency samples. Similarly to the Section 4.4.3, we define the $M_o \times 1$ vector $\mathcal{Y}$ as

$$\mathcal{Y} = \begin{bmatrix} \mathbf{y}(0) \\ \vdots \\ \mathbf{y}(M_f - 1) \end{bmatrix} = \overline{\mathbf{u}} + \overline{\mathbf{n}}_d + \overline{\mathbf{n}}, \tag{5.4}$$

where $M_o = M_r M_t M_f$, and

$$\overline{\mathbf{u}} = \begin{bmatrix} \mathbf{u}^T(0) & \dots & \mathbf{u}^T(M_f - 1) \end{bmatrix}^T \tag{5.5}$$

$$\overline{\mathbf{n}}_d = \begin{bmatrix} \mathbf{n}_d^T(0) & \dots & \mathbf{n}_d^T(M_f - 1) \end{bmatrix}^T \tag{5.6}$$

$$\overline{\mathbf{n}} = \begin{bmatrix} \mathbf{n}^T(0) & \dots & \mathbf{n}^T(M_f - 1) \end{bmatrix}^T. \tag{5.7}$$

In the formulation above, it is implicitly assumed that the channel sounding technique is such that the received signal in each MIMO subchannel is available. As described in Section 4.1, this can be obtained, e.g., by time division multiplexing.

Deterministic maximum likelihood estimation techniques such as the SAGE-based method in [80] represent the received signal as a combination of a large number of discrete waves. Consequently, parameters from each wave must be estimated. This leads to very high-dimensional parameter space. Hence, the algorithms often have convergence prob-

66

lems and the estimates contain artifacts due to local maxima in the likelihood function and high dimensionality of the parameter space.

The following assumptions are employed throughout this thesis:

(a) the process $\overline{\mathbf{n}}_d$ is zero-mean complex temporally white circular Gaussian;

(b) the channel can be treated as constant during the time it takes to measure one realization of the channel;

(c) the additive noise $\overline{\mathbf{n}}$ is an i.i.d. zero-mean circular complex Gaussian process with known covariance matrix, $\mathbf{R}_n = E[\overline{\mathbf{n}}\,\overline{\mathbf{n}}^H] = \sigma_n^2 \mathbf{I}$, and independent of $\overline{\mathbf{n}}_d$ and $\overline{\mathbf{u}}$.

Assumption (a) comes from the observation that a very large number of waves, having independent weights, reach the receiver from scattered sources. Therefore, the Central Limit Theorem can be used in this case to show that the received data are Gaussian distributed. The covariance matrix of $\overline{\mathbf{n}}_d$ is obtained by writing the DSC as a sum of a very large number of specular-like components, each one modeled similarly to (5.2). Hence, as shown in Publications V and VII, the covariance matrix of $\overline{\mathbf{n}}_d$ is given by

$$E[\overline{\mathbf{n}}_d\,\overline{\mathbf{n}}_d^H] = E[\mathbf{w}\mathbf{w}^H] \otimes E[\mathbf{h}\mathbf{h}^H], \tag{5.8}$$

where vector $\mathbf{h}$ of dimension $M_r M_t \times 1$ represents the spatial content of the DSC and is a function of the array response, and the vector $\mathbf{w}$ of dimension $M_f \times 1$ represents the frequency-dependent content of the DSC.

Based on the assumptions above, the PDF of the received signal $\mathcal{Y}$ is completely characterized by its mean, $E[\mathcal{Y}] = \overline{\mathbf{u}}$, and its $M_o \times M_o$ covariance matrix (see Publication VII)

$$\mathbf{R}_y = E[(\mathcal{Y} - \overline{\mathbf{u}})(\mathcal{Y} - \overline{\mathbf{u}})^H] = \mathbf{R}_w \otimes \mathbf{R}_h + \sigma_n^2 \mathbf{I}, \tag{5.9}$$

where $\mathbf{R}_w = E[\mathbf{w}\mathbf{w}^H]$, and $\mathbf{R}_h = E[\mathbf{h}\mathbf{h}^H]$.

Observe that this model is based on the assumption that the covariance matrix of the DSC can be factorized into a Kronecker-product (5.9). However, it is not assumed that the covariance matrix of the complete MIMO channel observation can be factorized into a Kronecker-product.

5.1.1 Delay and Frequency Domain Characterization

For the delay domain, we use the model in Section 3.2.2, which is based on the observation that the power delay profile (PDP) has an exponential decay over time and a base delay which is related to the distance between the transmitter and receiver. Hence, $\mathbf{w}$ is given by

$$\mathbf{R}_w = \text{toep}\big(\mathbf{v}(\boldsymbol{\Theta}_w), \mathbf{v}(\boldsymbol{\Theta}_w)^H\big), \tag{5.10}$$

where $\boldsymbol{\Theta}_w = \{\gamma, \beta_d, \tau_d\}$, and

$$\mathbf{v}(\boldsymbol{\Theta}_w) = \frac{\gamma}{M_f} \left[\frac{1}{\beta_d} \quad \frac{e^{-j2\pi\tau_d}}{\beta_d + j\frac{2\pi}{M_f}} \quad \cdots \quad \frac{e^{-j2\pi(M_f-1)\tau_d}}{\beta_d + j2\pi\frac{M_f-1}{M_f}} \right]. \tag{5.11}$$

5.1.2 Angular Domain Characterization

The diffuse scattering is characterized by its covariance matrix, and hence we will apply the modeling strategy described in Section 3.4.1 for its angular domain characterization. Assuming that for the diffuse scattering there is statistical independence between DoAs and DoDs, we can use the modeling strategy for the SVA model in Section 3.4.1.2 to characterize the covariance matrix of the channel in angular domain as

$$\mathbf{R}_h = \mathbf{R}_h^R \otimes \mathbf{R}_h^T, \tag{5.12}$$

where $\mathbf{R}_h^R$ and $\mathbf{R}_h^T$ denote the covariance matrix at the receiver and transmitter side, respectively.

From a parameter estimation point of view, the extension from the spatially uncorrelated to the correlated case is more complicated than the extension from SIMO to MIMO, as long as the Kronecker structure in equation (5.12) holds. Hence, we will limit the discussion to uni-directional estimation, but the results can be naturally extended to the double-directional case. We also assume for simplicity that an uniform linear array (ULA) is used at the receiver. Given these assumptions, the correlation at the receiver side is equivalently given by the SVA model in Section 3.4.1.2 and the von Mises distribution model in Section 3.4.1.5. Hence, we can write

$$\mathbf{R}_{h,m_1m_2}(\boldsymbol{\Theta}_h) = \int_{-\pi}^{\pi} \exp(b_{m_1m_2}\cos(\theta))f(\theta, \boldsymbol{\Theta}_h)\,d\theta, \tag{5.13}$$

where $f(\theta, \mathbf{\Theta}_h)$ is any angular PDF of θ, characterized by parameters $\mathbf{\Theta}_h$, $b_{m_1 m_2} = j2\pi d_{m_1 \to m_2}$, and $d_{m_1 \to m_2}$ is the distance between elements m_1 and m_2 in the receive array. An angular PDF must at least satisfy $f(\theta, \mathbf{\Theta}_h) = f(\theta + 2\pi k, \mathbf{\Theta}_h) \ \forall \ k \in \mathbb{Z}$, with $\phi \in [\phi_0, \phi_0 + 2\pi)$, $\phi_0 \in \mathbb{R}$. Hence, a Gaussian PDF which has an infinite support is not suitable. The von Mises distribution [22] defined in angular domain is more appropriate. Moreover, it allows for an analytical solution to equation (5.13), as shown in Section 3.4.1.5.

In channel measurements, multimodal angular PDFs are often found as a result of signals arriving from a number of different clusters. This can be modeled using a mixture of angular PDFs,

$$f(\theta, \mathbf{\Theta}_h) = \sum_{p=1}^{L} \epsilon_p f_p(\theta, \mathbf{\Theta}_{h,p}), \tag{5.14}$$

where L is the number of mixture components, $\sum_{p=1}^{L} \epsilon_p = 1$, ϵ_p are unknown mixture proportions, and $f_p(\theta, \mathbf{\Theta}_{h,p})$ is any valid angular PDF. With this definition of the angular PDF, the angular domain parameters are defined as $\mathbf{\Theta}_h = \{\mathbf{\Theta}_{h,1}, \dots, \mathbf{\Theta}_{h,P}\}$, with $\mathbf{\Theta}_{h,p} = \{\mu_p, \kappa_p, \epsilon_p\}$, $p = 1, \dots, L$. The flexibility of representation given by the mixture model is illustrated in Figure 5.1, where the power angular spectrum estimated based on a mixture of two von Mises PDFs is compared to the power angular spectrum estimated from a single von Mises PDF.

The cross correlation in equation (5.13) is shown in [12] and Publication III to be given by

$$\mathbf{R}_{h,m_1 m_2}(\mathbf{\Theta}_h) = \sum_{p=1}^{L} \epsilon_p \frac{I_0(\{\kappa_p^2 + b_{m_1 m_2}^2 + 2\kappa_p \, b_{m_1 m_2} \cos(\mu_p)\}^{\frac{1}{2}})}{I_0(\kappa_p)}. \tag{5.15}$$

Alternatively, it is possible to model the bi-directional distribution directly based on the generalized von Mises-Fisher distribution [105, 22], which accounts for dispersion in DoA and DoD simultaneously. In [105] the authors present a maximum likelihood estimator based on this distribution, but no closed-form solution to the cross correlation is presented.

5.2 Parameter Estimation

Let us denote by $\mathcal{Y}_m$ the m-th observation of $\mathcal{Y}$, $m = 1, \dots, M_s$. Assuming $\mathcal{Y}$ is circular complex Gaussian and that the realizations $\mathcal{Y}_m$ are i.i.d., we can write the log-likelihood
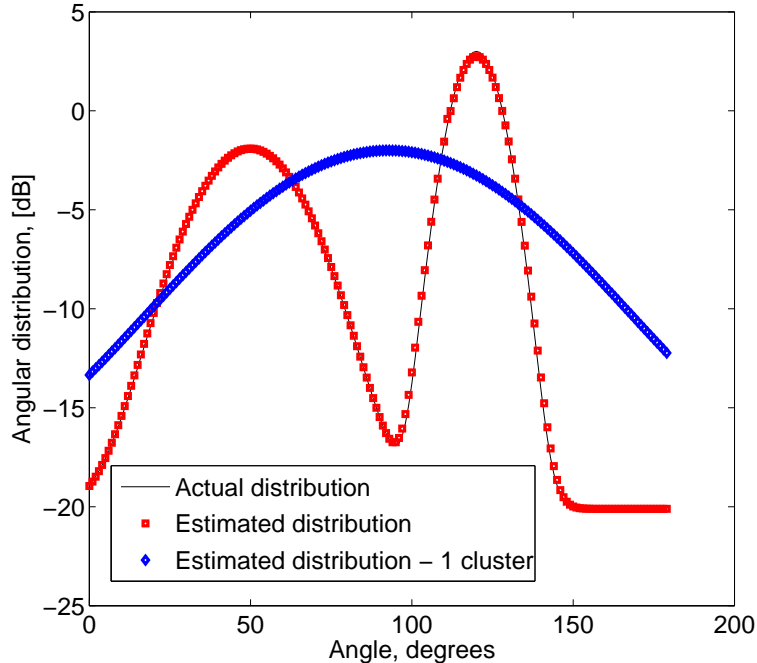
Figure 5.1: Comparison between the power angular spectrum estimated based on a mixture of two von Mises PDFs and the power angular spectrum estimated from a single von Mises PDF.

function as

$$\mathcal{L}(\mathcal{Y}_1, \ldots, \mathcal{Y}_{M_s}) = -M_o M_s \log \pi - M_s \log |\mathbf{R}_y| - \sum_{m=1}^{M_s} (\mathcal{Y}_m - \overline{\mathbf{u}})^H \mathbf{R}_y^{-1} (\mathcal{Y}_m - \overline{\mathbf{u}}), \quad (5.16)$$

where M_s is the number of observations. It is also assumed that the noise is circular complex white Gaussian with variance σ_n^2. The formulation of the problem is similar to the one used in the RIMAX estimator (see Section 4.4.3), except that the diffuse scattering is not assumed to be spatially white. Hence, the structure of the covariance matrix $\mathbf{R}_y$ is changed, and the procedure described in [10] cannot be applied directly. Also, direct optimization of the likelihood function using (5.9) is not feasible due to the high dimensionality of the matrices involved. In current sounding systems, typical values for M_f and M_r, M_t are in the range $M_f = [100, 2000]$, and $M_r, M_t = [4 \cdots 64]$. But with the rapid development of the channel sounders these values may grow. This leads to a dimension of $\mathbf{R}_y$ ranging from 400×400 to 128000×128000, or even higher. Hence, it is not feasible to compute the determinant and matrix inverse in (5.16) directly.

In Publications V and VII, we propose an estimation method that reduces the compu-
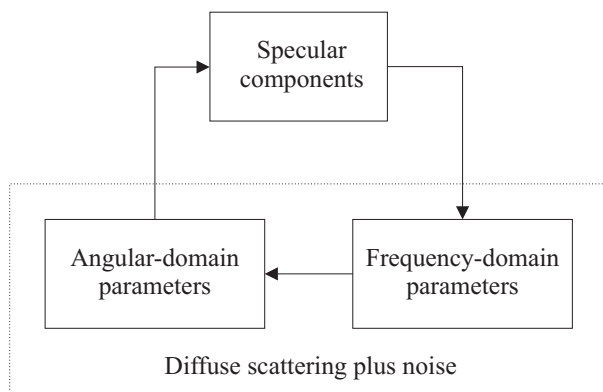
Figure 5.2: Two-step procedure for joint optimization of specular components and diffuse scattering parameters.

tational complexity by using the following iterative procedure:

(1) Optimize for the parameters of the specular components such as azimuth and elevation angle of arrival/departure, time delay, Doppler spread etc., using the previously estimated covariance matrix.

(2) Remove the contribution of the specular components from data and optimize for the covariance matrix of the diffuse scattering components plus noise variance.

(3) Repeat the procedure until convergence or a maximum number of iterations is reached.

Step 2 can be further decomposed into two steps:

(2.a) Optimize for the frequency-domain parameters and noise variance.

(2.b) Optimize for the angular-domain parameters, with $\mathbf{R}_w$ as calculated in the previous step.

This iterative procedure is illustrated in Figure 5.2.

A key benefit of the proposed method is the separate optimization of specular and diffuse scattering components. This reduces the number of variables for each local optimization. This approach is similar to the RIMAX algorithm in Section 4.4.3, where the DSC was assumed to be spatially white.

The further decomposition of step (2) into steps (2.a) and (2.b) is important due to the high dimensionality of the matrices involved. With this two step procedure it is possible to exploit the Toeplitz structure of $\mathbf{R}_w$ for the computation of the ML estimates. Also, the

covariance matrix manipulated in step (2.b) is only $\mathbf{R}_h$, which is typically much smaller in dimension than $\mathbf{R}_w$.

5.2.1 Specular Component

Most algorithms for parameter estimation of specular components described in Chapter 4 assume that any additive noise-like components are white. Hence, they cannot be directly applied to the model used in this paper, unless the covariance matrix of $\bar{\mathbf{n}}_d + \bar{\mathbf{n}}$ is the identity matrix. In order to avoid this problem and allow the use of well-known low complexity algorithms for parameter estimation of specular components, a *prewhitening* transform is applied to the data such that its covariance matrix becomes a constant times the identity matrix [76]. We define the prewhitening matrix $\mathbf{E}$, such that

$$E[(\mathbf{E}^{-H}\mathcal{Y} - \mathbf{E}^{-H}\bar{\mathbf{u}})(\mathbf{E}^{-H}\mathcal{Y} - \mathbf{E}^{-H}\bar{\mathbf{u}})^H] = \mathbf{E}^{-H}(\mathbf{R}_w \otimes \mathbf{R}_h + \sigma_n^2\mathbf{I})\mathbf{E}^{-1} = \mathbf{I}. \qquad (5.17)$$

Therefore, $\mathbf{E}^{-H}\mathcal{Y}$ can be used to estimate the parameters of the specular-alike propagation paths using any well-known algorithm, such as the SAGE-based procedure in [9, 80] (c.f. Section 4.4.1.1).

Matrix $\mathbf{E}$ is any square-root matrix of $\mathbf{R}_y$ such that $\mathbf{R}_y = \mathbf{E}^H\mathbf{E}$. It can be obtained, e.g., by the Cholesky decomposition of $\mathbf{R}_y$, since the presence of additive noise guarantees that $\mathbf{R}_y$ is positive definite. Another possibility to calculate $\mathbf{E}$ is through the eigenvalue decomposition of $\mathbf{R}_y$. The benefits of this implementation over the Cholesky decomposition is that the eigenvalues and eigenvectors of $\mathbf{R}_w$ and $\mathbf{R}_h$ can be used later on to simplify the estimator of the diffuse scattering component. Moreover, it will be shown in the next section that the computation of $\mathbf{V}_w^H$ and its multiplication by a vector can be done in a very efficient way. In Publications V and VII it is shown that $\mathbf{E}^{-H}$ can be defined as

$$\mathbf{E}^{-H} = (\mathbf{\Lambda}_w \otimes \mathbf{\Lambda}_h + \sigma_n^2\mathbf{I})^{-1/2}(\mathbf{V}_w^H \otimes \mathbf{V}_h^H), \qquad (5.18)$$

where $\mathbf{\Lambda}_w$ and $\mathbf{V}_w$ contain the eigenvalues and eigenvectors of $\mathbf{R}_w$, respectively, and $\mathbf{\Lambda}_h$ and $\mathbf{V}_h$ contain the eigenvalues and eigenvectors of $\mathbf{R}_h$, respectively. A computationally efficient computation of the product $\mathbf{E}^{-H}\mathcal{Y}$ is given in Publications V and VII.

5.2.2 Frequency-Domain Parameters

In the sequel we will assume that the specular components have been estimated and removed from the observation. Hence, the likelihood function is given by

$$\mathcal{L}(\mathcal{Y}_1, \ldots, \mathcal{Y}_{M_s}) = -M_o M_s \log \pi - M_s \log |\mathbf{R}_y| - \sum_{m=1}^{M_s} \mathcal{Y}_m^H \mathbf{R}_y^{-1} \mathcal{Y}_m. \qquad (5.19)$$

An estimator for the frequency-domain parameters is derived in [10]. It is assumed that the channel covariance matrix has the structure $\mathbf{R}_y = (\mathbf{R}_w + \sigma_n^2 \mathbf{I}) \otimes \mathbf{I}$, i.e., the channel is assumed to be spatially white. This is a special case of the situation expressed in equation (5.15), with $L = 1$ and $\kappa = 0$. Since we do not assume whiteness in the spatial domain, the method in [10] is not directly applicable here.

Using the decomposition of the estimation procedure outlined in Section 5.2 already allows some simplification in the optimization. This is due to lower dimensional searches. However, we still have not solved the problem of calculating the determinant and inverse of $\mathbf{R}_y$ at every iteration. These computations can be simplified by writing $\mathbf{R}_y$ as a function of its eigenvalues and eigenvectors, as in Section 5.2.1.

We can exploit the Kronecker structure of the eigenvalues and eigenvectors of $\mathbf{R}_y$ in order to simplify the optimization procedure. The logarithm of the determinant of $\mathbf{R}_y$ can be calculated as

$$\log |\mathbf{R}_y| = \sum_{j=1}^{M_o} \log \left((\boldsymbol{\lambda}_w \otimes \boldsymbol{\lambda}_h + \sigma_n^2 \mathbf{1}_{M_o})_{\{j\}} \right),$$

where $\boldsymbol{\lambda}_w$ and $\boldsymbol{\lambda}_h$ are vectors containing the eigenvalues of $\mathbf{R}_w$ and $\mathbf{R}_h$, respectively, $\mathbf{1}_{M_o}$ is a $M_o \times 1$ vector whose entries are equal to 1, and $(\cdot)_{\{j\}}$ denotes the j-th element of $(\cdot)$. It is clear that the computational complexity of calculating the determinant is reduced. Another important observation is that the exchange of the order in which the log is computed allows for easier implementation with finite precision. This is due to the fact that the eigenvalues $\boldsymbol{\lambda}_w$ can have a large spread, since they are an approximation to the PDP in (3.4). The computation of $\mathbf{R}_y^{-1}$ can also be simplified using the Kronecker structure of the eigenvalues and eigenvectors of $\mathbf{R}_y$ (see Publication V).

Further simplifications are possible if we take into account that $\mathbf{R}_h$ is fixed while optimizing for $\mathbf{R}_w$. In this case, the estimate of $\mathbf{R}_w$ is obtained from the likelihood

function of the transformed signal

$$\overline{\mathcal{Y}}_m = (\mathbf{I}_{M_f} \otimes \boldsymbol{\Lambda}_h^{-1/2} \mathbf{V}_h^H) \mathcal{Y}_m, \tag{5.20}$$

where it is assumed that $\mathbf{R}_h$ is nonsingular. A computationally efficient form for the likelihood function of $\overline{\mathcal{Y}}_m$ is given in Publication VII).

Even further reduction of complexity is possible in the calculation of the eigenvalues and eigenvectors of $\mathbf{C}_w$ since it is a large Toeplitz matrix. Consequently, it can be approximated by a circulant matrix [106, 107]. A circulant matrix can be diagonalized as

$$\mathbf{R} = \mathbf{F}\mathbf{D}\mathbf{F}^H, \tag{5.21}$$

where $\mathbf{F}$ is the unitary DFT matrix and $\mathbf{D}$ is a diagonal matrix with the eigenvalues of $\mathbf{R}$. Hence, the eigenvectors and eigenvalues of $\mathbf{R}$ are given by $\mathbf{V}_w = \mathbf{F}$, and $\boldsymbol{\Lambda}_w = \mathbf{F}^H \mathbf{R}\mathbf{F}$, respectively. In case M_o is a power of 2, the computational complexity of $\boldsymbol{\Lambda}_w$ and $\overline{\mathcal{Y}}_m$ in (5.20) can be reduced even further by using FFT. For other values of M_o, other algorithms that optimize the computation of the DFT can be used, like the Goertzel algorithm. There is no need to compute the off-diagonal elements of $\mathbf{F}^H \mathbf{R}_w \mathbf{F}$, and we use the following computationally efficient mapping from $\mathbf{v}(\boldsymbol{\Theta}_w)$ to $\boldsymbol{\lambda}_w$ [10]:

$$\boldsymbol{\lambda}_w = T(\mathbf{v}(\boldsymbol{\Theta}_w)) = \frac{1}{\sqrt{M_f}} \mathbf{F}^H (\mathbf{W}_1 \mathbf{v}(\boldsymbol{\Theta}_w) + \mathbf{W}_2 \mathbf{v}^*(\boldsymbol{\Theta}_w)), \tag{5.22}$$

where

$$\mathbf{W}_1 = \mathrm{diag}(\begin{bmatrix} M_f & M_f - 1 & \cdots & 1 \end{bmatrix}) \tag{5.23}$$

and

$$\mathbf{W}_2 = \begin{bmatrix} 0 & & \cdots & & 0 \\ & & & \iddots & 1 \\ \vdots & & 0 & 2 & 0 \\ & \iddots & \iddots & \iddots & \vdots \\ 0 & M_f - 1 & 0 & \cdots & 0 \end{bmatrix}. \tag{5.24}$$

5.2.3 Angular-Domain Parameters

In Section 5.1.2, the covariance matrix in angular domain, $\mathbf{R}_h$, was modeled as a function of a mixture of von Mises distributions. Assuming the number of mixture components

in angular domain, L, is known or reliably estimated, the angular parameters are the parameters of the mixture of von Mises distributions: $\boldsymbol{\Theta}_h = \{\mu_1, \kappa_1, \epsilon_1, \ldots, \mu_L, \kappa_L, \epsilon_L\}$, $p = 1, \ldots, L$, with $\sum_{p=1}^{L} \epsilon_p = 1$. Due to the model in (5.9), the path loss is already estimated as part of the delay-domain parameters.

For the estimation of the angular domain parameters, we assume that the frequency-domain parameters are fixed. The computational complexity can be simplified as in Section 5.2.2, by maximizing the likelihood function of the transformed signal

$$\widetilde{\mathcal{Y}}_m = (\boldsymbol{\Lambda}_w^{-1/2} \mathbf{F}^H \otimes \mathbf{I}_{M_r M_t}) \mathcal{Y}_m, \tag{5.25}$$

where it is assumed that $\mathbf{R}_w$ is nonsingular. A computationally efficient form for the likelihood function of $\widetilde{\mathcal{Y}}_m$ is given in Publication VII).

The optimization of the nonlinear likelihood functions of (5.20) and (5.25)´can be performed using the Levenberg-Marquardt algorithm [108]. It requires the computation of the gradient and an approximation of the Hessian, which can be found in Publication VII. Moreover, the derivatives presented in Publication VII are used for the derivation of the performance bounds in Section 5.3. Efficient implementations of the gradient and the approximate Hessian can be found in Publication VII.

5.2.4   Initialization

In this section we describe one approach for the initialization of the algorithm. The specular paths are initialized assuming $\mathbf{R}_y = \mathbf{I}$. Well-known estimators available in the literature, like those described in Chapter 4, can be used to get initial estimates for the parameters of the specular paths.

For the diffuse scattering, the frequency-domain parameters are initialized as in the RIMAX algorithm [10], and assuming $\mathbf{R}_h = \mathbf{I}$.

The angular-domain parameters can be initialized using the following procedure:

(1) Get initial estimate for μ_p, $p = 0, \ldots, L - 1$, using ESPRIT assuming L sources.

(2) Choose initial values for κ_p, $p = 0, \ldots, L - 1$, uniformly drawn from the interval $[0, 50]$, and ϵ_p, $p = 0, \ldots, L - 1$, randomly in the range $[0, 1]$.

(3) Refine the initial estimates using the method in Publications III and IV, with $\mathcal{Y}$

75

normalized by

$$P_y = \frac{\gamma}{\beta_d} e^{\beta_d \tau_d}.$$

If an arbitrary 2-D or 3-D antenna element arrangement is used, beamforming or ES-root MUSIC [85] can be applied in step (1).

5.2.5 Computational Complexity

The computational complexity of the algorithm is evaluated in terms of real multiplications. We assume the multiplication of two complex numbers corresponds to four real multiplications, and the multiplication of a complex and a real number corresponds to two real multiplications. Figure 5.3 shows the computational complexity as a function of the number of frequency samples, M_f, assuming 20 evaluations of the cost function during the optimization, and that 3 cycles of the estimation procedure are used. We assume that only the diffuse components are estimated. The complexity of calculating the eigendecomposition of $\mathbf{R}_h$ is of order $\mathcal{O}((M_t M_r)^3)$ [109]. The exact number of multiplications depends on the matrix structure, but the order $\mathcal{O}((M_t M_r)^3)$ remains. Conditioning of the matrix plays a role as well.

Figure 5.3 illustrates the complexities of different solutions. It is clear that the optimized method reduces the complexity by several orders of magnitude compared to the maximum likelihood estimation, especially if FFTs are used when multiplying by $\mathbf{V}_w$.

The effectiveness of this reduction depends on the number of cycles. A reasonable criterion for convergence is to stop the algorithm if after any two iterations the relative change for all parameters is less than a pre-defined threshold, e.g., 10^{-2}. For this threshold value, the parameters usually converge in less than 5 iterations for all versions of the algorithm.

5.3 Performance Bounds

The $\{i, k\}$-th element of the Fisher Information Matrix (FIM) for a circular complex white Gaussian variable are given by [76]

$$\boldsymbol{\mathcal{I}}_{ik} = M_s 2\Re\left\{ \left(\frac{\partial \overline{\mathbf{u}}^H}{\partial \Theta_i} \right) \mathbf{R}_y^{-1} \left(\frac{\partial \overline{\mathbf{u}}}{\partial \Theta_k} \right) \right\} + M_s \mathrm{tr}\left\{ \mathbf{R}_y^{-1} \left(\frac{\partial \mathbf{R}_y}{\partial \Theta_i} \right) \mathbf{R}_y^{-1} \left(\frac{\partial \mathbf{R}_y}{\partial \Theta_k} \right) \right\}. \quad (5.26)$$
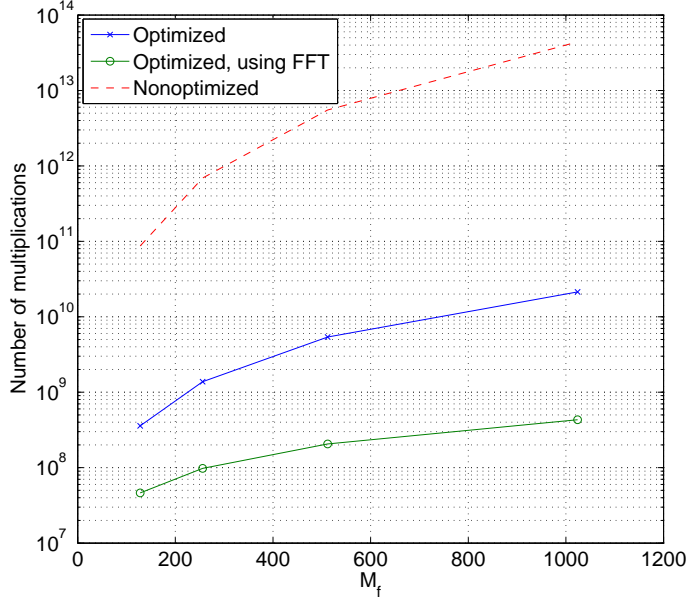
Figure 5.3: Comparison of computational complexity of direct optimization of likelihood function and the optimized algorithm as a function of the number of frequency samples, M_f. The optimized method reduces the complexity by several orders of magnitude compared to the maximum likelihood estimation, especially if FFT is used when multiplying by $\mathbf{V}_w$.

Hence, the FIM is block diagonal if $\boldsymbol{\Theta}_{\mathrm{sp}}$ and $\boldsymbol{\Theta}_{dn}$ contain uncorrelated parameters, i.e.,

$$\boldsymbol{\mathcal{I}} = \begin{bmatrix} \boldsymbol{\mathcal{I}}(\boldsymbol{\Theta}_{\mathrm{sp}}) & \mathbf{0} \\ \mathbf{0} & \boldsymbol{\mathcal{I}}(\boldsymbol{\Theta}_{dn}) \end{bmatrix}, \tag{5.27}$$

where $\boldsymbol{\mathcal{I}}(\boldsymbol{\Theta}_{\mathrm{sp}})$ is the FIM for the specular components, $\boldsymbol{\Theta}_{dn} = \{\boldsymbol{\Theta}_{wn}, \boldsymbol{\Theta}_h\}$, and $\boldsymbol{\mathcal{I}}(\boldsymbol{\Theta}_{dn})$ is the FIM for the diffuse scattering parameters plus noise variance. As a consequence, its inverse is also block diagonal [109]. This means that the parameters of the specular and diffuse components are asymptotically decoupled, and the respective CRLBs can be derived independently. The CRLB for the parameters of the specular components can be found in [9, 10]. The CRLB for the parameters of the diffuse scattering components is given by (5.26) as

$$\boldsymbol{\mathcal{I}}_{ik}(\boldsymbol{\Theta}_{dn}) = M_f \mathrm{tr}\left\{\mathbf{R}_y^{-1}\left(\frac{\partial \mathbf{R}_y}{\partial \Theta_i}\right)\mathbf{R}_y^{-1}\left(\frac{\partial \mathbf{R}_y}{\partial \Theta_k}\right)\right\}. \tag{5.28}$$

Let us define the matrices containing the partial derivatives with respect to all N_p

77

elements of the parameter vector $\boldsymbol{\Theta}_{dn}$, as

$$\mathbf{D}_1 = \left[\text{vec} \left\{ \left(\mathbf{R}_y^{-1} \left(\frac{\partial \mathbf{R}_y}{\partial (\boldsymbol{\Theta}_{dn})_1} \right) \right)^T \right\} \quad \cdots \quad \text{vec} \left\{ \left(\mathbf{R}_y^{-1} \left(\frac{\partial \mathbf{R}_y}{\partial (\boldsymbol{\Theta}_{dn})_{Np}} \right) \right)^T \right\} \right] \tag{5.29}$$

$$\mathbf{D}_2 = \left[\text{vec} \left\{ \mathbf{R}_y^{-1} \left(\frac{\partial \mathbf{R}_y}{\partial (\boldsymbol{\Theta}_{dn})_1} \right) \right\} \quad \cdots \quad \text{vec} \left\{ \mathbf{R}_y^{-1} \left(\frac{\partial \mathbf{R}_y}{\partial (\boldsymbol{\Theta}_{dn})_{Np}} \right) \right\} \right]. \tag{5.30}$$

Using (5.29) and (5.30), the FIM can be expressed in a compact form as

$$\mathcal{I} = M_s \mathbf{D}_1^T \mathbf{D}_2 \tag{5.31}$$

The partial derivatives of $\mathbf{R}_y$ with respect to the diffuse scattering component parameters is given by

$$\frac{\partial \mathbf{R}_y}{\partial \Theta_i} = \frac{\partial \mathbf{R}_w}{\partial \Theta_i} \otimes \mathbf{R}_h, \qquad \Theta_i \in \boldsymbol{\Theta}_w \tag{5.32}$$

$$\frac{\partial \mathbf{R}_y}{\partial \theta_i} = \mathbf{R}_w \otimes \frac{\partial \mathbf{R}_h}{\partial \Theta_i}, \qquad \Theta_i \in \boldsymbol{\Theta}_h \tag{5.33}$$

$$\frac{\partial \mathbf{R}_y}{\partial \sigma_n^2} = \mathbf{I}. \tag{5.34}$$

The partial derivatives of $\mathbf{R}_w$ and $\mathbf{R}_h$ with respect to the propagation parameters can be found in Publication VII.

5.4 Simulation Results

In this Section simulation examples are presented in order to illustrate the performance of the described parameter estimation procedure. The receiver is equipped with an ULA having $M_r = 8$ antennas and the transmitter uses $M_t = 1$ antenna. The number of frequency points is $M_f = 128$, and the number of channel realizations is $M_s = 5$. For the frequency-domain parameters, typical values often observed in channel sounding experiments are used: $\sigma_n^2 = 0.1$, $\gamma = 1$, $\beta_d = 0.07$, and $\tau_d = 0.1$. The angular-domain parameters are defined as $\mu = \{60°, 120°\}$, $\kappa = \{10, 50\}$, $\epsilon = \{0.4, 0.6\}$, corresponding to two clusters in the angular domain.

One specular component is assumed to be present, and it is modeled as

$$\mathbf{u}(k) = \gamma \mathbf{a}(\theta_R) \exp(-j2\pi k\tau), \tag{5.35}$$

where γ is the complex gain, $\mathbf{a}(\theta_R)$ is the steering vector for receive azimuth angle θ_R,

and τ is the normalized delay. For the simulation, the values are set as $\gamma = 0.8e^{j*\pi/5}$, $\theta_R = 80°$, and $\tau = 0.12$.

The received signal is generated as

$$\mathbf{y}(k) = \mathbf{u}(k) + \mathbf{R}^{1/2}\mathbf{n}_2(k) + \mathbf{n}(k), \tag{5.36}$$

where $\mathbf{n}_2(k)$ is a circular complex white Gaussian process and $\mathbf{R}^{1/2}$ is obtained by the Cholesky decomposition of $\mathbf{R}_w \otimes \mathbf{R}_h$. This implies that the covariance matrix of $\mathbf{R}^{1/2}\mathbf{n}_2(k)$ is given by $\mathbf{R}_w \otimes \mathbf{R}_h$. The vector $\mathbf{n}(k)$ is a circular complex white Gaussian process representing the measurement noise.

The iterative procedure described in Section 5.2 is repeated 5 times, starting with the estimation of the specular component and proceeding as illustrated in Figure 5.2. The model order, i.e., number of clusters and specular paths, is assumed known. The frequency-domain parameters are computed using the approximation of a Toeplitz matrix as a circulant matrix described in Section 5.2.2. The parameters are initialized as described in Section 5.2.4. In Figures 5.4 and 5.5, we compare the power delay profile (PDP) and power angular profile (PAP) obtained using the estimation procedure described in this article with the actual PDP and PAP, respectively. The curves overlap almost perfectly. In the example, $M_s \ll M_o$, i.e., the full sample covariance matrix is rank deficient. Still, the estimator is able to provide high-precision estimates for the time-delay distribution, angular distribution, and specular component. The PAP is compared to the output of the Bartlett beamformer, showing the gain in using the combined procedure to estimate both signal components iteratively. The beamformer is only able to estimate the angle of the specular component, but it does not provide any useful information about the diffuse scattering component.

The algorithms that approximate the mean angle and angular variance using two separate paths around the mean are called *Spread F* [16], where F denotes the underlying algorithm to estimate the paths. Table 5.1 shows the estimates obtained using the proposed method and Spread ESPRIT [16]. The results are an average over 300 runs. The parameters of the DSC and specular components are the same as in the previous simulation. The angular spread is shown in degrees using the mapping $\sigma_\mu \approx \kappa^{-1/2}$ [22]. Hence, for the simulated values of $\kappa = \{10, 50\}$ we obtain $\sigma_\mu = \{18.12°, 8.10°\}$.

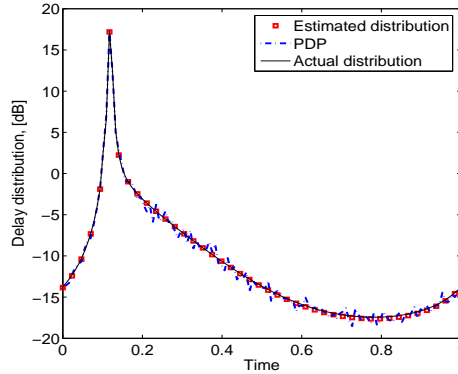The estimator proposed in this paper overperforms Spread ESPRIT for all parameters

Figure 5.4: Comparison of estimated power delay profile and actual power delay profile. The curves overlap almost perfectly. The specular component is identified as a sharp peak at $\tau_d = 0.12$, while the diffuse component corresponds to the exponential curve.
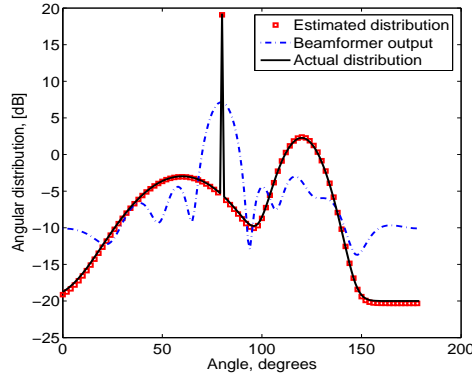

Figure 5.5: Comparison of estimated power angular profile and actual power angular profile. The curves overlap almost perfectly. Also shown is the output of the Bartlett beamformer. The specular component is identified as a sharp peak at $\theta = 80°$, while the diffuse component corresponds to the mixture of von Mises distributions.

of the diffuse component, while presenting similar performance for the specular component. One problem for the application of the Spread F techniques is that it is very difficult in a real-world environment to identify which of the identified waves belong to a distributed scatterer in particular and which one is a specular component. This issue limits the application of Spread F techniques to well separated sources with small angular spread, as already noted in [16].

In Figures 5.6–5.10, we compare the MSE of the estimates after two cycles with the CRLB as a function of the number of channel realizations, M_s. The angular-domain parameters are set to $\theta = \{50°, 100°\}$, $\kappa = \{5, 150\}$, $\epsilon = \{0.4, 0.6\}$, corresponding to two clusters in the angular domain. The frequency-domain parameters remain unchanged. No specular components are present. It can be observed that all parameters converge close to

Table 5.1: Comparison between the proposed method and Spread ESPRIT

	Correct values	Proposed method	Spread ESPRIT
μ_1	$60°$	$59.98°$	$56.66°$
$\sigma_{\mu,1}$	$18.12°$	$18.14°$	$9.20°$
μ_2	$120°$	$119.99°$	$119.15°$
$\sigma_{\mu,2}$	$8.10°$	$8.07°$	$3.09°$
θ	$80°$	$79.99°$	$79.97°$
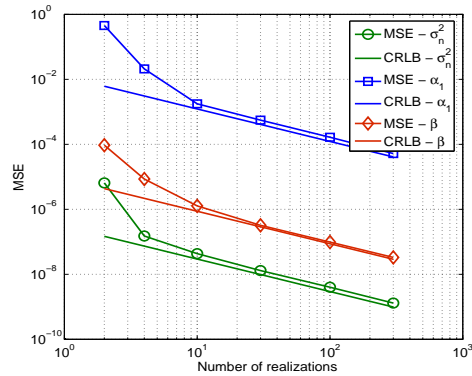
Figure 5.6: CRLB of frequency-domain parameters $\{\gamma, \beta_d\}$ and noise variance as a function of the number of channel realizations, M_s. The MSE after two iterations of the estimation procedure is shown for comparison.

the CRLB for relatively small sample size. The exception is the relative delay, τ_d, which presents a noticeable gap with respect to its CRLB. However, no bias is observed, since the curve is parallel to the CRLB.

In order to verify the robustness of the algorithm, we apply the estimator to data that do not follow exactly the assumptions used for its derivation. We generate the data as a
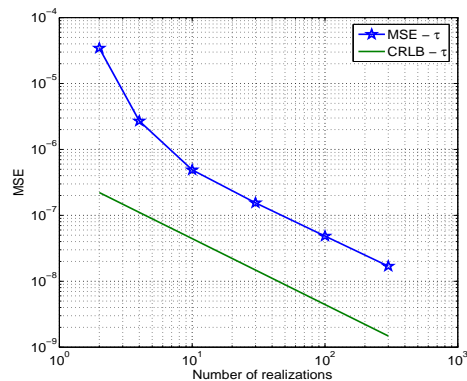

Figure 5.7: CRLB of base delay as a function of the number of channel realizations, M_s. The MSE after two iterations of the estimation procedure is shown for comparison.
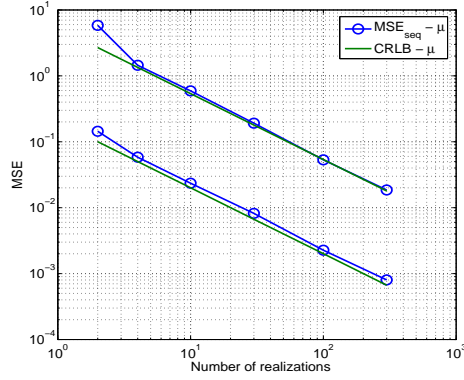
Figure 5.8: CRLB of mean angle as a function of the number of channel realizations, M_s. The MSE after two iterations of the estimation procedure is shown for comparison.
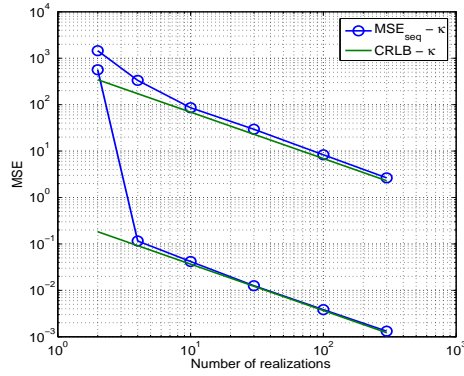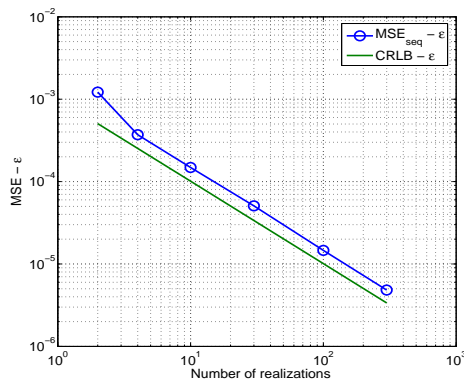

Figure 5.9: CRLB of dispersion parameter as a function of the number of channel realizations, M_s. The MSE after two iterations of the estimation procedure is shown for comparison.

Figure 5.10: CRLB of mixture proportion of the first angular cluster as a function of the number of channel realizations, M_s. The MSE after two iterations of the estimation procedure is shown for comparison. The maximum number of mixture components is assumed to be known.
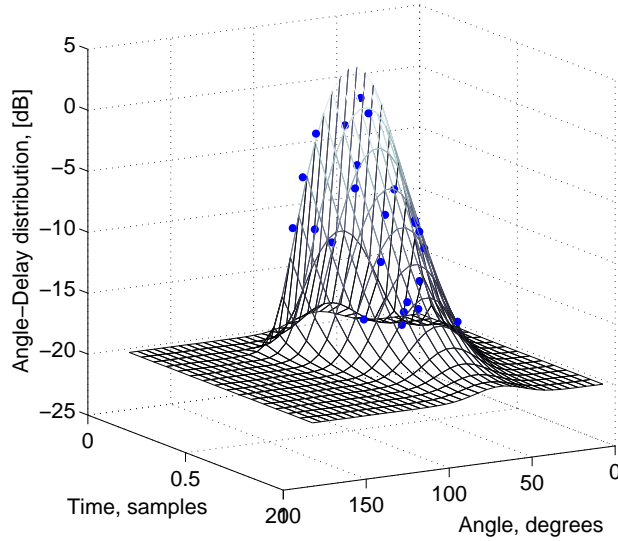
Figure 5.11: Estimated joint angle-delay distribution and the actual individual paths used to generate the data, denoted by the dots. The estimated distributions provide a good fit for the data.

sum of individual propagation paths,

$$\mathbf{y}(k) = \sum_{l=1}^{L_1} \mathbf{u}_l(k) + \mathbf{n}(k), \tag{5.37}$$

where L_1 is the number of individual paths, and $\mathbf{u}_l(k)$ are defined as in (5.2). For this simulation, we use $L_1 = 24$, the noise variance is 0.01, and $M_s = 4$. Convergence is achieved after 4 iterations, assuming the parameters converge after changing by less than 5×10^{-3}. The specular paths are not estimated individually, but rather the joint angle-delay distribution of diffuse scattering is used to characterize the data, assuming $L = 1$. Figure 5.11 shows the estimated joint angle-delay distribution and the individual paths used for generating the data. It can be observed that the estimated distributions provide a good fit for the data.

5.5 Search for New Specular Paths

In this section, we propose a procedure for detection and estimation of parameters of specular paths that is based on the estimator described in Section 5.2. The proposed method is particularly useful for the estimation of specular paths with low power, which may not be easily distinguished from distributed scattering by techniques based on deterministic mod-
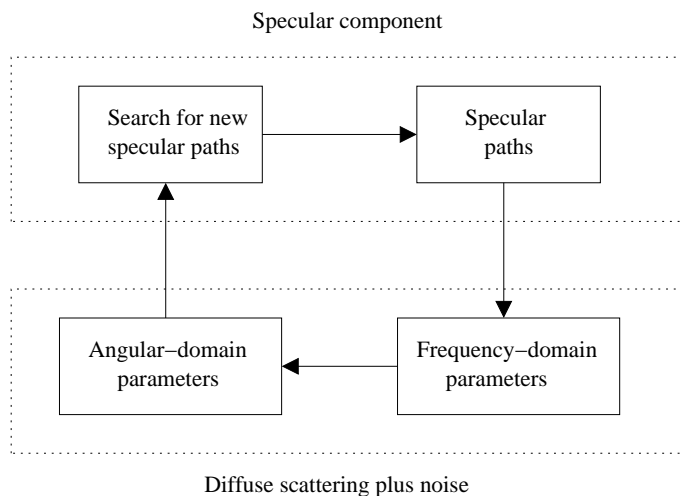
Specular component

Figure 5.12: Iterative procedure for joint optimization of specular component and diffuse scattering parameters, including the search for new specular paths.

els. Typically, such techniques require a large number of discrete waves to be estimated in order to characterize the channel, and it is not straightforward to identify which of the estimated waves are actual specular paths and which are an attempt to describe the diffuse component. The estimator described in Section 5.2 assumes a stochastic model, where the DSC is modeled by a random process. Hence, the specular paths can be easily identified as the deterministic part of the model, while the DSC corresponds to the stochastic part. Moreover, this model requires a reduced set of parameters to be estimated, which usually results in estimates with lower variance. Figure 5.12 shows how the procedure for searching new paths is inserted into the estimator described in Section 4.3.2.

It is assumed that at least one iteration of the estimator described in Section 5.2 has been executed. Hence, an estimate of the strongest specular paths is assumed to be available, as well as an estimate of the diffuse scattering component. We estimate the new specular paths following the approach in Section 5.2.1, where the data is multiplied by a pre-whitening transformation.

Vector $\overline{\mathbf{u}}$ can be written as (see Publication VI)

$$\overline{\mathbf{u}} = \sum_{k=0}^{K-1} \gamma_k \mathbf{c}(\tau_k) \otimes \mathbf{a}(\theta_{R,k}, \theta_{T,k}), \qquad (5.38)$$

where the $M_f \times 1$ vector $\mathbf{c}(\tau)$ is defined as

$$\mathbf{c}(\tau) = \begin{bmatrix} 1 & e^{-j2\pi\tau} & \cdots & e^{-j2\pi(M_f-1)\tau} \end{bmatrix}^T. \qquad (5.39)$$

84

Let us also define

$$\mathbf{B}(\tau, \theta_R, \theta_T) = (\mathbf{\Lambda}_w \otimes \mathbf{\Lambda}_h + \sigma_n^2 \mathbf{I})^{-\frac{1}{2}} (\mathbf{V}_w^H \mathbf{c}(\tau) \otimes \mathbf{V}_h^H \mathbf{a}(\theta_R, \theta_T)). \qquad (5.40)$$

The ML estimates for a single wave are then given by

$$\{\widehat{\tau}, \widehat{\theta}_R, \widehat{\theta}_T\} = \arg \max_{\tau, \theta_R, \theta_T} \frac{|\sum_{m=1}^{M_s} \mathbf{B}^H(\tau, \theta_R, \theta_T) \mathcal{Y}_m'|^2}{|\mathbf{B}(\tau, \theta_R, \theta_T)|^2}, \qquad (5.41)$$

and

$$\widehat{\gamma} = \frac{\sum_{m=1}^{M_s} \mathbf{B}^H(\widehat{\tau}, \widehat{\theta}_R, \widehat{\theta}_T) \mathcal{Y}_m'}{M_s |\mathbf{B}(\widehat{\tau}, \widehat{\theta}_R, \widehat{\theta}_T)|^2}. \qquad (5.42)$$

Based on the initialization procedure proposed in [9, 80], the search in equation (5.41) can be further simplified. First, the base delay is estimated as

$$\widehat{\tau} = \arg \max_\tau \frac{|\sum_{m=1}^{M_s} \overline{\mathbf{B}}^H(\tau) \mathcal{Y}_m'|^2}{|\overline{\mathbf{B}}(\tau)|^2}, \qquad (5.43)$$

where $\overline{\mathbf{B}}(\tau) = (\mathbf{c}_\tau^H \mathbf{V}_w \otimes \mathbf{1}^H \mathbf{V}_h)(\mathbf{\Lambda}_w \otimes \mathbf{1} + \sigma_n^2 \mathbf{I})^{-1/2}$, and $\mathbf{1} = [1 \cdots 1]^T$. With the estimated $\widehat{\tau}$, the angular parameters are estimated as

$$\widehat{\theta}_R = \arg \max_{\theta_R} \frac{|\sum_{m=1}^{M_s} \mathbf{B}^H(\widehat{\tau}, \theta_R, \theta_T) \mathcal{Y}_m'|^2}{|\mathbf{B}(\widehat{\tau}, \theta_R, \theta_T)|^2}, \qquad (5.44)$$

and

$$\widehat{\theta}_T = \arg \max_{\theta_T} \frac{|\sum_{m=1}^{M_s} \mathbf{B}^H(\widehat{\tau}, \theta_R, \theta_T) \mathcal{Y}_m'|^2}{|\mathbf{B}(\widehat{\tau}, \widehat{\theta}_R, \theta_T)|^2}. \qquad (5.45)$$

The main advantage of this approach is that only 1-D searches are performed, hence reducing the computational complexity. However, the 1-D searches are suboptimal, and the detection performance is reduced compared to the full search in (5.41).

5.5.1 Application to Detection of Weak Specular Paths

An example application of the procedure above is the detection of weak specular paths that would otherwise be neglected. In a MIMO radar, this would imply the detection of a target that would otherwise be neglected. The application is illustrated by the following simulation results. Parameters for DSC and noise are the same ones used in Section 5.4.
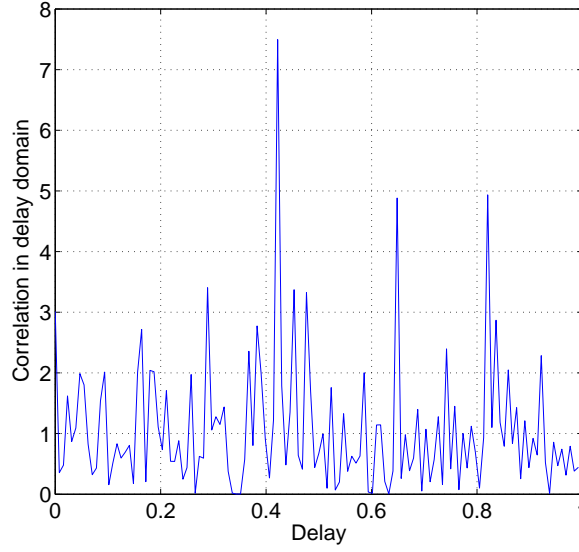
Figure 5.13: Output of the 1-D correlation for the estimate of τ. The strongest specular path can be identified.

Two specular paths are present, and modeled as

$$\mathbf{u}(f) = \sum_{k=0}^{1} \gamma_k \mathbf{a}(\theta_{R,k}) \exp(-j2\pi f \tau_k), \tag{5.46}$$

where γ_k is the complex gain, $\mathbf{a}(\theta_{R,k})$ is the steering vector for receive azimuth angle $\theta_{R,k}$, and τ_k is the normalized delay. For the simulation, the values are set as $\gamma_k = \{0.2e^{j*\pi/5}, 0.02e^{j*\pi/3}\}$, $\theta_{R,k} = \{80°, 150°\}$, and $\tau_k = \{0.12, 0.42\}$. The received signal is generated as in Section 5.4.

Figures 5.13 and 5.14 show the output of the 1-D correlations in (5.43) and (5.44). The second specular path can be clearly identified and its parameters can be estimated. Finally, Figures 5.15 and 5.16 show the power delay profile (PDP) and power angular profile (PAP) obtained using the estimation procedure described in this article, and compares them to the actual PDP and PAP, respectively. The curves overlap almost perfectly.
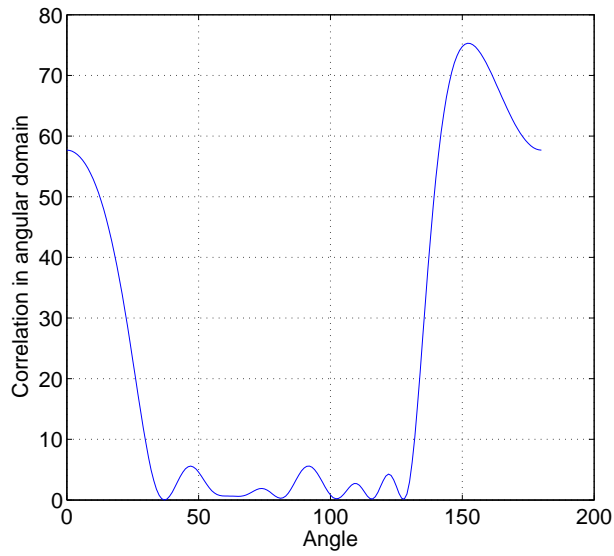
Figure 5.14: Output of the 1-D correlation for the estimate of $\theta_{R,1}$, using previously estimated $\widehat{\tau}$.
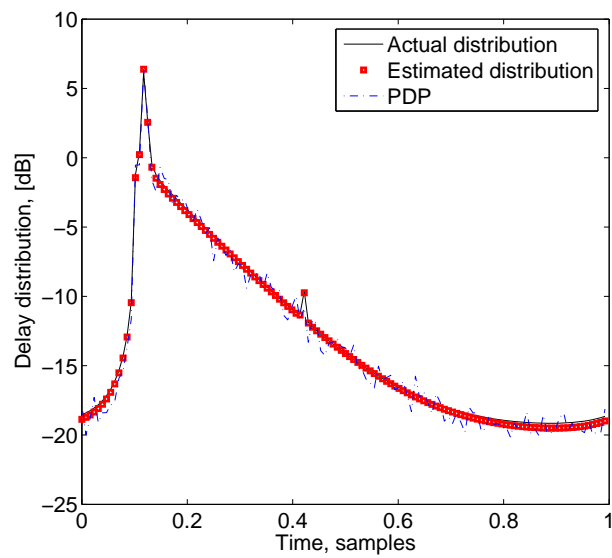

Figure 5.15: Comparison of estimated power delay profile and actual power delay profile. The curves overlap almost perfectly.
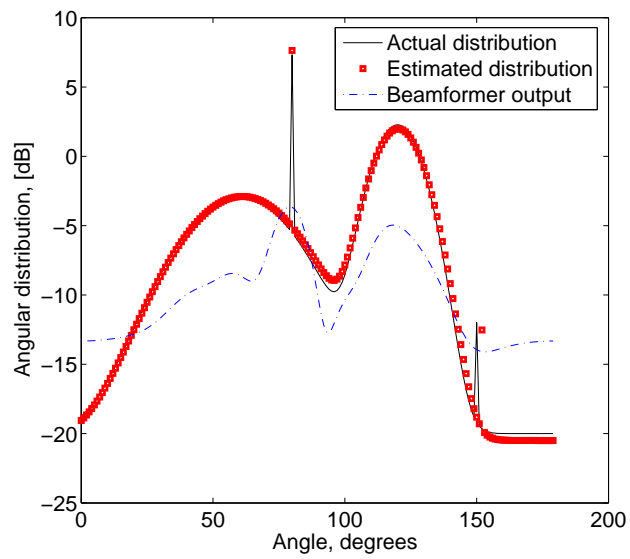
Figure 5.16: Comparison of estimated power angular profile and actual power angular profile. The curves overlap almost perfectly. Also shown is the output of the Bartlett beamformer.

Chapter 6

Summary

Multiple antenna techniques are a key enabling technology in modern and next-generation wireless communications systems. Such techniques are considered for the high link capacity gains that are achievable from spatial multiplexing, but also for the system capacity benefits, improved link reliability, and extended range that are possible from spatial diversity, beamforming, spatial division multiple access, and interference cancellation techniques. In fact, the very demanding performance targets set for next-generation systems are virtually impossible to achieve without an efficient utilization of multiple antennas both at transmitter and receiver side.

Accurate channel models are important tools for the development of techniques that exploit the MIMO channel efficiently, and are fundamental tools in network planning, link- and system-level studies, MIMO radar, and transceiver development. Realistic models are developed with the aid of MIMO channel measurements, which require high-precision parameter estimation techniques to extract the information on the propagation environment. In particular, the spatial information is of interest in MIMO measurement campaigns.

Most estimation algorithms are based on the assumption that the channel can be modeled as a combination of rays that travel from the transmitter to the receiver reflecting on objects scattered around the environment. Such models usually require a large number of rays to characterize the environment, leading to very high-dimensional models. As a consequence, estimation algorithms based on such models become highly complex as well. Hence, it is important to condense the relevant information to a few parameters. A powerful way to solve this problem and obtain models with only a few parameters is to utilize a stochastic model instead of a deterministic model.

Such a model is suitable to describe diffuse scattering, which is the part of the received

signal that cannot be resolved into distinct specular paths. It should be noted that diffuse scattering is a significant part of the rich scattering that gives diversity and multiplexing gains in MIMO systems.

In this thesis, estimation methods are derived that jointly estimate the parameters of the concentrated propagation paths and the distributed scattering component that are frequently observed in MIMO channels. In particular, the parameters of the scattering component is estimated in both spatial and temporal domains. A stochastic channel model is assumed. The power-delay profile of the scattering component is modeled using an exponential distribution, which is typically observed in measurement campaigns. The power angular profile is modeled using a mixture of angular von Mises distributions. The simulation results show that this procedure converges to the estimates of both specular and diffuse components with high fidelity. Convergence is achieved with only few iterations.

Computationally efficient methods were derived for finding the approximate ML estimates. The structure of the covariance matrices is fully exploited. Complexity studies show that the reduction in the number of real multiplications is approximately three to five orders of magnitude. Computationally efficient methods to compute the gradients and Hessians are presented as well, which are useful for the implementation of the optimization routines.

Furthermore, the Cramér-Rao lower bound (CRLB) for the problem was established and the simulations show that the variance of the estimates converges close to the bound for a relatively small number of cycles of the estimation procedure and small number of channel realizations (small sample size). For some parameters the CRLB is not attained, but no error floor indicating bias is observed.

Possible topics of future research include the extension of the derived techniques for multiple clusters in angle- and delay-domain. This extension requires new computationally efficient methods, since the Kronecker structure of the DSC covariance matrix is lost. Also of interest is the application of the estimation method to measured data from channel sounding campaigns. Extensions of the proposed estimators to dynamic, time-varying propagation environments is also of great interest. Such estimators should be able to capture the dynamic behavior of the channel with few parameters with relatively low computational complexity. Due to the close relationship between MIMO channel sounding and MIMO radars, potential future research topics include extending the proposed methods to target detection, discrimination and tracking in MIMO radars. In addition,

waveform diversity, i.e. designing waveforms in order to improve the overall performance such as propagation path tracking or detection and identification of targets in interference and noise is of interest.

Bibliography

[1] "Third Generation Partnership Project," http://www.3gpp.org, July 2002.

[2] "WiMAX Forum," http://www.wimaxforum.org/home.

[3] S. Cherry, "The wireless last mile," *IEEE Spectrum*, vol. 40, no. 9, pp. 18–22, Sep. 2003.

[4] A. F. Molisch, *Wireless Communications*, John Wiley & Sons, NJ, USA, 2005, 668 pages.

[5] D. Gesbert, M. Shafi, and D.-S. Shiu, "From theory to practice: An overview of MIMO space-time coded wireless systems," *IEEE Journal on Selected Areas in Communications*, vol. 21, no. 3, pp. 281–302, Apr. 2003.

[6] A. Hottinen, O. Tirkkonen, and R. Wichman, *Multi-Antenna Transceiver Techniques for 3G and Beyond*, John Wiley & Sons, NJ, USA, 2nd. edition, 2006, 342 pages.

[7] D. Tse and P. Viswanath, *Fundamentals of Wireless Communication*, Cambridge University Press, Cambridge, UK, 2005, 586 pages.

[8] L. M. Correia, Ed., *Mobile Broadband Multimedia Networks: Techniques, Models and Tools for 4G*, Academic Press, London, UK, 2006, 600 pages.

[9] B. H. Fleury, M. Tschudin, R. Heddergott, D. Dahlhaus, and K. I. Pedersen, "Channel parameter estimation in mobile radio environments using the SAGE algorithm," *IEEE Journal on Selected Areas in Communications*, vol. 17, no. 3, pp. 434–450, Mar. 1999.

[10] A. Richter, *Estimation of Radio Channel Parameters: Models and Algorithms*, Ph.D. thesis, Technische Universtat Ilmenau, 2005, http://www.db-thueringen.de/servlets/DocumentServlet?id=4815.

[11] J. W. Wallace and M. Jensen, "Modeling the indoor MIMO wireless channel," *IEEE Trans. on Antennas and Propagation*, vol. 50, no. 5, pp. 591–599, May 2002.

[12] A. Abdi and M. Kaveh, "A space-time correlation model for multielement antenna systems in mobile fading channels," *IEEE Journal on Selected Areas in Communications*, vol. 20, no. 3, pp. 550–560, April 2002.

[13] A. Richter, M. Landmann, and R. S. Thomä, "Parameter estimation results of specular and dense multipath components in micro- and macro-cell scenarios," in *Proc. of WPMC 2004*, Abano Terme, Italy, Sep. 2004.

[14] A. Richter, "The contribution of distributed scattering in radio channels to channel capacity: Estimation and modeling," in *Conference Record of the Thirty-Eighth Asilomar Conference on Signals, Systems and Computers*, Nov. 2006, pp. 951–955.

[15] D. Astély, B. Ottersten, and A. L. Swindlehurst, "A generalized array manifold model for local scattering in wireless communications," in *Proc. IEEE Int. Conf. on Acoustics, Speech, and Signal Processing, ICASSP '97*, 1997, vol. 5, pp. 4021–4024.

[16] M. Bengtsson and B. Ottersten, "Low-complexity estimators for distributed sources," *IEEE Transactions on Signal Processing*, vol. 48, no. 8, pp. 2185–2194, Aug. 2000.

[17] O. Besson and P. Stoica, "Decoupled estimation of DOA and angular spread for a spatially distributed source," *IEEE Transactions on Signal Processing*, vol. 48, no. 7, pp. 1872–1882, Jul. 2000.

[18] Q. Wan, J. Yuan, and Y. N. Peng, "Estimation of nominal direction of arrival and angular spread using the determinant of the data matrix," in *Proc. of the 4th Int. Workshop on Mobile and Wireless Communications Network*, 2002, pp. 76–79.

[19] E. Fishler, A. Haimovich, R. Blum, L. Cimini, D. Chizhik, and R. Valenzuela, "Performance of MIMO radar systems: Advantages of angular diversity," in *Conference Record of the Thirty-Eighth Asilomar Conference on Signals, Systems and Computers*, Nov. 2004, vol. 1, pp. 305 – 309.

[20] E. Fishler, A. Haimovich, R. Blum, D. Chizhik, L. Cimini, and R. Valenzuela, "MIMO radar: an idea whose time has come," in *Proc. of the IEEE Radar Conference*, Apr. 2004, pp. 71 – 78.

[21] "International Telecommunication Union," http://www.itu.int, July 2002.

[22] K. V. Mardia, *Statistics of Directional Data*, Academic Press, London and New York, 1972, 357 pages.

[23] G. J. Foschini and M. Gans, "On limits of wireless communication in a fading environment when using multiple antennas," *Wireless Personal Communications*, , no. 6, pp. 311–335, 1998.

[24] V. V. Veeravalli, Y. Liang, and A. M. Sayeed, "Correlated MIMO wireless channels: Capacity, optimal signaling, and asymptotics," *IEEE Transactions on Information Theory*, vol. 51, no. 6, pp. 2058–2072, Jun. 2005.

[25] B. Widrow, P. E. Mantey, L. J. Griffiths, and B. B. Goode, "Adaptive antenna systems," *Proceedings of IEEE*, vol. 55, no. 12, pp. 2143–2159, Dec. 1967.

[26] S. Applebaum, "Adaptive arrays," *IEEE Transactions on Antennas and Propagation*, vol. 24, no. 5, pp. 585–598, Sep. 1976.

[27] W. F. Gabriel, "Adaptive arrays – an introduction," *Proceedings of IEEE*, vol. 64, no. 2, pp. 239–272, Feb. 1976.

[28] J. Winters, "Optimum combining in digital mobile radio with cochannel interference," *IEEE Transactions on Vehicular Technology*, vol. 33, no. 3, pp. 144–155, Aug. 1984.

[29] L. C. Godara, "Application of antenna arrays to mobile communications, part II: Beam-forming and direction-of-arrival considerations," *Proceedings of the IEEE*, vol. 85, no. 8, pp. 1195–1245, Aug. 1997.

[30] IST-WINNER, "D2.7 assessment of advanced beam forming and MIMO technologies," Feb. 2005, https://www.ist-winner.org/DeliverableDocuments/D2.7v1.1.pdf.

[31] S. M. Alamouti, "A simple transmit diversity technique for wireless communications," *IEEE Journal on Select Areas in Communications*, vol. 16, no. 8, pp. 1451–1458, Oct. 1998.

[32] D. P. Palomar, J. M. Cioffi, and M. A. Lagunas, "Joint Tx-Rx beamforming design for multicarrier MIMO channels: A unified framework for convex optimization," *IEEE Transactions on Signal Processing*, vol. 51, no. 9, pp. 2381–2401, Sep. 2003.

[33] A. F. Naguib, N. Seshádri, and A. R. Calderbank, "Increasing data rate over wireless channels," *IEEE Signal Processing Magazine*, vol. 17, no. 3, pp. 76–92, May 2000.

[34] G. J. Foschini, "Layered space-time architecture for wireless communication in a fading environment when using multi-element antennas," *Bell Lab Techn. J.*, pp. 41–59, Autumn 1996.

[35] G. J. Foschini, D. Chizhik, M. J. Gans, C. Papadias, and R. A. Valenzuela, "Analysis and performance of some basic space-time architectures," *IEEE Journal on Selected Areas in Communications*, vol. 21, no. 3, pp. 303–320, Apr. 2003.

[36] A. F. Molisch and M. Z. Win, "MIMO systems with antenna selection," *IEEE Microwave Magazine*, vol. 5, no. 1, pp. 46–56, Mar. 2004.

[37] A. F. Molisch, M. Z. Win, Y.-S. Choi, and J. H. Winters, "Capacity of MIMO systems with antenna selection," *IEEE Transactions on Wireless Communications*, vol. 4, no. 4, pp. 1759–1772, Jul. 2005.

[38] K. Yu and B. Ottersten, "Models for MIMO Propagation Channels, A Review," *Special Issue on Adaptive Antennas and MIMO Systems, Wiley Journal on Wireless Communications and Mobile Computing*, vol. 2, no. 7, pp. 653–666, Nov. 2002.

[39] R. B. Ertel, P. Cardieri, K. W. Sowerby, T. S. Rappaport, and J. H. Reed, "Overview of spatial channel models for antenna array communication systems," *IEEE Personal Communications*, vol. 5, no. 1, pp. 10–22, Mar. 1998.

[40] D. Didascalou, M. Döttling, N. Geng, and W. Wiesbeck, "An approach to include stochastic rough surface scattering into deterministic ray-optical wave propagation modeling," *IEEE Transactions on Antennas and Propagation*, vol. 51, no. 7, pp. 1508–1515, Jul. 2003.

[41] V. Degli-Esposti, D. Guiducci, A. de' Marsi, P. Azzi, and F. Fuschini, "An advanced field prediction model including diffuse scattering," *IEEE Transactions on Antennas and Propagation*, vol. 52, no. 7, pp. 1717–1728, Jul. 2004.

[42] M. Barbiroli, C. Carciofi, G. Falciasecca, M. Frullone, P. Grazioso, and A. Varini, "A new statistical approach for urban environment propagation modeling," *IEEE Transactions on Vehicular Technology*, vol. 51, no. 5, pp. 1234–1241, Sep. 2002.

[43] Q. H. Spencer, B. D. Jeffs, M. A. Jensen, and A. L. Swindlehurst, "Modeling the statistical time and angle of arrival characteristics of an indoor multipath channel," *IEEE Journal on Selected Areas in Communications*, vol. 18, no. 3, pp. 347–360, Mar. 2000.

[44] W. Newhall, R. Mostafa, K. Dietze, J. Reed, and W. Stutzmad, "Measurement of multipath signal component amplitude correlation coefficients versus propagation delay," in *IEEE Radio and Wireless Conference, 2002*, Aug. 2002, pp. 133–136.

[45] T. Rappaport, S. Seidel, and R. Singh, "900-mhz multipath propagation measurements for us digital cellular radiotelephone," *IEEE Transactions on Vehicular Technology*, vol. 39, no. 2, pp. 132–139, May 1990.

[46] R. Roy and T. Kailath, "ESPRIT – estimation of signal parameters via rotational invariance techniques," *IEEE Transactions on Acoustics, Speech, and Signal Processing*, vol. 37, no. 7, pp. 984–995, Jul. 1989.

[47] H. Krim and M. Viberg, "Two decades of array signal processing research," *IEEE Signal Processing Magazine*, vol. 13, no. 4, pp. 67–94, Jul. 1996.

[48] R. U. Nabar, H. Bölcskei, V. Erceg, D. Gesbert, and A. J. Paulraj, "Performance of multiantenna signaling techniques in the presence of polarization diversity," *IEEE Transactions on Signal Processing*, vol. 50, no. 10, pp. 2553–2562, Oct. 2002.

[49] S. Sirianunpiboon, S. D. Howard, and A. R. Calderbank, "Diversity gains across line of sight and rich scattering environments from space-polarization-time codes," in *IEEE Information Theory Workshop on Information Theory for Wireless Networks*, Jul. 2007, pp. 1 – 5.

[50] D.-S. Shiu, G. J. Foschini, M. J. Gans, and J. M. Kahn, "Fading correlation and its effect on the capacity of multielement antenna systems," *IEEE Transactions on Communications*, vol. 48, no. 3, pp. 502–513, Mar. 2000.

[51] J. P. Kermoal, L. Schumacher, K. I. Pedersen, P. E. Mogensen, and F. Frederiksen, "A stochastic MIMO radio channel model with experimental validation," *IEEE Journal on Selected Areas in Communications*, vol. 20, no. 6, pp. 1211–1226, Aug. 2002.

[52] K. Yu, M. Bengtsson, B. Ottersten, D. McNamara, P. Karlsson, and M. Beach, "Modeling of wide-band MIMO radio channels based on NLoS indoor measurements," *IEEE Transactions on Vehicular Technology*, vol. 53, no. 3, pp. 655–665, May 2004.

[53] D. P. McNamara, M. A. Beach, P. N. Fletcher, and P. Karlsson, "Initial investigation of multiple-input multiple-output (mimo) channels in indoor environments," in *Symposium on Communications and Vehicular Technology*, Oct. 2000, pp. 139 – 143.

[54] J. Wallace and M. Jensen, "Statistical characteristics of measured MIMO wireless channel data and comparison to conventional models," in *Proc. of IEEE Vehicular Technology Conference, VTC 2001 Fall*, 2001, vol. 2, pp. 1078–1082.

[55] A. Saleh and R. Valenzuela, "A statistical model for indoor multipath propagation," *IEEE Journal on Selected Areas in Communications*, vol. 5, no. 2, pp. 128–137, Feb. 1987.

[56] W. C. Jakes, *Microwave Mobile Communications*, Wiley, New York, 1974, 656 pages.

[57] D.-S. Shiu, Ed., *Wireless Communication Using Dual Antenna Arrays*, Kluwer Academic, Boston, USA, 2000, 144 pages.

[58] J. Wallace, H. Özcelik, M. Herdin, E. Bonek, and M. Jensen, "A diffuse multipath spectrum estimation technique for directional channel modeling," in *Proc. of IEEE International Conference on Communications*, Jun. 2004, vol. 6, pp. 3183–3187.

[59] H. Özcelik, M. Herdin, W. Weichselberger, J. Wallace, and E. Bonek, "Deficiencies of 'Kronecker' MIMO radio channel model," *IEEE Electronic Letters*, vol. 39, no. 16, pp. 1209–1210, Aug. 2003.

[60] K. Yu and B. Ottersten, "Models for MIMO Propagation Channels, A Review," *Special Issue on Adaptive Antennas and MIMO Systems, Wiley Journal on Wireless Communications and Mobile Computing*, vol. 2, no. 7, pp. 653–666, Nov. 2002.

[61] A. M. Sayeed, "Deconstructing multiantenna fading channels," *IEEE Transactions on Signal Processign*, vol. 50, no. 10, pp. 2563–2579, Oct. 2002.

[62] D. Gesbert, H. Bölcskei, D. A. Gore, and A. J. Paulraj, "Outdoor MIMO wireless channels: Models and performance prediction," *IEEE Transactions on Communications*, vol. 50, no. 12, pp. 1926–1934, Dec. 2002.

[63] P. Almers, F. Tufvesson, and A. F. Molisch, "Keyhole effect in MIMO wireless channels: Measurements and theory," *IEEE Transactions on Wireless Communications*, vol. 5, no. 12, pp. 3596–3604, Dec. 2006.

[64] G. T. 25.996, "3rd Generation Partnership Project; technical specification group radio access network; spatial channel model for MIMO simulations," http://www.3gpp.org, V7.0.0.

[65] L. M. Correia, Ed., *Wireless Flexible Personalised Communications COST 259: European Co-operation in Mobile Radio Research*, John Wiley & Sons, NJ, USA, 2001, 512 pages.

[66] A. F. Molisch, H. Asplund, R. Hedder, M. Steinbauer, and T. Zwick, "The COST259 directional channel model – part I: Overview and methodology," *IEEE Transactions on Wireless Communications*, vol. 5, no. 12, pp. 3421–3433, Dec. 2006.

[67] H. Asplund, A. A. Glazunov, A. F. Molisch, K. I. Pedersen, and M. Steinbauer, "The COST259 directional channel model – part II: Macrocells," *IEEE Transactions on Wireless Communications*, vol. 5, no. 12, pp. 3434–3450, Dec. 2006.

[68] M. Steinbauer, A. F. Molisch, and E. Bonek, "The double-directional radio channel," *IEEE Antennas and Propagation Magazine*, vol. 43, no. 4, pp. 51–63, Aug. 2001.

[69] T. Fügen, J. Maurer, C. Kuhnert, and W. Wiesbeck, "A modelling approach for multiuser MIMO systems including spatially-colored interference," in *IEEE GLOBECOM 2004*, Nov. 2004, pp. 938–942.

[70] K. I. Pedersen, P. E. Mogensen, and B. H. Fleury, "A stochastic model of the temporal and azimuthal dispersion seen at the base station in outdoor propagation environments," *IEEE Transactions on Vehicular Technology*, vol. 49, no. 2, pp. 437–447, March 2000.

[71] J. B. Andersen and K. I. Pedersen, "Angle-of-arrival statistics for low resolution antennas," *IEEE Transactions on Antennas and Propagation*, vol. 50, no. 3, pp. 391–395, Mar. 2002.

[72] IST-WINNER, "Wireless world initiative new radio," https://www.ist-winner.org.

[73] IST-WINNER, "D1.1.1 WINNER II interim channel models," Nov. 2006, https://www.ist-winner.org/WINNER2-Deliverables/D1.1.1.pdf.

[74] IST-WINNER, "D5.4 final report on link level and system level channel models," Nov. 2005, https://www.ist-winner.org/DeliverableDocuments/D5.4.pdf.

[75] J. A. Khoja, M. A. Al-Shalash, and V. K. Prabhu, "Dynamic system simulator for the modeling of CDMA systems," in *International Mobility and Wireless Access Workshop*, Oct. 2002, pp. 50 – 58.

[76] S. M. Kay, *Fundamentals of Statistical Signal Processing, Volume I: Estimation Theory*, Prentice-Hall International, Inc., Englewood Cliffs, NJ, USA, 1993, 625 pages.

[77] J. Medbo, F. Harrysson, H. Asplund, and J.-E. Berg, "Measurements and analysis of a MIMO macrocell outdoor-indoor scenario at 1947 MHz," in *Proc. of IEEE 59th Vehicular Technology Conference, VTC 2004 Spring*, May 2004, vol. 1, pp. 261 – 265.

[78] K. Haneda and J. ichi Takada, "High-resolution estimation of NLOS indoor MIMO channel with network analyzer based system," in *Proc. of IEEE International Symposium on Personal, Indoor and Mobile Radio Communication*, Sep. 2003, vol. 1, pp. 675 – 679.

[79] K. Sulonen, P. Suvikunnas, L. Vuokko, J. Kivinen, and P. Vainikainen, "Comparison of MIMO antenna configurations in picocell and microcell environments," *IEEE Journal on Selected Areas in Communications*, vol. 21, no. 5, pp. 703–712, Jun. 2003.

[80] B. H. Fleury, P. Jourdan, and A. Stucki, "High-resolution channel parameter estimation for MIMO applications using the SAGE algorithm," in *2002 International Zurich Seminar on BroadBand Communications. Access, Transmission, Networking*, Feb 2002, pp. 30–1 – 30–9.

[81] Y. C. Eldar and A. V. Oppenheim, "MMSE whitening and subspace whitening," *IEEE Transactions on Information Theory*, vol. 49, no. 7, pp. 1846–1851, Jul. 2003.

[82] J. Capon, "High-resolution frequency-wavenumber spectrum analysis," *Proceedings of the IEEE*, vol. 57, no. 8, pp. 1408–1418, Aug. 1969.

[83] G. Bienvenu and L. Kopp, "Adaptivity to background noise spatial coherence for high resolution passive methods," in *Proc. of IEEE International Conference on Acoustics, Speech and Signal Processing*, Apr. 1980, vol. 5, pp. 307 – 310.

[84] P. Stoica and A. Nehorai, "MUSIC, maximum likelihood, and cramer-rao bound," *IEEE Transactions on Acoustics, Speech, and Signal Processing*, vol. 37, no. 5, pp. 720–741, May 1989.

[85] F. Belloni, A. Richter, and V. Koivunen, "Extension of root-MUSIC to non-ULA array configurations," in *Proceedings IEEE International Conference on Acoustics, Speech, and Signal Processing (ICASSP)*, Toulouse, France, May 2006, pp. 897–900.

[86] B. Ottersten, M. Viberg, and T. Kailath, "Performance analysis of the total least squares ESPRIT algorithm," *IEEE Transactions on Signal Processing*, vol. 39, no. 5, pp. 1122–1135, May 1991.

[87] J. F. Böhme, "Estimation of source parameters by maximum likelihood and nonlinear regressions," in *IEEE International Conference on Acoustics, Speech, and Signal Processing*, Mar. 1984, vol. 9, pp. 271 – 274.

[88] A. J. Weiss and B. Friedlander, "Maximum likelihood signal estimation for polarization sensitive arrays," *IEEE Transactions on Antennas and Propagation*, vol. 41, no. 7, pp. 918–925, Jul. 1993.

[89] J. Li, P. Stoica, and D. Zheng, "Efficient direction and polarization estimation with a COLD array," *IEEE Transactions on Antennas and Propagation*, vol. 44, no. 4, pp. 539–547, Apr. 1996.

[90] A. P. Dempster, N. M. Laird, and D. B. Rubin, "Maximum likelihood from incomplete data via the EM algorithm," *Journal of the Royal Statistical Society. Series B (Methodological)*, vol. 39, no. 1, pp. 1–38, 1977.

[91] T. K. Moon, "The expectation-maximization algorithm," *IEEE Signal Processing Magazine*, vol. 13, no. 6, pp. 47–60, Nov. 1996.

[92] J. A. Fessler and A. O. Hero, "Space-alternating generalized expectation-maximization algorithm," *IEEE Transactions on Signal Processing*, vol. 42, no. 10, pp. 2664–2677, Oct 1994.

[93] B. H. Fleury, X. Yin, K. G. Rohbrandt, P. Jourdan, and A. Stucki, "Performance of a high-resolution scheme for joint estimation of delay and bidirection dispersion in the radio channel," in *IEEE 55th Vehicular Technology Conference, VTC 2002 Spring*, May 2002, vol. 1, pp. 522–526.

[94] J. F. Böhme, "Separated estimation of wave parameters and spectral parameters by maximum likelihood," in *IEEE International Conference on Acoustics, Speech, and Signal Processing*, Apr. 1986, vol. 11, pp. 2819 – 2822.

[95] A. G. Jaffer, "Maximum likelihood direction finding of stochastic sources: a separable solution," in *IEEE International Conference on Acoustics, Speech, and Signal Processing*, Apr. 1988, pp. 2893 – 2896.

[96] H. Akaike, "A new look at the statistical model identification," *IEEE Transactions on Automatic Control*, vol. AC-19, no. 6, pp. 716–723, Dec. 1974.

[97] G. Schwartz, "Estimating the dimension of a model," *Ann. Stat.*, vol. 6, pp. 461–464, 1978.

[98] J. Rissanen, "Modeling by shortest data description," *Automatica*, vol. 14, pp. 465–471, 1978.

[99] M. Wax and T. Kailath, "Detection of signals by information theoretic criteria," *IEEE Transactions on Acoustics, Speech, and Signal Processing*, vol. 33, no. 4, pp. 387–392, Apr. 1985.

[100] P. Stoica and Y. Selén, "Model-order selection: a review of information criterion rules," *IEEE Signal Processing Magazine*, vol. 21, no. 4, pp. 36–47, Jul. 2004.

[101] P. Stoica, Y. Selén, and J. Li, "On information criteria and the generalized likelihood ratio test of model order selection," *IEEE Signal Processing Letters*, vol. 11, no. 10, pp. 794–797, Oct. 2004.

[102] T. Trump and B. Ottersten, "Estimation of nominal direction of arrival and angular spread using an array of sensors," *Signal Processing*, vol. 50, no. 1-2, pp. 57–69, Apr. 1996.

[103] D. Astély and B. Ottersten, "The effects of local scattering on direction of arrival estimation with music," *IEEE Transactions on Signal Processing*, vol. 47, no. 12, pp. 3220–3234, Dec. 1999.

[104] X. Yin and B. H. Fleury, "Nominal direction and direction spread estimation for slightly distributed scatterers using the sage algorithm," in *IEEE 61st Vehicular Technology Conference, VTC 2005 Spring*, May 2005, vol. 1, pp. 25–29.

[105] X. Yin, T. Pedersen, N. Czink, and B. H. Fleury, "Parametric characterization and estimation of bi-azimuth dispersion of path components," in *Proceedings of the 7th IEEE International Workshop on Signal Processing Advances for Wireless Communications (SPAWC)*, Jul. 2006, pp. 1–6.

[106] S. Feng-Wen, J. Yimin, and J. Baras, "On the convergence of the inverses of Toeplitz matrices and its applications," *IEEE Transactions on Information Theory*, vol. 49, no. 1, pp. 180–190, Jan. 2003.

[107] P. Sherman, "Circulant approximations of the inverses of Toeplitz matrices and related quantities with applications to stationary random processes," *IEEE Transactions on Signal Processing*, vol. 33, no. 6, pp. 1630–1632, Dec. 1985.

[108] D. Marquardt, "An algorithm for least-squares estimation of nonlinear parameters," *SIAM Journal on Applied Mathematics*, vol. 11, pp. 431–441, 1963.

[109] G. H. Golub and C. F. V. Loan, *Matrix Computations*, The Johns Hopkins University Press, Maryland, USA, 1989, 728 pages.